Master Thesis in Chemistry and Business Studies

Shaping Tomorrow's Ethylene
A Prospective Life Cycle Assessment of Emerging Production Alternatives

Author:

Andreas Neft
Matriculation-Nr.: 22-738-355
Address: Riedgrabenweg 18, 8050 Zürich
Telephone: +41 (0)76 721 47 34
E-Mail: andreasfranz.neft@uzh.ch

Submission Date:

28th of November 2024

Supervisors at the University of Zurich:

Prof. Dr. Stefan Seeger – Department of Chemistry
Dr. Sandro Olveira – Department of Chemistry

Supervisor at the Paul-Scherrer-Institute:

Christian Bauer – Researcher at the Technology Assessment Group

Executive Summary

Recent catastrophic floods in Valencia underscore the IPCC's warnings about the increasing frequency and severity of extreme weather events driven by Anthropogenic Climate Change. The Petrochemical Industry, as a significant contributor to GHG emissions, remains locked into carbon-intensive processes facing growing pressure to reduce GHG emissions. Ethylene, a key product of this sector with high production volumes and diverse applications, serves as a critical case study for addressing the industry's environmental challenges.

This study evaluates two innovative production pathways – Biomass-to-Olefins and H_2+CCU-to-Olefins –, incorporating several low-carbon technologies, against the conventional Steam Cracking route using cradle-to-gate prospective Life Cycle Assessments focused solely on Global Warming Potential (GWP) under the functional unit of 1 t of ethylene. The analysis covers several future scenarios by implementing Integrated Assessment Models, geographies, and varying process set-ups and modifications retrieved from literature sources to assess the decarbonization potential of these routes and their feasibility in breaking the sector's carbon lock-in.

The Biomass-to-Olefins route consistently demonstrates the best GWP performance, achieving cradle-to-gate values as low as -2911.1 kg CO_2-eq./t ethylene in future scenarios due to its CO_2 sequestration properties. The H_2+CCU-to-Olefins route initially exhibits the highest GWP due to its reliance on carbon-intensive electricity, but significant improvements are observed in scenarios with decarbonized energy grids, reducing impacts as low as -2804.4 kg CO_2-eq./t ethylene, ultimately surpassing the conventional Steam Cracking process in future scenarios. In contrast, the Steam Cracking route offers limited GWP reduction potential due to its dependence on the fossil feedstock upstream chain and technological maturity. Regional electricity mixes play a critical role, with novel routes performing substantially better in cleaner energy systems, emphasizing the importance of renewable energy adoption.

Process modifications further enhance GWP performance. In Steam Cracking, adopting low-emission or electric furnaces combined with CCS achieves up to a 40% GWP reduction, although improvements remain constrained by fossil feedstock dependency. The Biomass-to-Olefins pathway benefits from process integration, optimized feedstocks and CCS, achieving GWP reductions of up to 330%. The H_2+CCU-to-Olefins pathway is heavily influenced by electricity demand and its source, with modifications such as replacing PEMEC with SOEC or incorporating other energy-efficient process designs reducing GWP by up to 30%. The findings underscore the necessity of integrating renewable energy, sustainable feedstocks and advanced technologies to reduce GWP impact of ethylene production. While Steam Cracking offers limited scope for improvement, the Biomass-to-Olefins and H_2+CCU-to-Olefins pathways present promising low-carbon alternatives, contingent upon a global transition to renewable electricity While the novel routes show promising GWP performances, trade-offs with other environmental impacts and resources as well as their resource-intensive nature highlight the need to reduce overall consumption alongside technological shifts. This Master Thesis contributes to a better understanding of low-carbon pathways for the Petrochemical Sector and their role in mitigating climate change, while future research should explore economic feasibility, downstream impacts, and trade-offs, such as land use and resource availability, to ensure sustainable and feasible decision-making in the Petrochemical Sector.

Acknowledgement

First and foremost, I would like to express my sincerest gratitude to my supervisors Prof. Dr. Stefan Seeger and Dr. Sandro Olveira at the University of Zurich as well as Christian Bauer at the Paul Scherrer Institute, for their invaluable guidance and expertise throughout the course of my research. Their insightful advice and constant support, particularly during our regular follow-up meetings, have been fundamental in shaping the direction and the successful completion of this Master Thesis. These meetings have not only ensured adherence to the required academic standards, but also served as source for inspiration, fostering the development of new ideas.

Furthermore, I would like to extend a special thank you to Christian Bauer's PhD student, Alvaro Hahn, for his generous assistance with Python coding and his counsel in establishing the necessary life cycle inventories. His contributions significantly enhanced the technical aspects of this Master Thesis and enriched my understanding of key methodologies.

Most importantly, I am deeply grateful to my parents whose unwavering support and belief in me have been a cornerstone of my academic journey. Their unconditional love, encouragement and sacrifices have provided me with the strength and determination to persevere, particularly during challenging moments. I am forever thankful for their role in enabling me to pursue my goals.

Finally, I would like to express my appreciation to everyone, who has been part of this journey, for their patience, encouragement and support. As I conclude this chapter, I look forward to applying the knowledge and skills I have gained throughout my academic course to contribute to solving real-world problems.

Table of Contents

List of Figures

List of Tables

List of Equations

List of Abbreviations

Abbreviation	Name
AEC	Alkaline Electrolysis
AGR	Acid Gas Removal
BA	Bosnia-Herzegovina
BoP	Balance of Plant
BTX	Benzene, Toluene and Xylene
c-LCA	comparative Life Cycle Assessment
CCS	Carbon Capture Storage
CCU	Carbon Capture Utilization
CH	Switzerland
CN	China
CO_2-eq.	CO_2 equivalent
DAC	Direct Air Capture
DME	Dimethyl ether
FRM	Free Radical Mechanism
EUR	Europe
FT	Fischer Tropsch
GHG	Green House Gas
GLO	Global
GWP	Global Warming Potential
HER	Hydrogen Evolution Reaction
HVC	High Value Chemical
IAM	Integrated Assessment Model
IPCC	Intergovernmental Panel on Climate Change
LCA	Life Cycle Assessment
LCI	Life Cycle Inventory
LCIA	Life Cycle Impact Assessment
LPG	Liquified Petroleum Gas
MEA	Monoethanolamine
MeOH	Methanol
MK	North Macedonia
MSW	Municipal Solid Waste
MTO	Methanol-to-Olefins
NaOH	Natrium hydroxide
NO	Norway
OER	Oxygen Evolution Reaction
p-LCA	prospective Life Cycle Assessment
PEMEC	Proton Exchange Membrane Electrolysis
$PM_{2.5}$	Particulate Matter
PSC	Point Source Capture
REMIND	Regional Model of Investments and Development
RoW	Rest of World

RS	Serbia
SAPO	Silicium Aluminum Phosphate
SDG	Sustainable Development Goal
SMR	Steam Methane Reforming
SN	Stoichiometric Number
SOEC	Solid Oxide Electrolysis
SSP	Shared Socioeconomic Pathway
TLE	Transfer Line Exchanger
TW	Taiwan
VOC	Volatile Organic Matter
WGS	Water Gas Shift
AEC	Alkaline Electrolysis
AGR	Acid Gas Removal

1. Introduction

1.1 Problem Statement and Aim of Master Thesis – Climate Crisis and the Chemical Industry

1.1.1 The Anthropogenic Climate Change and The Paris Agreement

Recent heavy rainfall, amounting to hundreds of liters per square meter, has led to severe flooding in southeastern Spain, resulting in over 200 casualties and causing extensive damage valued in the billions (s. **Figure 1**) (Hall, 2024 & SRF, 2024). To contextualize, the city of Chiva experienced 491 liters per square meter within an eight-hour period - surpassing the typical annual rainfall of nearby Valencia, which averages 461 liters per square meter (Kixmüller, 2024). Although such extreme events are influenced by a complex interaction of factors, scientists from Brunel University London emphasize that anthropogenic climate

Figure 1: Picture taken from the city of Catarroja, 10 km away from Valencia after the floods (Arber, 2024; p. 1)

change plays a critical role in intensifying these rainfall extremes. In this catastrophe in particular, the Mediterranean Sea has recently reached an unprecedented temperature of 28.47 °C, the highest on record, which facilitates increased evaporation and moisture uptake into the atmosphere. This moisture is then likely to condense and precipitate as temperatures cool during the autumn months, which fuels these heavy rainfalls (von Eichhorn, 2024).

The authors of the latest Intergovernmental Panel on Climate Change (IPCC) report also reaffirm the strong link between the rise in extreme weather events – such as the recent flooding in Spain – and Anthropogenic Climate Change (IPCC, 2023). According to this report, the human-driven climate change has already profoundly impacted the atmosphere, cryosphere, biosphere, oceans and ecosystems, favoring and intensifying the severity and frequency of extreme weather events. These escalating conditions contribute to food and water insecurity, pose significant risks to human health and lead to economic instability, all of which impede progress toward achieving the Sustainable Development Goals (SDGs). The reason for these developments is clear:

> *"Human-caused climate change is a consequence of more than a century of net GHG emissions from [unsustainable] energy use, land-use and land-use change, lifestyle and patterns of consumption, and production (...)."* (IPCC, 2023, p. 44)

The numbers from the IPPC report underpin these developments: By 2019, atmospheric CO_2 levels reached 410 parts per million, a level unprecedented in at least 2 Mio. years, with CH_4 and N_2O concentrations of 1886 and 332 parts per billion, respectively at historic highs, as well (s. **Figure 2**). These cumulative greenhouse gas emissions (GHG) from 1850 to 2019 exceeded 2400 Gt, driving a global surface temperature rise of over 1.09°C since pre-industrial times (s. **Figure 3**).
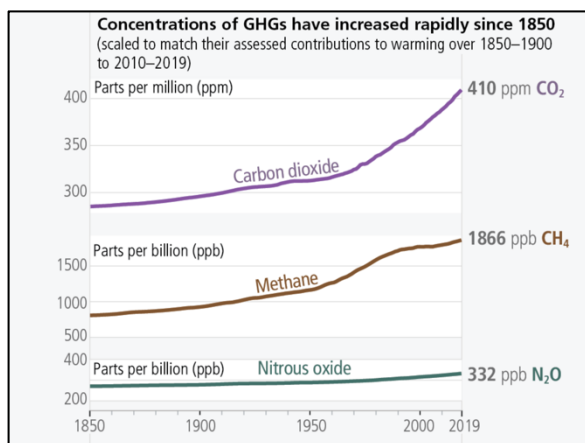
Figure 2: Measured CO_2, CH_4 and N_2O concentrations throughout the years 1850-2020 (IPCC, 2023, p. 43)
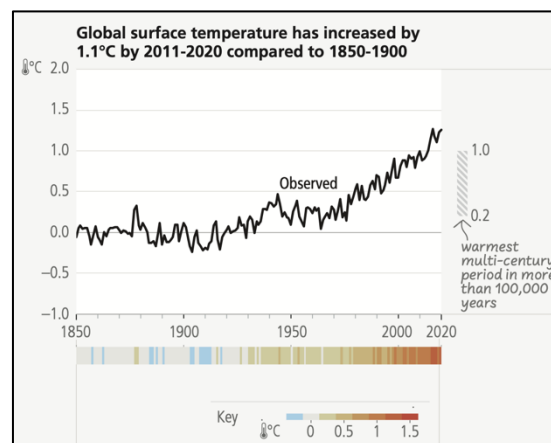
Figure 3: Observed global surface temperature throughout the years 1850-2020 (IPCC, 2023, p. 43)

Furthermore, the annual CO_2-equivalent (CO_2-eq.) emissions reached 59 Gt/year in 2019, a 12% increase compared to 2010 (s. **Figure 4**), with the energy sector contributing the largest share (34%). Other significant sectors include industry (24%), agriculture, forestry, and land use (22%), transport (15%) and buildings (6%) (IPCC, 2023). In response to these concerning developments, the 2015 Paris Agreement with over 196 parties sought to limit global temperature rise to

Figure 4: Annual GHG emissions in CO_2-eq./year throughout out the years 1850-202 (IPCC, 2023, p. 43)

well below 2°C above pre-industrial levels, with an aim to restrict it to 1.5°C – a milestone in the multilateral climate change process (UN Climate Change, 2015). To meet this goal, urgent action is necessary because the world needs to aim at peaking global GHG emissions by 2025 and reducing them by 43% by 2030 to stay on track (IPCC, 2023; UN Climate Change, 2015).

1.1.2 The (Petro-)Chemical Industry as one of the biggest (polluting) industries in a unique situation

The previous chapter emphasized that rapid climate change is driven by human activities with severe impacts on various ecosystems threatening our livelihoods, while industries as a sector significantly contribute to it. Therefore, especially the chemical industry, the third-largest industry polluter after cement and iron, must act (Bauer et al., 2022). As a key economic player, this industry also generated $4.7 trillion in revenues in 2022, contributing 4% of global Gross Domestic Product. It employs more than 15 million people, while synthesizing products integral to over 96% of all manufactured goods (Gabrielli et al., 2023). The Petrochemical Industry in particular, is a fundamental sector within the chemistry sphere

serves as cornerstone in organic chemistry (Chemie, 2024). It acts as a bridge between the Petroleum and Chemical Industry and is carbon-intensive, responsible for 10% of global GHG emissions due to its high reliance on fossil fuels as source of energy and feedstock (Bauer et al., 2022; Chemie, 2024). Despite energy efficiency improvements in this sector, the Petrochemical Industry remains in a carbon lock-in situation as over 99% of its production depends on fossil resources. Moreover, it only changes slowly due to the requirement of large investments to modify its business models, operating and safety standards as well as its complex value chains (Bauer et al., 2022; Gabrielli et al., 2023; Meng et al., 2023). This carbon lock-in situation can be described as followed:

> *"Carbon lock-in is the "self-perpetuating inertia that is created by large fossil-fuel-based energy systems and that inhibits the emergence of alternative energy technologies" and can be seen as a special case of path dependency in the economy, relying on increasing economies of scope, scale, and networks related to fossil fuel resources."* (Bauer et al., 2020, p. 3)
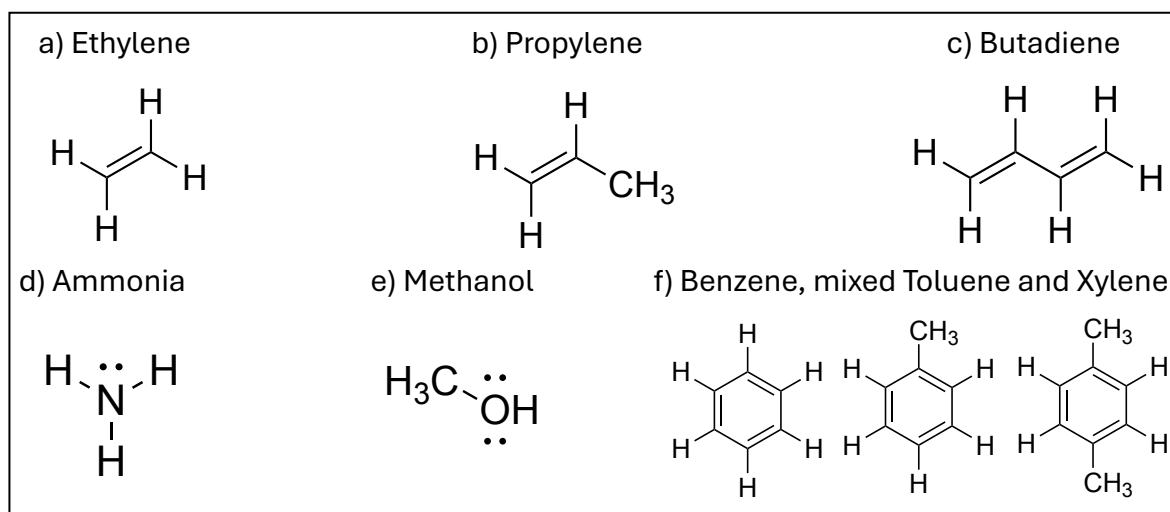
Figure 5: LEWIS-structures of the primary chemicals: light olefins (ethylene, propylene, butadiene), ammonia, MeOH and mixed aromatics (benzene, toluene, xylene)

A significant part of the petrochemical sector's emissions comes from producing primary chemicals namely methanol (MeOH), ammonia, aromatics (mixed benzene, xylene and toluene (BTX)) and light olefins (notably ethylene, propylene and butadiene), which are the backbone of most chemicals and are produced at a million tons scale mostly from a combination of high-temperature heat and fossil resources (s. **Figure 5a-f**) (Gabrielli et al., 2023; Galàn-Martìn et al., 2021; IEA, 2023).

In fact, according to Bauer et al., 2022 and Cefic, 2023, these primary chemicals are mostly derived from coal, natural gas liquids, and refined petroleum products with multiple downstream applications ranging from textiles and detergents, over various fuel types to wind turbines and furniture. Despite increasing use of different feedstocks and advanced processes, the core Steam Cracking process, which produces most of the primary chemicals or their precursors, remains unchanged.

Global production capacity for petrochemicals, particularly in Asia, the Middle East, and in former Soviet states, is expected to increase to meet the growing demand especially for light olefins for plastic production (Gabrielli et al., 2023). Indeed, between 1950 and 2020, the production of petrochemicals surged from 2 Mt to over 420 Mt, with a 12% increase between

2015 and 2020 alone, and is projected to double over the next 30 years, while ethylene plays a central role in this development (Rootzèn et al., 2023). With an annual production volume of over 162 Mt in 2020, ethylene is the most produced plastic precursor in the world and serves as a raw material for producing a wide range of polymers and chemical products, including different kinds of plastics, rubbers, detergents and adhesives (Meng et al., 2023). Identified by CAS Number 74-85-1, ethylene is a colorless gas with a sweet odor, lighter than air, and highly flammable. It has a molecular weight of 28.05 g/mol and features a carbon-carbon double bond with two hydrogen atoms attached to each carbon atom (s. **Figure 5a**) (PubChem, 2024).

In conclusion, the Chemical Industry is a hard-to-abate sector trapped in a carbon lock-in situation due to its great fossil dependency and energy intensiveness with not only a substantial contribution to the Anthropogenic Climate Change, but also complex value chains affecting almost every other sector. Hereby, the production of ethylene, the most important plastic precursor, serves as a good proxy for this sector and thus, will be the main objective of this Master Thesis.

1.1.3 Goal of Master Thesis: Evaluation of decarbonization strategies for ethylene production

Despite these circumstances described in Chapter 1.1.2, there is promising progress in the development of low-carbon technologies to mitigate the environmental impact of ethylene production addressing its carbon lock-in situation. This chapter provides a brief overview of these technologies, highlighting their advantages and drawbacks.
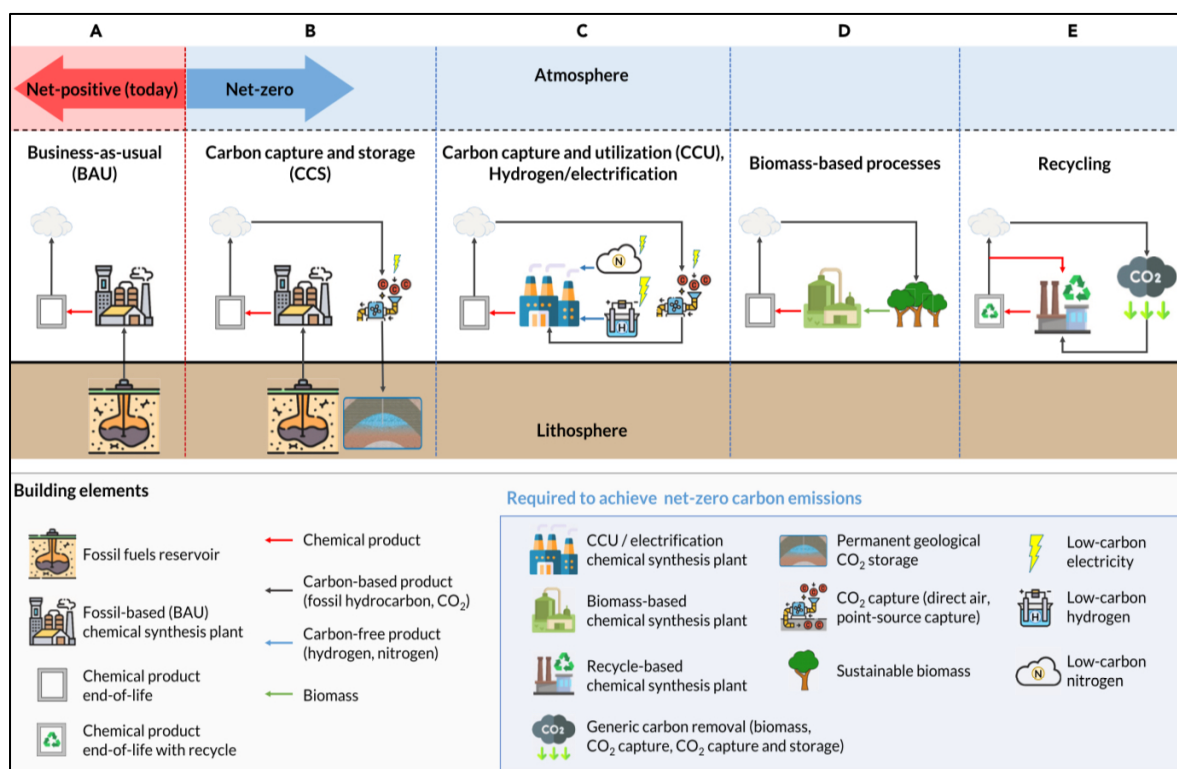
Figure 6: Different net-zero pathways and their simplified process set-ups (CCS, CCU in combination with H2 and electrification, biomass-based process and recycling) in comparison to the conventional route (Business as-usual) (Gabrielli et al., 2023, p. 4)

According to Gabrielli et al, 2023, the key to decarbonize hard-to-decarbonize production processes, in general terms, lies in combining carbon-free energy sources with CO_2-neutral carbon feedstocks. In the case of ethylene production, four primary approaches have been identified to achieve this objective: Carbon Capture and Storage (CCS), Carbon Capture and Utilization (CCU) combined with green hydrogen production, biomass-based processes, and recycling (s. **Figure 6B-E**). This Master Thesis will not elaborate on recycling due to the follwing reasons.

Firstly, the recyling sphere offers various technologies with complex reaction set-ups, which would be out of scope of this Master Thesis (Quicker, 2023). Secondly, even though recycling will play a crucial role in reducing CO_2 emissions and resource use, recycling comes with a lot of drawbacks. This includes lower quality of recycled material (down-cycling), materials and additives, which are harmful to human health espeically in long-lasting plastics, and complex chemical structures amounting to over 13000 chemicals used in plastics according to the UN Envirenement Programme, making recycling difficult or even impossible (Singh and Walker, 2024; Wiesinger, 2024). Thirdly, all recycling processes produce residual waste, which is incinerated yielding to unavoidable CO_2 emissions (Gabrielli et al., 2023).

Business as Usual (BAU)

Fossil feedstocks are the primary source of carbon and hydrogen atoms as well as the energy needed for product synthesis in the fossil-based industry. This results in net-positive CO_2 emissions over a product's lifetime while most emissions come from synthesis and the end-of-life processes, such as combustion or decomposition, of carbon-based products. Additional emissions stem from fossil fuel extraction, preparation, and supply chain leakages, which can account for up to 20% of total emissions (s. **Figure 6A**).

Efforts within BAU scenarios aim to improve efficiency and reduce carbon intensity. Strategies include reducing coal use, waste heat recovery, electrifying processes and adopting co-generation systems. Due to high maturity levels, there are only limited future energy and emissions reductions expected, necessitating more transformative solutions for significant progress (these two sections draw upon Gabrielli et al., 2023).

CCS

In CCS, petrochemicals like ethylene continue to be synthesized from fossil feedstocks but CO_2 emissions from the energy-intensive steam cracking process are captured and permanently stored in geological formations, such as saline aquifers, depleted oil and gas reservoirs or get injected into the deep-ocean (s. **Figures 6B**, **7**), which account for a storage capacity of approximately 7000-55000 Gt (Bisinella et al., 2021; Gabrielli et al., 2023). CO_2 capture technology has already been developed in the 1920s, was utilized to boost oil production in the USA during the energy crisis in the 1970s through the Enhanced Oil Recovery (EOR) process and has gained attraction for climate change mitigation in recent decades (Cruz et al., 2021). Among the different carbon capture technologies presented in **Figure 7**, chemical absorption is chosen as it is the only proven carbon capture technology for flue gases (Bisinella et al., 2021). In addition to chemical absorption, temperature-vacuum swing adsorption (s. TSA/VSA in **Figure 7**) utilized in direct air capture (DAC) systems is also accounted for because it is the implemented technology in the commercially available *Climeworks* system (Deutz and Bardow, 2021).

In spite of the fact that CCS offers significant storage potential, high maturity, commercial availability while maintaining current petrochemical production processes, there are challenges (Gabrielli et al., 2023; Markowitsch et al., 2023). These include uncertainty around the availability and acceptance of storage sites, high costs, energy demands and continued dependency on fossil feedstocks (Gabrielli et al., 2023). Furthermore, this technology still relies on fossil carbon feedstock and current technologies cannot capture all CO_2 due to technology restraints (Galàn-Martìn et al., 2021; Meunier et al., 2020). However, commercial projects like *Shell*'s Quest facility as part of the *Athabasca Oil Sands Project* demonstrate CCS's viability, capturing over 1 Mt of CO_2 annually by storing it underground via pipeline (Shell, 2021). Therefore, two commercially available technologies for CO_2 capture – DAC and Point Source Capture (PSC) – will be discussed in greater detail in Chapter 3.1.
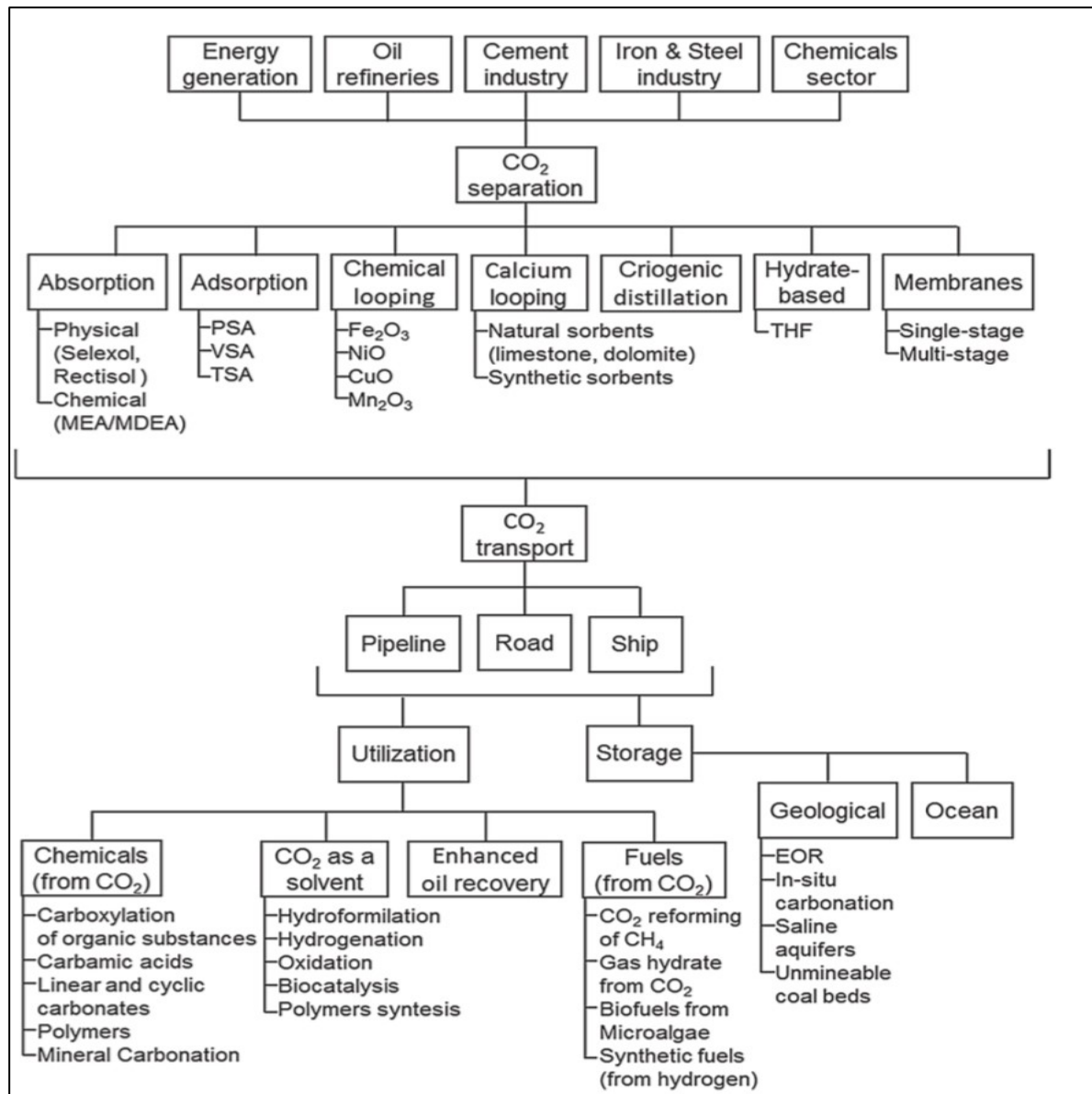
Figure 7: *Overview of different CO_2 separation technologies, possible CO_2 transport pathways as well as different storage and utilization possibilities (Cruz et al., 2021, p. 2)*

CCU & electrolytic H₂

CCU sources carbon from captured CO_2 rather than from fossil fuels, converting it into chemicals using H_2 produced via electrolysis. Unlike CCS where CO_2 is stored, CCU repurposes it, requiring the development of a new chemical industry to break CO_2's strong molecular bonds (s. **Figure 6C**) (Gabrielli et al., 2023). Currently, there are three main methods for producing

	Terminology	Technology	Feedstock/Electricity source
PRODUCTION VIA ELECTRICITY	**Green Hydrogen**	Electrolysis	Wind | Solar | Hydro Geothermal | Tidal
	Purple/Pink Hydrogen		Nuclear
	Yellow Hydrogen		Mixed-origin grid energy
PRODUCTION VIA FOSSIL FUELS	**Blue Hydrogen**	Natural gas reforming + CCUS Gasification + CCUS	Natural gas | coal
	Turquoise Hydrogen	Pyrolysis	Natural gas
	Grey Hydrogen	Natural gas reforming	
	Brown Hydrogen	Gasification	Brown coal (lignite)
	Black Hydrogen		Black coal

Figure 8: Different types of H₂ (Global Energy Infrastructure, 2021, p. 1)

green H_2 via electrolysis (s. **Figure 8**). Although Alkaline Electrolysis (AEC) is the most mature and widely used process, this Master Thesis selects Proton Exchange Membrane Electrolysis (PEMEC) as the baseline scenario in Chapter 3.2.1.1.1 if the electrolysis operates with renewable energy (Bareiß, et al., 2019; Global Energy Infrastructure, 2021). This makes sense as PEMEC has been rapidly scaled up, can operate solely on water, functions at higher pressures, and features more compact and dynamic PEM stacks, which is particularly advantageous in the context of fluctuating energy demands and intermittent nature of renewable energy sources (Bareiß et al., 2019; Bauer et al., 2022). Solid Oxide Electrolysis (SOEC), while still under research and not yet commercially available, offers significant efficiency improvements over PEMEC and thus, will be considered as an emerging technology in this Master Thesis (s. Chapter 3.2.2.1) (Ahbabi Saray et al., 2024; Vilbergsson et al., 2023). Regardless of the type of electrolysis, the overall reaction of water splitting remains the same (s. **Equation 1**).

Equation 1: Overall Reaction of Water Splitting

$$2H_2O \rightarrow 2H_2 + O_2; \Delta H_R^0 = +285.83 \; kJ/mol$$

The main benefit of CCU is the replacement of fossil-based carbon with CO_2 in chemical production enabling the production of ethylene via the platform chemical MeOH using H_2 without CO_2 emissions (s. Chapter 3.2.1.1.1) under the assumption that all the required energy is sourced from renewable energy (Gabrielli et al., 2023; Zhao et al., 2018).

This scenario holds true only when DAC is employed. If the CO_2 is captured from point source emissions, often originating from the combustion of fossil fuels, the situation becomes more complex. In such cases, the captured CO_2 can be considered "recycled" but remains of fossil origin. While fossil CO_2 is temporarily stored in chemicals for a longer time – particularly in plastics – the captured CO_2 is ultimately released into the atmosphere when these materials are incinerated or decompose at the end of their life cycle. In contrast, with DAC, the release of CO_2 at the end of the product's life creates a closed-loop system. This is because the CO_2 originally captured from the atmosphere during the DAC process is simply returned to the air, maintaining a balance rather than contributing additional emissions. Furthermore,

this pathway, especially H_2 production and CCU, requires vast amounts of renewable energy, which poses a significant economic challenge compared to conventional production methods (Bauer et al., 2022; Vilbergsson et al., 2023). Though, projects like *ThyssenKrupp*'s *"Carbon2Chem"* pilot plant showcases CCU's potential, repurposing steel production flue gases in combination with electrolytic H_2 to create chemicals like MeOH (Stagge et al., 2024).

Biomass-based processes
Biomass absorbs CO_2 during growth and stores it into biomass matter via photosynthesis (s. **Equation 2**), which is composed of different concentrations of cellulose, lignin and hemicellulose, offering a "natural" carbon capture solution (s. **Figure 6D**) (Bauer et al., 2022; Vaithyanathan et al., 2023).

Equation 2: *Chemcial Reaction of Photosynthesis*

$$6CO_2 + 6H_2O \rightarrow C_6H_{12}O_6 + 6O_2$$
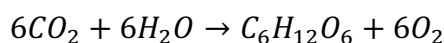
As depicted in **Figure 6D**, biomass can be converted into useful products via various methods, including chemical processes (such as acid hydrolysis), biological treatments (such as fermentation), and thermochemical techniques (such as gasification) (Vaithyanathan et al., 2023). In this Master Thesis, the thermochemical route is selected, as it is more extensively researched and better understood than the other approaches (Osman et al., 2021). Among the available thermochemical processes, biomass gasification represents the most advanced technology, with significant progress dating back to the 1980s (Babu, 2005; Vaithyanathan et al., 2023). It converts biomass into syngas, which can then be used to produce platform chemicals like MeOH and ultimately ethylene as seen in Chapter 3.2.1.1.2 (Bauer et al., 2022; Zhao et al., 2018).

Biomass-based processes offer the advantage of creating a circular carbon system by replacing fossil carbon with renewable biogenic sources. Once biogenic carbon is converted into a chemical product, it is eventually released back into the atmosphere as CO_2, which can then be recaptured and stored in biomass, completing the cycle. Additionally, biomass is relatively inexpensive, and widely available (Wang et al., 2024). However, biomass, due to its unfavorable chemical structure, has lower energy density and higher water content and its availability is limited, with competition from industrial sectors. Ensuring sustainable sourcing is also a challenge (Gabrielli et al., 2023). However, demonstration plants, like *Enerkem*'s municipal solid waste (MSW)-to-MeOH facility in Edmonton, Canada established in 2014, exemplifies the potential of biomass conversion, transforming municipal waste into bio-MeOH (Enerkem, 2024).

Bottom line, there are promising approaches to mitigate the carbon lock-in situation of ethylene production. Yet, it is an imperative to look at these technologies from a holistic point of view to consider potential trade-offs between environmental burdens (Palm et al., 2024). A widely studied and recognized approach is performing a life cycle assessment (LCA; s. Chapter 2.2), which is going to be the methodology applied in this Master Thesis to scrutinize different ethylene production pathways.

1.1.4 Problem Statement

To the best of the author's knowledge based on the extensive Literature Review in Chapter 2.1, no prospective Life Cycle Assessment (p-LCA) has yet been conducted on various ethylene production processes, comparing conventional Steam Cracking and the two innovative routes of MeOH production through either direct hydrogenation of CO_2 – sourced from air or point source emissions combined with electrolytic H_2 (H_2+CCU) – or via pre-treated syngas from biomass gasification, followed by the subsequent Methanol-to-Olefins (MTO) process. While previous studies have examined these production routes already, they typically rely on baseline scenarios without accounting for potential technological advancements, modifications in process design or future developments (s. Chapter 2.1). This Master Thesis aims to evaluate the environmental performance of these two novel ethylene production pathways – Biomass-to-Olefins and H_2+CCU-to-Olefins – in comparison to the conventional Steam Cracking process. The analysis is conducted under the functional unit (FU) of producing 1 t of ethylene, considering not only current technological conditions but also future scenarios and potential process modifications. The assessment employs p-LCAs from a cradle-to-gate perspective and focuses exclusively on GWP as climate impact category, without addressing other environmental dimensions. Since the location specifics, as described in Chapter 3.1, can play an important part, two regions, Switzerland and China, were selected and compared against each other's baseline cases and future scenarios.

1.2 Methodology

The primary objective of this Master Thesis is to model and evaluate various ethylene production processes applying the p-LCA methodology and compare them to the current state-of-the-art production method, examining how GWP outcomes shift over time and under different process modifications (Sacchi et al., 2022). These modifications include alternative feedstocks (e.g., miscanthus or wood chips instead of bark chips), process integrations (such as repurposing waste heat for carbon capture), and novel technologies (like e-furnaces for Steam Cracking). Future scenarios were set to the 2030 (BASE), 2050 (BASE) and 2050 (PkBudg500), which are further discussed in Chapter 2.2.2, aligning with the climate goals of the European Union (Council of the European Union, 2024. Hereby, this Master Thesis Project was structured into four distinct phases.

In Phase 1, the existing literature on mitigation pathways in the Chemical Industry was reviewed to capture the full scope of the field and gain insights into state-of-the-art research. Specific technologies, including CCS and hydrogen production for instance, were examined both in isolation and as part of integrated chemical production processes. This procedure provided a deeper understanding of the single processes on the one hand and on the other hand, contextualize their roles and impacts within the broader chemical production chain. Additionally, trends in production processes related to environmental performance were identified, which informed subsequent sanity checks of the Master Thesis' results. For example, the electricity mix used in electrolytic hydrogen production significantly impacts global warming potential (GWP). Finally, this foundational review helped define a research gap and refine the research question.

Phase 2 focused on familiarizing with the software tool *brightway2*, an open-source program widely used at the Paul Scherrer Institute to translate Life Cycle Inventory (LCI) data into impact scores (Brightway, 2024). The *Activity Browser* open-source software was also

employed as it provides a graphical user interface for the *brightway2* framework, facilitating tasks such as project and database management, LCI modeling, and data analysis (Steubing et al., 2020). This phase included learning to format Excel files for upload into *brightway2* and applying the Python programming language to streamline the data upload process.

The 3rd phase was the most critical, focusing on data collection and structuring for various processes and scenarios. An extensive bibliographical review had to be conducted, followed by sanity checks against existing data sources such as *ecoinvent* and other literature references to ensure consistency. The iterative nature of this process was necessary due to challenges such as conflicting data, missing parameters, and inconsistent data structures. Data from industry sources was particularly difficult to obtain due to confidentiality. Nevertheless, iterations continued until the data quality was deemed satisfactory, with consistent mass balances and well-defined input and output parameters for each process. Further challenges arose from geographic mismatches in the data: parameters in the literature did not always align with the intended locations or were missing entirely from the *ecoinvent* database. To resolve this, geographic scope was broadened systematically: if data were unavailable for Switzerland, European data were sought, followed by global parameters. In cases involving China, data from India were sometimes used as a substitute, based on similar assumed GWP impacts, before global (GLO) data set came into play. Additionally, when specific parameters were absent, proxy data were employed as appropriate. For instance, in the absence of data for catalyst waste in MeOH and MTO production, zeolite waste was used as it was considered the best available approximation for this type of waste.

In Phase 4, all gathered data was consolidated, structured, and analyzed. The results underwent a final validation process to ensure reliability and coherence.

2. Theoretical Background

This chapter lays out the current knowledge in the Literature Review section (s. Chapter 2.1) first, before it delves deeper into the fundamentals required to understand the different concepts employed including the LCA (s. Chapter 2.2) as well as the Sensitivity Analysis (s. Chapter 2.3).

2.1   Literature Review

To examine the existing body of knowledge of the various decarbonization strategies discussed in the previous Chapter 1.1.3, and to identify research gaps, a Literature Review is presented. The review focuses on papers, which have been published within the last six years to provide an accurate and up-to-date understanding of the current state of the field incorporating LCAs.

The literature review is divided into two sections: The first section evaluates research papers that explore low-carbon technologies, specifically CCS, CCU, green H_2 and biomass gasification. This part aims to identify the key factors that should be considered when conducting LCAs for these technologies. The second section reviews studies, that have integrated these low-carbon technologies into the production of primary chemicals, providing insights into their LCA performance.

Hydrogen

Bareiß et al., 2019 explored the environmental performance of PEMEC compared to the conventional H_2 production via Steam Methane Reforming (SMR) through a cradle-to-gate comparative LAC (c-LCA). The study concluded that PEMEC is a viable alternative to SMR, offering significant reductions in GHG emissions if powered exclusively by renewable energy. The findings indicated that the electricity mix is the primary determinant of CO_2-eq. emissions of H_2 production, accounting for 96% of total GHG emissions, whereas the impact of electrolyser components is negligible (contributing only 4% of total emissions).

Vilbergsson et al., 2023 conducted a cradle-to-gate c-LCA of H_2 production in Iceland and continental Europe to assess the viability from a GWP standpoint of producing H_2 via electrolysis in regions with abundant renewable energy (e.g. Iceland) and transporting it to areas with high H_2 demand (such as continental Europe), versus producing H_2 closer to the demand site. The study found as in Bareiß et al, 2019's paper that the GWP impact of H_2 production is largely determined by the energy mix used, with transportation playing a relatively minor role. Consequently, from an LCA perspective, it is feasible to import H_2 from Iceland to continental Europe from a GWP prespective. The authors concluded that prioritizing local electrification should take precedence over H_2 production in regions without readily available green H_2 sources.

Weidner et al., 2022 examined a p-LCA of grey, green, and blue H_2 (s. **Figure 8**) within the Planetary Boundaries (PB) framework, considering scenarios for 2019, 2035, and 2050. The study observed minimal changes in the environmental impacts of blue and grey H_2, as the operational phase of SMR is already highly efficient. However, green H_2 showed substantial reductions in climate change-related impact categories when future data sets were considered.

Additionally, the authors noted a burden shift from reduced global warming impacts to increased pressure on biogeochemical flows due to expanded use of resources (especially rare earth metals). This underscores the importance of not only decarbonizing electricity sources but also improving metal recycling and mining practices for electrolyser stack production, which contradicts the point made in Bareiß et al., 2019`s paper when future scenarios are considered, as well.

Krishnan et al., 2024 reached similar conclusions as Weidner, et al., 2020 in a p-LCA comparing AEC and PEMEC of grey H_2 to SMR under a baseline (2020) and future scenario (2030). The study reaffirmed that electricity source is the dominant factor influencing environmental impacts as it was the case in Bareiß et al., 2019's and Vilbergsson et al., 2023's paper. However, the authors also observed that electrolyser stacks, contain rare earth metals, which also play a critical role, emphasizing the need to develop more efficient stacks with reduced demand for critical raw materials and energy as stressed in Weidner et al., 2022's paper. In conclusion, the paper found no clear winner between AEC and PEMEC, but both technologies significantly outperformed grey H_2 in all impact categories except for mineral and metal resource use.

CCS/CCU
Bisinella et al., 2021 performed a c-LCA of MSW incineration with and without the application of CCS. Their findings demonstrated that incorporating CCS leads to substantial improvements in mitigating climate change impacts without introducing significant trade-offs in other environmental categories. The positive effects of CCS are further amplified when the energy required for CCS operations is sourced from systems with reduced reliance on fossil fuels.

Raadal and Modahl, 2022 conducted a cradle-to-gate c-LCA of steam production at a Norwegian paper mill, comparing systems with CCS, CCU, and no capture technology. Their study emphasized that replacing fossil fuels with renewable energy sources should be prioritized over CO_2 recycling. They also found that CCS offers greater reductions in CO_2-eq. emissions compared to CCU, as long as fossil fuels remain part of the energy mix. However, once fossil-based electricity is fully replaced with renewable sources, CCU becomes the more favorable option.

Biomass
Sammarchi et al., 2022 led two cradle-to-grave c-LCAs: one for a coal power plant with CCS and another for a coal plant co-firing biomass wit CCS. The study, carried out within a chemical plant in Inner Mongolia, revealed substantial CO_2 reduction potential in both scenarios. However, the LCA results highlighted a significant increase in upstream emissions from the electricity and heat supply required for energy-intensive processes such as CCS and biomass preparation, limiting the overall mitigation potential. Additionally, the reliance on diesel and fertilizers in the biomass supply chain led to negative impacts on local ecosystems and water resources. Despite these challenges, the combination of CCS and biomass could result in negative CO_2 emissions, representing net CO_2 savings.

Wang et al., 2024 conducted a cradle-to-gate c-LCA to evaluate the thermal efficiency and GWP of a biomass gasification plant equipped with chemical looping air separation, coupled with a semi-closed supercritical CO_2 and organic Rankine cycle system. The study demonstrated that combining biomass with CCS offers significant emission reduction potential, primarily due to biomass's carbon neutrality. Moreover, the fuel and material preparation stages were identified as the largest contributors to emissions.

Novel production technologies of primary chemicals

Hoppe et al., 2018 conducted a cradle-to-gate c-LCA on the production of CH_4, MeOH and syngas as basic chemicals, as well as their derived polymers – polyethylene, polypropylene, and polyoxymethylene – to evaluate key resource efficiency indicators of selected CCU routes. These routes were based on different sources of CO_2 combined with H_2 produced via electrolysis sourced by wind energy. The study concluded that CO_2-based chemicals exhibit lower global warming impacts compared to conventional processes, despite having higher raw material input and total material requirement, which goes in hand with the results from Weidner et al., 2022 and Krishnan et al., 2024. The authors emphasized that the feasibility of recycling CO_2 into hydrocarbons is highly dependent on the energy source and the amount of energy used in H_2 production as Bareiß et al., 2019 stressed, as well.

Zhao et al., 2018 compared various ethylene production processes using a cradle-to-gate c-LCA, including different types of pathways including steam cracking, coal-to-olefins (with and without CCS), natural gas-to-olefins, CO_2-to-olefins, and biomass-to-olefins via MeOH (with and without CCS), as well as coal-to-olefins via the Fischer-Tropsch (FT) process (with and without CCS) and biomass-to-ethylene via bioethanol. The study found that CCS offers significant CO_2 reduction potential within chemical production, with biomass-to-olefins via MeOH combined with CCS achieving the lowest CO_2 emissions, which amplifies the point made in Bisinella et al., 2021's paper. However, although coal-to-olefins via FT could significantly reduce reliance on petroleum, this route would result in a considerable increase in environmental burdens, exhibiting the highest CO_2 emissions among the examined processes.

Biernacki et al., 2018 conducted a cradle-to-gate c-LCA comparing MeOH production from natural gas to MeOH production from biogas generated by a wastewater treatment plant in Germany, with H_2 derived from water electrolysis using surplus electricity. They assessed the impacts with and without considering the upstream chains. The study concluded that renewable MeOH had a lower environmental impact in 5 out of 11 impact categories when the upstream chain was included. However, when upstream chains were excluded, renewable MeOH exhibited lower impacts across all categories, which emphasized the importance of including the upstream stages, particularly those related to biomass cultivation and preparation, as well as emissions from wind electricity, in LCA assessments.

Zuiderveen et al., 2024 performed a cradle-to-grave p-LCA integrating the PB framework, comparing mixed plastic waste (MPW)-to-BTX, biomass-to-BTX, and fossil feedstock-to-BTX routes. The study revealed that the MPW-to-BTX pathway had the lowest environmental impact, followed by biomass-to-BTX, which, while having higher environmental impacts due to biomass cultivation, offers the greatest CO_2 reduction potential. Fossil feedstock-to-

BTX showed limited future emission reduction potential, while the MPW-to-BTX and bio-mass-to-BTX routes demonstrated high future reduction potentials. Additionally, chemical recycling was shown to provide greater climate benefits than incineration with energy recovery.

Liu et al., 2024 conducted a cradle-to-gate c-LCA on the state-of-the-art liquid sunlight production method, comparing it with traditional pathways such as coal gasification-to-MeOH, coal-coking-to-MeOH, natural gas-to-MeOH, biomass-to-MeOH, and CO_2-capture-to-MeOH. The study concluded that adopting 100% clean electricity in all cases would reduce cumulative environmental impacts, with the energy source being the most sensitive factor as it was already articulated in previous papers (Bareiß et al., 2019; Hoppe et al., 2018; Vilbergsson et a., 2023). Although natural gas-to-MeOH was considered the most viable approach, CO_2-capture-to-MeOH becomes comparable to natural gas-to-methanol when powered by renewable sources such as wind, nuclear, or hydro energy.

In conclusion, most of the studies reviewed conducted cradle-to-gate LCAs comparing various processes to assess their environmental impacts comprehensively. These studies have already examined the different low-carbon technologies brought up in Chapter 1.1.3 from multiple perspectives, with some integrating these technologies into chemical production processes. Most of the studies demonstrated that low-carbon technologies improve the environmental performance of these processes. A recurring conclusion across the literature is that the electricity source, particularly for H_2 production, is critical to minimizing GWP impact. Additionally, CCS or CCU systems can significantly reduce environmental burdens, although some burden-shifting – particularly in resource use – has also been observed when applying these technologies.

However, only a few studies have incorporated p-LCAs, which account for future technological developments. These studies have shown remarkable results: while the environmental impacts of conventional processes are expected to remain relatively constant, low-carbon technologies are projected to become more efficient and environmentally sustainable as they increasingly rely on renewable energy sources. Hence, p-LCAs are included in this Master Thesis (s. Chapter 1.1.4).

2.2 LCA

This sub-chapter provides an overview of the LCA methodology (s. Chapter 2.2.1), before different facets of LCAs are explained in greater detail. These different aspects cover Integrated Assessment Models (IAMs), which incorporate future projections for p-LCA (s. Chapter 2.2.2) and the *ecoinvent* data base as source of background data (s. Chapter 2.2.3). Furthermore, the impact assessment method employed in this Master Thesis is described (s. Chapter 2.2.4) as well as economic allocation as a methodological approach tackling multi-functionality challenges (s. Chapter 2.2.5).

2.2.1 Overview

The LCAs conducted in this Master Thesis follow the guidelines of the International Organization for Standardization (ISO) – ISO 14044:2006 as well as ISO 14040:2006 –, which systematically quantify a broad range of environmental impacts of a product or service (ISO,

2006a, 2006b).This helps to compare different processes taking all impacts, in this case from cradle-to-gate, into account by giving them a final environmental value at the gate. According to these two ISO-standards as graphically presented in **Figure 9**, LCAs should involve a goal and scope definition by addressing the system boundaries of the product (s. Chapter 3.1) and defining the main objective (s. Chapter 1.1.4) of this study. This is followed by a LCI analysis (s. Chapter 3.1), which collects the necessary data, quantifying the in- and outputs of each unit operation obtained through literature data. In the end, a Life Cycle Impact Assessment (LCIA) is conducted to evaluate the sig-

Figure 9: LCA according to ISO14044:2006 and ISO 14040:2006 (CEM-WAVE, 2021, p. 1)

nificance of potential environmental impacts (s. Chapter 3.3). Finally, these impact results are analyzed at the life cycle interpretation stage (s. Chapter 3.4), which should be compared with each other rather in relative instead of absolute terms.

2.2.2 Integrated Assessment Models

To model future scenarios, this Master Thesis employs IAMs based on the Shared Socioeconomic Pathway 2 (SSP2) from the Regional Model of Investments and Developments (REMIND) (Riahi et al., 2017).

According to Carbon Brief Ltd, 2018, 2024 and Luderer et al., 2020, IAMs are crucial for generating future inventories as they combine complex data of physical and social systems. They utilize different SSPs to explore various futures, which formalize these futures into consistent story lines reflecting a long list of assumption including global population growth, technological advancement, mitigation policy environments and drivers of demand, energy and resource. These models focus on minimizing the economic cost of achieving climate mitigation goals and assuming fully functioning markets but do not explicitly address broader social and political dynamics. The REMIND model, developed by the Potsdam Institute of Climate Research in Germany, assumes a significant deployment of renewable energies even without climate policies due to falling costs.
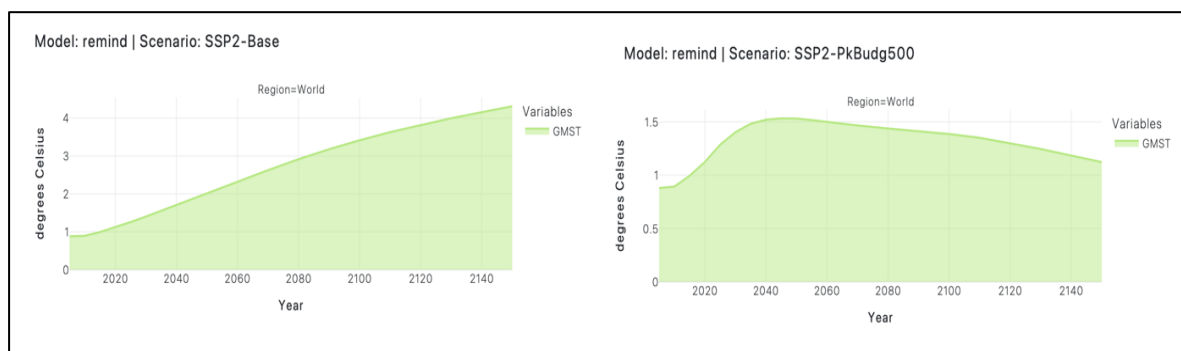
Figure 10: Different developments of global average surface temperature according to the SSP2-base and the SSP2-PkBudg500 scenario (Premise Dash, n.d., p. 1)

This Master Thesis adopts the SSP2 pathway, which envisions moderate global economic and technological growth alongside uneven development, resulting in slow progress towards achieving several SDGs. Population growth is expected to stabilize in the latter half of the century, accompanied by a gradual decline in energy intensity throughout the 21st century (Carbon Brief Ltd., 2018).

Within this SSP2 route, two scenarios are considered (Premise Dash, n.d.):

- The base scenario (BASE): Represents a continuation of global warming throughout the century (s. **Figure 10**), adjusted to the years 2020, 2030, and 2050.
- The optimistic scenario (PkBudg500): Assumes a peak carbon budget of 500 Gt CO_2-eq., limiting global warming by mid-century and allowing for a subsequent decline, which is modeled for the year 2050 (s. **Figure 10**).

While IAMs provide valuable insights, they have inherent limitations. They cannot fully capture positive synergies from climate mitigation efforts, potential cost savings from avoided damages or the influence of political, behavioral, and consumption factors. Consequently, IAMs are used not as prescriptive forecasts but as tools to support policy decision-making by comparing different pathways (Carbon Brief Ltd., 2018).

2.2.3 *Ecoinvent v3.9* data base

The *ecoinvent* v*3.9* database, released on October 13th, 2023, includes over 20000 high-quality LCI datasets covering approximately 3500 products (ecoinvent 2023, 2024). This extensive database functions as a repository of activities associated with specific geographical locations, representing a wide range of industrial and agricultural processes and their resulting products including chemicals, heat, electricity, forestry, textiles, transport and several other categories (ecoinvent, 2024). Hence, it is currently the most used LCA database (Barahmand and Eikeland, 2022). Rather than reflecting the unique practices of individual companies or sites, each dataset in *ecoinvent* represents an average production scenario for a given location (ecoinvent, 2024).

Each entry provides information on technosphere and biosphere flows, encompassing resource consumption, energy and fuel use as well as emissions (ecoinvent, 2024). In this Master Tesis, these datasets (system model: "allocation, cut-off by classification") are used as background information and supplemented by foreground data derived from literature sources to complete LCAs (s. Chapter 3.1).

2.2.4 LCIA calculation method

Based on Lalonde, 2024, LCIAs convert raw emissions and resource data into quantifiable impact scores, categorizing environmental impacts across various processes. This is achieved using impact categories and characterization factors. Impact categories address specific environmental issues by aggregating the effects of emissions that contribute to the same problem. Characterization factors, on the other hand, assess the relative impact within each category by converting emissions into impact scores.

This Master Thesis employs the Environmental Factor (EF) v3.1 European Norm (EN) 15804 LCIA method, which standardizes environmental impact assessments across European non-construction sectors, as developed by the Joint Research Centre of the European Commission (European Commission, 2016; Lalonde, 2024). This method differs from other EF v3.1 versions in its treatment of biogenic CO_2, setting characterization factors for biogenic CO_2

uptake and emission at -1 and +1, respectively (European Commission, 2016). EF v3.1 EN15804 includes 19 impact categories assigned with their own impact index, from acidification and eutrophication to material resources as it can be viewed in **Table 1** (European Commission, 2016).

Table 1: Impact categories according to EF v3.1 EN15804 method

Impact category	Index	Unit
Acidification	Accumulated exceedance	mol H^+-eq.
Climate change	Global warming potential (GWP 100)	kg CO_2-eq.
Climate change: biogenic	Global warming potential (GWP 100)	kg CO_2-eq.
Climate change: fossil	Global warming potential (GWP 100)	kg CO_2-eq.
Climate change: land use and land use change	Global warming potential (GWP 100)	kg CO_2-eq.
Ecotoxicity: freshwater	Comparative toxic unit for ecosystems (CTUe)	CTUe
Energy resources: non-renewable	Abiotic depletion potential: fossil fuels	MJ, net calorific value
Eutrophication: freshwater	Fraction of nutrients reaching freshwater end compartment (phosphorus)	kg P-eq.
Eutrophication: marine	Fraction of nutrients reaching freshwater end compartment (nitrogen)	kg N-eq.
Eutrophication: terrestrial	Accumulated exceedance	mol N-eq.
Human toxicity: carcinogenic	Comparative toxic unit for human (CTUh)	CTUh
Human toxicity: non-carcinogenic	Comparative toxic unit for human (CTUh)	CTUh
Ionising radiation: human health	Human exposure efficiency relative to Uranium 235	kBq U235-eq.
Land use	Soil quality index	[]
Material resources: metals/minerals	Abiotic depletion potential: elements (ultimate reserves)	kg Sb-eq.
Ozone depletion	Ozone depletion potential	kg CFC-11-eq.
Particulate matter formation	Impact on human health	disease incidence
Photochemical oxidant formation: human health	Tropospheric ozone concentration increase	kg NMVOC-eq.
Water use	User deprivation potential (deprivation-weighted water consumption)	m^3 world-eq. deprived

In example: climate change is measured by the GWP index, expressed in CO_2-eq. units describing cumulative direct and indirect radiative forcing (s. **Table 1**), which allows relative comparisons among GHGs (especially the Kyoto gases: CO_2, CH_4, N_2O, SF_6, NF_3 and (per-)fluorinated hydrocarbons) based on the climate potency of each gas against CO_2. CO_2 as a

reference GHG is connoted with a potency GWP = 1, CH_4 as an example is 28 times as climate potent as CO_2, thus having a GWP value of 28 (Ziegler et al., 2024).

These values or also called characterization factors and are continuously reevaluated by the IPCC in their assessment reports. A higher GWP value means that a particular gas is more climate potent than a gas with a smaller GWP value (Ziegler et al., 2024). Due to the fact that CO_2 for instance exhibits a much smaller GWP value compared to CH_4, yet stays much longer in the atmosphere than CH_4, it is important to define time frames to make GWP results comparable (Umwelt Bundesamt, 2022; Ziegler et al., 2024). The most commonly used time frame is 100 years and also deployed in this Master Thesis. All GWP values of EF v3.1 EN 15804 are also set to 100 years (s. **Table 1**: GWP 100), which is in line with the international GHG reporting time horizon of GWP-values (Umwelt Bundesamt, 2022).

This measure is central to understanding the role of GHGs in global warming as GHGs absorb and re-emit infrared radiation, thereby fueling global temperature rise (Ziegler et al., 2024). Besides that, it is the most cited mid-point category of interest due to environmental pressures exerted by GHGs leading to atmospheric temperature change (Katumwesigye et al., 2023). Consequently, GWP is a vital metric for tracking progress toward emissions reduction goals and is integral to carbon footprint calculations required in sustainability reporting of companies, making it the chosen index in this research (Ziegler et al., 2024).

2.2.5 Allocation Methods

In LCAs, allocation methods distribute the input and output flows of a process among different product systems, following ISO 14040:2006, although allocation should be avoided where possible, either by dividing the unit process or expanding the product system. If these approaches are not feasible, allocation methods are used (Dolezal et al., 2014). It is important to consistently employ one out several options such as physical or economic allocation when similar products or processes are compared with each other (Carbon Chain, n.d.).

For multi-product processes like the MTO and Steam Cracking process (s. Chapters 3.1.1 and 3.1.2), this Master Thesis uses economic allocation to address the issue of multi-functionality. It weights products by their shares of the total proceeds, which builds on the products' masses and prices. This approach is chosen because it is the most suitable method to assign emissions between different co-products differing substantially in value. That is the case for the MTO and Steam Cracking process, and as a result, this allocation methodology can reflect why emissions occur (the whole paragraph is drawn upon Carbon Chain, n.d.).

Based on Guinèe et al., 2004, products (economic value $\geq$ 0) and waste streams (economic value $<$ 0) are first categorized based on their economic value. Using a three-year average price (P_i) and the quantity of each product (Q_i), the economic proceeds of each product are calculated ($Q_i \times P_i$, s. **Equation 3**), which stabilizes the results against uncertain price fluctuations. This is followed by summing these proceeds to determine the total value ($\sum_i Q_i \times P_i$, s. **Equation 3**). The allocation factor (AF) is then derived by dividing the economic proceeds of each product by the total value (s. **Equation 3**). This AF is then applied to all material and energy flows in both steam cracking and MTO processes. This method ensures that environmental impacts are proportionally distributed across co-products based on their economic contribution.

Equation 3: *Economic Allocation*

$$AF = \frac{Q_i \times P_i}{\sum_i Q_i \times P_i}$$

This allocation method relies on several key factors, including the reference years for prices, the type of production chain, and the geographical location (Guinèe et al., 2004). While global instead of country specific prices were included in the allocation method due to difficulties at acquiring country specific prices, the refence years were set to 2020-2022 (s. **Appx. Tables 1-8** in Appendix 6.1). However, this approach has limitations: A primary drawback is the assumption of uniform profitability across regions, which can be skewed by varying price types, such as production costs, retail prices and wholesale prices (Cherubini et al., 2011). Detailed descriptions of the economic allocation models applied to different process modifications and future scenarios are provided in the Appendix (s. **Appx. Tables 1-8** in Appendix 6.1).

2.3   Sensitivity Analysis

Sensitivity Analysis evaluates the robustness of results against variations in data, assumptions, and models, and commonly conducted either through local or global Sensitivity Analysis. Local sensitivity analysis examines the effect of a single input parameter on model outputs, keeping all other inputs constant. This method is widely used due to its simplicity and highlights which input variables have the most significant influence on the results. However, local Sensitivity Analysis is limited to changes around one specific parameter, only providing a partial view of the system (whole section is based on Wei et al., 2015).

To address these limitations, global Sensitivity Analysis assesses the influence of input variability across a full range of uncertainty factors, offering a comprehensive view of the system's response to changes in multiple parameters. This approach explores the entire input space, allowing for a more thorough examination of input-output relationships. Compared to local analysis, global Sensitivity Analysis evaluates how variations across all parameters affect model outputs, yielding a more robust assessment of influential factors (whole passage is drawn upon Wei et al., 2015).

In this Master Thesis, a derivative approach from local Sensitivity Analysis is conducted: this Sensitivity Analysis examines how changes of one reference input, identified as very impactful to the overall GWP result during the life cycle interpretation, affects the overall GWP result. For example, in the electrolysis process, the primary GWP contributor is the electricity source, which is originally modeled using the European electricity mix. By altering the electricity source to coal-based electricity, the study evaluates how GWP scores differ to the original scenario. This analysis provides insights into whether specific processes are particularly sensitive to variations in major contributing factors, indicating potential for significant impact fluctuations due to changes in production processes.

3. Results and Discussion

This section of the Master Thesis presents p-LCAs of three ethylene production pathways introduced in the previous Chapter 1.1.3: Steam Cracking and MTO using MeOH produced either through direct hydrogenation of CO_2 from CCU with electrolytic H_2 or through post-treated syngas of biomass gasification. The objective is to assess the GWP impacts of these two innovative pathways relative to the conventional Steam Cracking route and across the two selected locations, Switzerland and China, both in the present and in future projections. Additionally, several c-LCAs are conducted of these pathways individually to analyze how results vary with modifications to each process.

This chapter begins by detailing the system boundaries, describing each baseline production process and possible modifications with their respective LCIs (s. Chapter 3.1). Afterwards, the assumptions underlying future inventories are reported and discussed (s. Chapter 3.2), before LCIAs for all early on discussed LCAs are presented (s. Chapter 3.3) and interpreted (s. Chapter 3.4). Finally, a Sensitivity Analysis is performed to assess the influence of key parameters identified during life cycle interpretation (s. Chapter 3.5).

3.1 System Boundaries of different Ethylene Production Processes

General remarks and assumptions have to be outlined prior to discussing the processes in detail. Firstly, all (sub-)processes are assumed to be located on-site meaning that there is no transportation needed to transfer (intermediate) products from one process to the other. Therefore, no transportation except the captured and stored CO_2 is included in these LCAs. Secondly, two regions were chosen for the ethylene production plant as outlined in Chapter 1.1.4: Switzerland, as an example for a region with a relatively high share of renewables in its energy mix, and China as the country with the strongest growing ethylene production capacities of the world (Bork, 2021). Thirdly, the FU is chosen to be 1 t of ethylene produced to account for the large production scale of ethylene (Meng et al., 2023). The LCI values in the tables provided in this chapter have to be read always as per kg of respective product while the complete LCI tables for of Biomass-to-Olefins, the H_2+CCU-to-Olefins as well as their process modifications aligned to 1 t of ethylene are provided in the Appendix (s. **Appx. Tables 9-12** in Appendix 6.3). Finally, as discussed in Chapter 1.1.4, this Master Thesis focuses exclusively on the cradle-to-gate impacts of ethylene production, excluding downstream value chains due to their complexity: Ethylene can be utilized in a wide range of applications, including consumer electronics, automotive components and food packaging derived from ethylbenzene and polyethylene, as well as solar panels, coatings, adhesives, detergents and even paper made from ethylene oxide derivatives. These products follow diverse end-of-life pathways, such as recycling, decomposition, or incineration, which are beyond the scope of this study (Cefic, 2023).

3.1.1 Steam Cracking as Reference Case

3.1.1.1 Baseline Scenario

Steam cracking is widely regarded as the state-of-the-art technology for ethylene production, the most energy-intensive primarily due to its significant steam and heat requirements and one of the most critical processes within the chemical industry, (Caprio, 2017; Gholami et al., 2021). While the technology has been in use since the 1960s and has undergone economic

and scale advancements, the fundamental principles of the process have remained unchanged (Gholami et al., 2021).
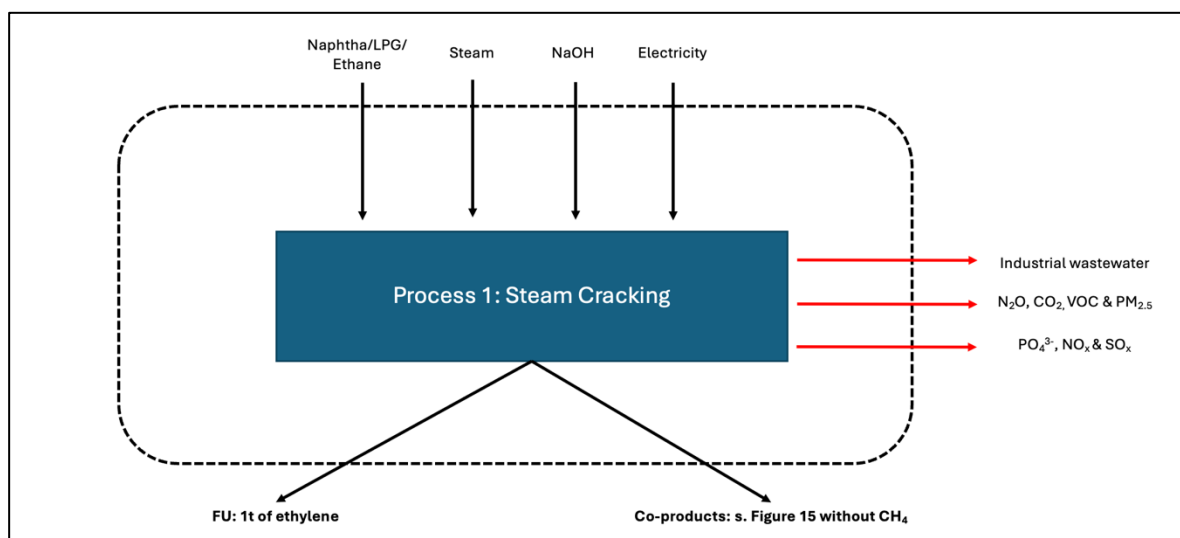
Figure 11: System Boundaries of Steam Cracking including all accounted in- and outflows as well as the respective emissions

The Steam Cracking's primary aim is to thermally decompose hydrocarbons, typically derived from naphtha – a mixture of alkanes, alkenes, aromatics, and sulfur compounds – as well as liquefied petroleum gas (LPG) – comprising propane and (iso-)butane – or ethane into a variety of products (s. Naphtha/LPG/Ethane as input in **Figure 11** and **Table 2**) (Plastics Europe, 2017). The choice of feedstock varies by region: European steam crackers predominantly use naphtha (s. **Figure 12**), whereas ethane has become more common in the U.S. due to the shale gas boom (Fattouh and Brown, 2014).

Based on Ren et al., 2006, the Steam Cracking process can be divided into three main sections: convection, pyrolysis/radiant, fractionation/separation section. In the convection section, naphtha is preheated to approximately 923 K through a series of heat exchangers, which is assumed to come solely from heat recovered from Transfer Line Exchanger (TLE) cooling down the cracked gas (s. **Figure 13**). Afterwards, the preheated naphtha is vaporized with superheated (dilution) steam in a certain ratio, which is crucial to mitigate the specific energy consumption of the production unit (s. **Figure 13** and steam as input in **Figure 11** and **Table 2**) (Gholami et al., 2021).

Figure 12: Bar chart of different steam cracking feedstock used in EU15 1 Norway + as of 2020 Hungary and Slovakia (Petrochemicals Europe, 2023, p.1)

Following preheating, the steam-naphtha mixture enters the radiant section at which the pyrolysis occurs (s. **Figure 13**) (Ren, et al., 2006). The mixture is passed through a long and narrow Ni-Cr-radiant coil in a firebox equipped with burners, which are entirely fueled by CH_4. Methane is retrieved as one of the steam cracker's products to externally heat the coil

in the radiant section to temperatures ranging from 1023 K to 1373 K (Ren, et al., 2006; Ye et al., 2022). The produced gases from burning fuels are vented through the convection zone into the air (s. volatile organic compounds (VOC), CO_2, particulate matter smaller than 2.5 micrometers ($PM_{2.5}$) and N_2O as emissions in **Figure 11** and **Table 2**) (Ren, et al., 2006). The combination of a short residence time (< 1 second) and low hydrocarbon pressure are key factors that enhance olefin yields as the naphtha-steam mixture undergoes cracking into various smaller products (Gholami et al., 2021).
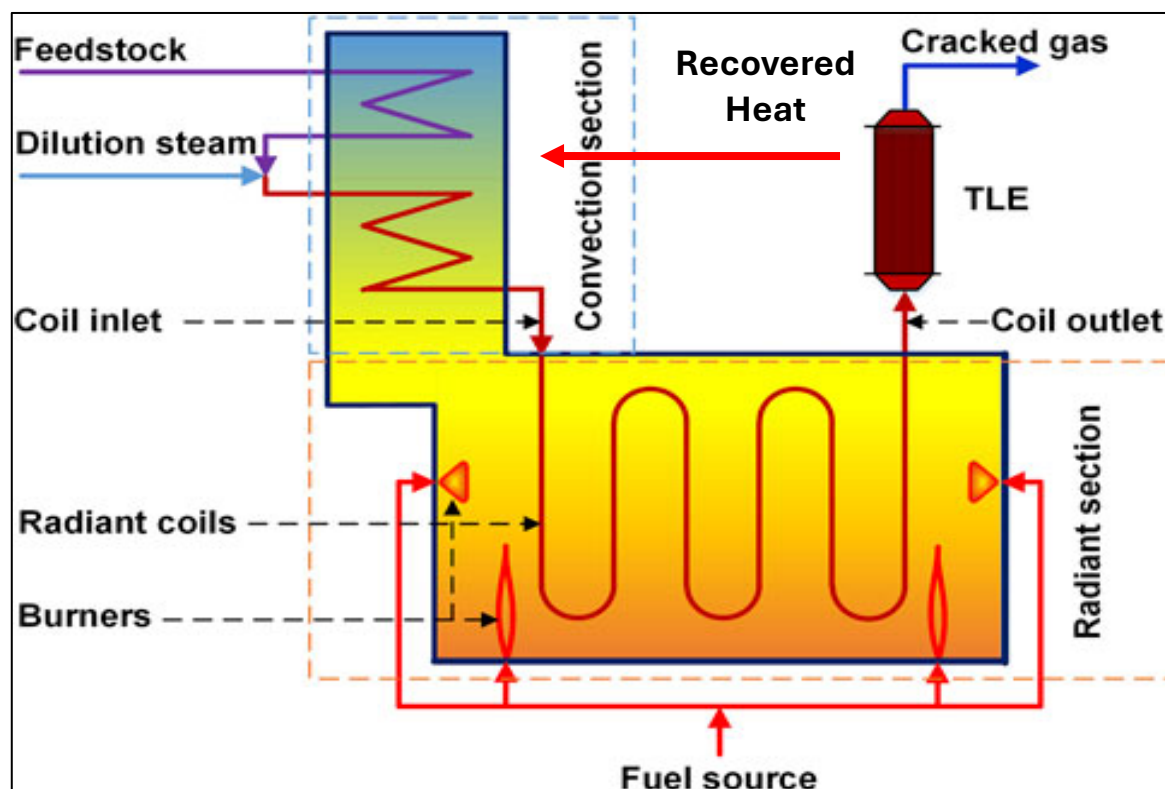
Figure 13: Schematic process structure of steam cracking including the convection and radiant section without the fractionation & separation section (based on Ren et al., 2021, p.3)

The cracking process follows the free radical mechanism (FRM), first proposed in the pioneer work of F. O. Rice during 1930s, which is inherently characterized by a vast number of radicals and other chemical species as well as reactions, which in turn tends to grow as the molar mass of the feed molecules increases (Moreira, 2015). To illustrate the different reactions, the steam cracking of ethane, the simplest case of the FRM, is displayed based on the work of Gholami et al., 2021.

During initiation (s. **Equation 4**), the unimolecular dissociation of ethane primarily occurs at the C-C bond forming two methyl radicals as the bond energy between the C-C bond is with 345 kJ/mol significantly weaker than the 413 kJ/mol of bond energy between the C-H bond. The possibility of the interaction between two dissociated radicals is very low (Gholami et al., 2021).

Equation 4: Initiation Reaction of the Steam Cracking Process

$$CH_3 - CH_3 \rightarrow CH_3^* + CH_3^*$$
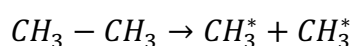
In the propagation phase, the resulting radicals undergo a series of propagation reactions which mainly follows three different general routes: these radicals can either decompose by breaking into a smaller radical and a compound, create a compound with the same number of carbon atoms by losing one H-atom or form a saturated molecule by taking one H-atom out of the surrounding hydrocarbon molecules. In the ethane case, the methyl radical abstracts a hydrogen atom from another ethane molecule forming methane while producing an ethyl radical (s. **Equation 5**) (section based on Gholami et al., 2021).

Equation 5: *Propagation Reaction – Case 1*

$$CH_3^* + C_2H_6 \rightarrow C_2H_5^* + CH_4$$
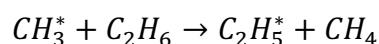
Equation 6: *Propagation Reaction – Case 2*

$$C_2H_5^* \rightarrow C_2H_4 + H^*$$
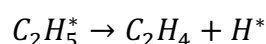
Equation 7: *Propagation Reaction – Case 3*

$$H^* + C_2H_6 \rightarrow H_2 + C_2H_5^*$$
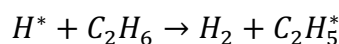
Etc.

The ethyl radical in turn can decompose itself to ethylene and to a hydrogen radical (s. **Equation 6**), which can further react with an ethane molecule again forming H_2 and another ethyl radical (s. **Equation 7**). These propagation steps can theoretically continue infinitely. However, two radicals will eventually come together forming either a saturated (s. **Equations 8, 9** as an example) or unsaturated molecules (s. **Equation 10** as an example), which marks the termination of the FRM (section based on Gholami et al., 2021).

Equation 8: *Termination Reaction – Example 1*

$$H^* + H^* \rightarrow H_2$$
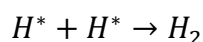
Equation 9: *Termination Reaction – Example 2*

$$C_2H_5^* + C_2H_5^* \rightarrow C_4H_{10}$$
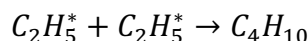
Equation 10: *Termination Reaction – Example 3*

$$C_2H_5^* + CH_3^* \rightarrow C_2H_4 + CH_4$$
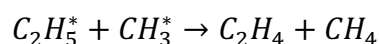
Etc.

The cracking of heavier feedstocks like naphtha is more complex than that of lighter alkanes, involving in addition to the FRM multiple parallel reactions including molecular reactions (s. **Figure 14**) and (unwanted) secondary reactions (as an example, s. **Equations 11, 12**) as they, among others, decompose olefins again (Gholami et al., 2021).

Equation 11: Secondary Reaction – Example 1

$$C_2H_4 + H^* \rightarrow C_2H_5^*$$
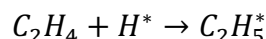
Equation 12: Secondary Reaction – Example 2

$$C_3H_6 + H^* \rightarrow C_3H_5^* + H_2$$
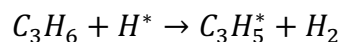
According to **Figure 14**, the primary cracking breaks heavier hydrocarbons into smaller compounds, which create the primary cracking network (s. reaction I), which are further broken down (secondary cracking) into lighter products. These cracked products are rich in olefins with yield and composition depend on the operating conditions (s. reaction II-IV). From this stage onwards, molecular reactions are involved: the most important ones are dehydrogenation and cycloaddition (in particular the Diels-Alder reaction: s**. Equation 13**) whereas other molecular reactions such as isomerization only play a minor role. The dehydrogenation (s. **Equation 14**) can produce extremely unsaturated hydrocarbons such as acetylene and propyne (s. reaction IV), which are undesired impurities in C_2 and C_3 cuts due to their noticeable reactivity and thus, are removed through catalytic hydrogenation and extractive distillation. Heavier hydrocarbons can be formed via Diels-Adler reaction (s. reaction V), which is prone to excessive dehydrogenation (s. reaction VI). These are the natural precursors of condensed polyaromatic materials known as coke in their solid state (s. reaction VII). Decoking is required regularly, which implies a furnace shutdown to burn off coke from the walls with high pressure steam (whole paragraph is drawn upon Gholami et al., 2021).
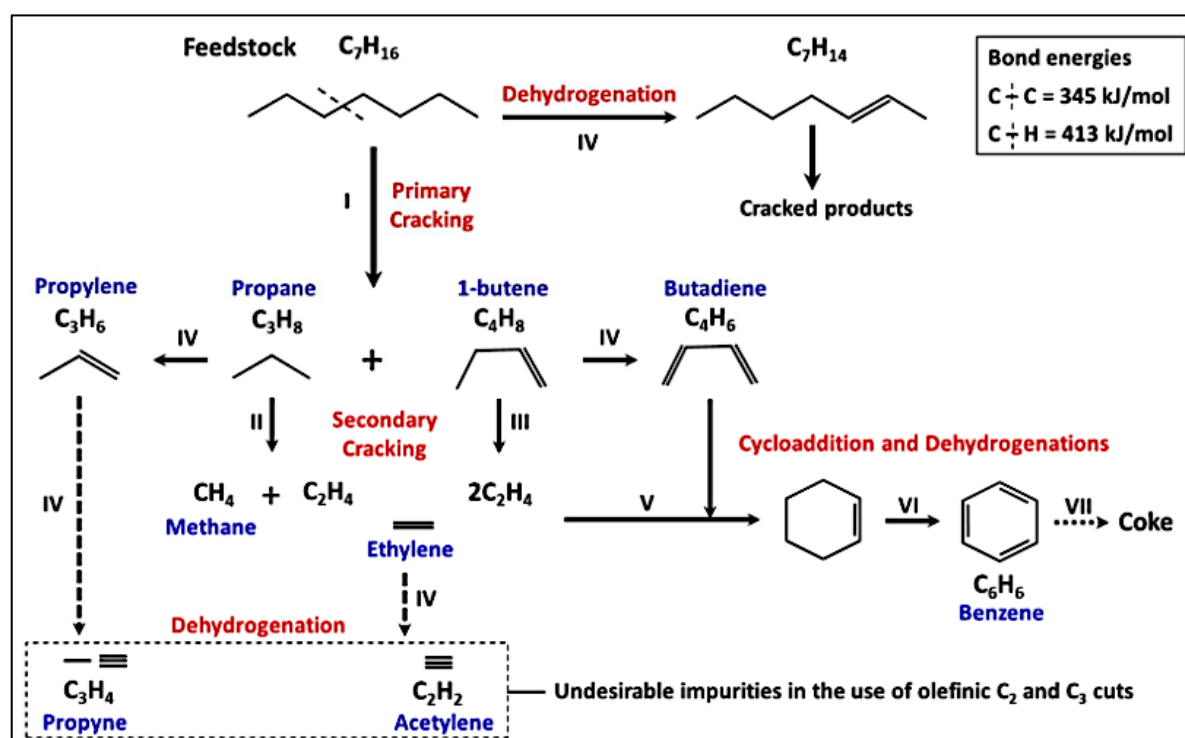
Figure 14: Main reactions involved in the cracking process of higher alkanes (Gholami et al., 2021, p. 8)

Equation 13: Diels-Alder Reaction

$$C_4H_6 + C_2H_4 \rightarrow C_6H_{10}$$
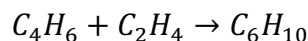
Equation 14: Dehydrogenation Reaction of Cyclohexene

$$C_6H_{10} \rightarrow C_6H_6 + 2H_2$$
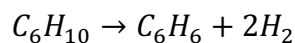
Based on Gholami et al., 2021 and Ren et al., 2006, the cracked gas enters the fractionation and separation section following the pyrolysis stage and is immediately quenched in a TLE from 823 K-923 K to 573 K to prevent secondary reactions from occurring whose recovered heat is re-integrated to the convection zone (s. **Figure 13**). The cooled cracked gas undergoes several caustic scrubbing processes with natrium hydroxide to remove acid gases before it is subjected to distillation (s. NaOH as input and the NO_x, PO_4^{3-}, SO_2 and industrial wastewater as emissions in **Figure 11** and **Table 2**). Afterwards, refrigeration and extraction steps separate petrochemical products from each other (i.e. de-propanizer to separate propylene/propane and C_3-splitter to split propylene from propane). In order to keep these processes in operation, electricity is needed, as well (s. electricity as input in **Figure 11** and **Table 2**). As it has already been mentioned in Chapter 2.2.5, this multifunctionality problem of having several co-products is solved by applying economic allocation (s. **Appx. Tables 1-7** in Appendix 6.1.1).

*Table 2: LCI of Steam Cracking as baseline scenario incl. all in- and outputs as well as emissions according to system boundaries defined in **Figure 11**, which have not been adjusted to the respective AF, yet. Co-products are listed in the Appendix (s. **Appx. Table 1** in Appendix 6.1.1).*

	Unit/kg ethylene	Value	Source
Allocation Factor:	[ ]	0.35130	s. Appendix 6.1.1
Product:			
Ethylene	kilogram	1.00000	Pre-defined FU
Inputs:			
Feedstock	kilogram	3.33000	Young et al., 2022
Steam	kilogram	1.40000	Yang & You, 2017; Rodriguez-Vellejo et al., 2020
Electricity	kilowatt hour	0.09000	Ye et al., 2022
NaOH	kilogram	0.00070	Yang & You, 2017
Natural Gas (fuel)	cubic meter	---	Ye et al., 2022
Emissions:			
CO_2	kilogram	1.82000	Rodriguez-Vellejo et al., 2020; Ye et al., 2022; Yang & You, 2017
$PM_{2.5}$	kilogram	0.00100	Ye et al., 2022
VOC	kilogram	0.00400	Ye et al., 2022
N_2O	kilogram	0.00003	Ye et al., 2022
H_2O	cubic meter	0.00022	Ye et al., 2022
PO_4^{3-}	kilogram	0.00010	Ye et al., 2022
SO_2	kilogram	0.00800	Ye et al., 2022
NO_x	kilogram	0.00400	Ye et al., 2022

All values for the respective parameters of the Steam Cracking process were collected from different literature resources and represented in **Table 2**. Ye et al., 2022 presented the most comprehensive LCI of Steam Cracking especially when it comes to emissions compared to other sources such as Rodriguez-Vellejo et al., 2020 or Yang & You, 2017. Though, the CO_2 emissions are weighted between these three sources, as Ye et al., 2022 reported a value of 2.32 kg CO_2/kg ethylene, which is inconsistent with the mass balance. On the other hand, Yang & You, 2017 and Rodriguez-Vellejo et al., 2020 reported the same value of 1.31 kg CO_2/kg ethylene. That is why the value for CO_2 emission in this Master Thesis for the Steam Cracking route is weighted to 1.82 kg CO_2/kg ethylene. Since Young et al., 2022 provides a holistic overview of different product yields dependent on different feedstocks (s. **Figure 15**), these yields are used to calculate the different mass inputs for the different feedstocks. The plant-installation is assumed to be insignificant in the GWP results, why it is not listed in **Table 2**.

3.1.1.2   Process Modifications

Different Feedstocks

While the Steam Cracking process operates independently of the specific feedstock used in principle, variations in feedstock properties and plant design can significantly affect the fractionation and separation stages (Caprio, 2017; Ren et al., 2006). Indeed, although many steam crackers are designed to process a variety of feedstocks, the cracking reaction must be carefully optimized based on the composition

Feedstock (i):	Ethane	Propane	Butane	Naphtha	Gas Oil
Product:					
Hydrogen (H_2)	6.2%	1.9%	1.4%	1.1%	0.9%
Methane (CH_4)	5.8%	26%	22%	14%	11%
Ethyne (C_2H_2)	0.68%	0.53%	0.43%	0.36%	0.40%
Ethylene (C_2H_4) ($Y_{i,ethy}$)	80%	44%	41%	30%	28%
Propyne (C_3H_4)	0.03%	0.58%	0.93%	0.60%	0.63%
Propylene (C_3H_6)	1.9%	17%	19%	17%	14%
Butatriene (C4H4)	0.08%	0.09%	0.10%	0.09%	0.12%
Butadiene (C4H6)	2.8%	3.3%	4.4%	4.8%	5.8%
Butene (C4H8)	0.30%	1.1%	3.1%	5.8%	3.6%
Benzene (C6H6)	0.86%	2.4%	3.0%	6.4%	5.5%
Toluene (C7H8)	0.13%	0.48%	0.89%	3.1%	3.5%
Styrene (C8H8)	0.05%	0.23%	0.27%	1.1%	1.2%
Xylene (C8H10)	0.00%	0.06%	0.13%	1.2%	0.92%
Ethylbenzene (C8H10)	0.02%	0.01%	0.01%	0.79%	0.37%
Pyrolysis gasoline	0.54%	1.4%	2.0%	11%	7.3%
Fuel Oil	0.33%	1.1%	1.1%	2.7%	16%
Total Mass Balance	99.7%	99.6%	99.6%	99.9%	99.9%

Figure 15: Product composition and distribution with the corresponding yields in terms per kg of feedstock (Young et al., 2022, p. 5)

of the feedstock and the target products (Caprio, 2017). In addition to ethylene, common by-products include propylene, butadiene, and hydrogen, with smaller amounts of acetylene, BTX-compounds and butene also being produced (s. **Figure 15**) (Plastics Europe, 2017).

The product composition in Steam Cracking remains relatively stable but its distribution varies depending on several factors such as feedstock type, residence time, operating temperature, and the steam-to-hydrocarbon ratio (Gholami et al., 2021; Ren et al., 2006). For instance, higher temperatures and shorter residence times generally increase ethylene yields, although higher temperatures also accelerate coke formation, reducing the lifespan of cracking tubes. Conversely, longer residence times can lead to unwanted secondary reactions as olefins decompose, while shorter residence times enhance the yields of ethylene and propylene (Gholami et al., 2021). Product yields also vary with different feedstocks according to **Figure 15** (Young et al., 2022).

*Table 3: LCI of Steam Cracking with different feedstocks as process modification incl. all in- and outputs as well as emissions according to system boundaries defined in Chapter 3.1.1.2 – Different Feedstocks, which have not been adjusted to the respective AFs, yet. Co-products are listed in the Appendix (s. **Appx. Tables 2, 3** in Appendix 6.1.1)*

	Unit/kg ethylene	Value	Source
Allocation Factor:			
Ethane	[ ]	0.5827	s. Appendix 6.1.1
LPG	[ ]	0.6552	s. Appendix 6.1.1
Product:			
Ethylene	kilogram	1.00000	Pre-defined FU
Inputs:			
Either Ethane as feedstock	kilogram	1.25000	Young et al., 2022
or LPG as feedstock	kilogram	2.35000	Young et al., 2022
Steam	kilogram	1.40000	Yang & You, 2017; Rodriguez-Vellejo et al., 2020
Electricity	kilowatt hour	0.09000	Ye et al., 2022
NaOH	kilogram	0.00070	Yang & You, 2017
Natural Gas (fuel) needed only for the ethane case	cubic meter	0.59000	Ye et al., 2022 Calculation based on Ye et al., 2022
Emissions:			
Fossil CO_2	kilogram	1.82000	Rodriguez-Vellejo et al., 2020; Ye et al., 2022; Yang & You, 2017
$PM_{2.5}$	kilogram	0.00100	Ye et al., 2022
VOC	kilogram	0.00400	Ye et al., 2022
N_2O	kilogram	0.00003	Ye et al., 2022
H_2O	cubic meter	0.00022	Ye et al., 2022
PO_4^{3-}	kilogram	0.00010	Ye et al., 2022
SO_2	kilogram	0.00800	Ye et al., 2022
NO_x	kilogram	0.00400	Ye et al., 2022

Despite these variations, the LCI values of the Steam Cracking baseline process remain unchanged except the steam cracking feedstock as it is assumed that the core process does not vary significantly across feedstocks built on **Table 3** (Caprio, 2017). However, economic allocation, as described in Chapter 2.2.5, accounts for the differing product mixes that result from different feedstock types, whose calculation can be found in the Appendix (s. **Appx. Tables 2,3** in Appendix 6.1.1). For the LPG and ethane cases an AF of 0.6552 and 0.5827 were calculated with feedstock inputs of 2.35 and 1.25 kg/kg ethylene according to Young et al., 2022. Additionally, it is important to mention that in the ethane case additional fuel in the form of natural gas is needed. According to Ye et al., 2022 all methane produced from Stream Cracking can be completely utilized to fully operate the radiant section. On this basis, a methane value was calculated according to Young et al., 2022, which is higher than the amount

if ethane is utilized as feedstock. The difference of methane reported for the naphtha case and the amount of methane in the ethane case must come from natural gas as fuel. The opposite case can be seen in the Steam cracking with LPG as feedstock. More methane is produced than needed for to operate the radiant section, which is why excess methane is accounted in the economic allocation (s. **Appx. Tables 2,3** in Appendix 6.1.1).

E-Furnace
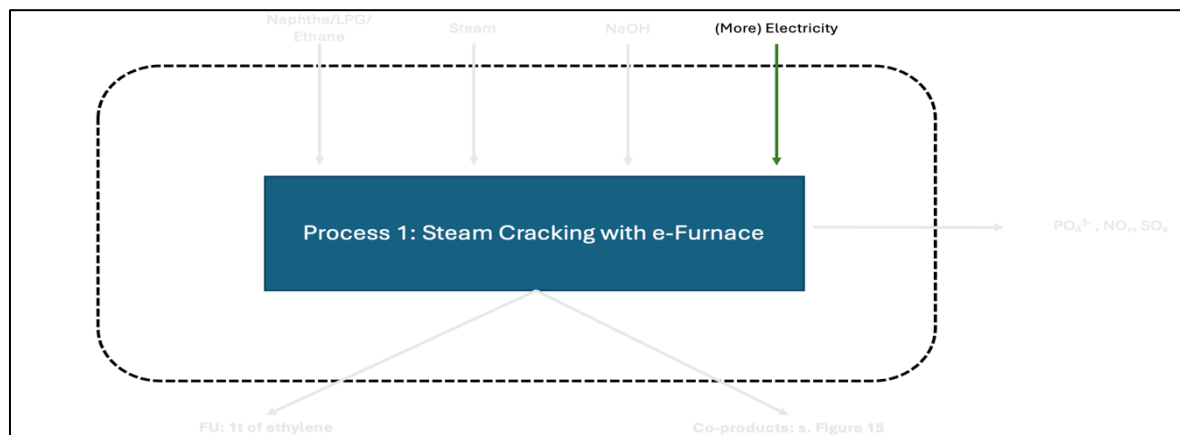
Figure 16: System Boundaries of Steam Cracking with an e-Furnace including all in- and out flows as well as emissions, highlighting the changes made compared to the baseline scenario

Based on Gu et al., 2022, the primary emissions directly associated with the Steam Cracking process (Scope 1 emissions) originate from the combustion of fuel used to heat the firebox to the necessary cracking temperatures. Hence, it is worth considering the substitution of fossil fuels with electricity as heat source (s. **Figure 17**).
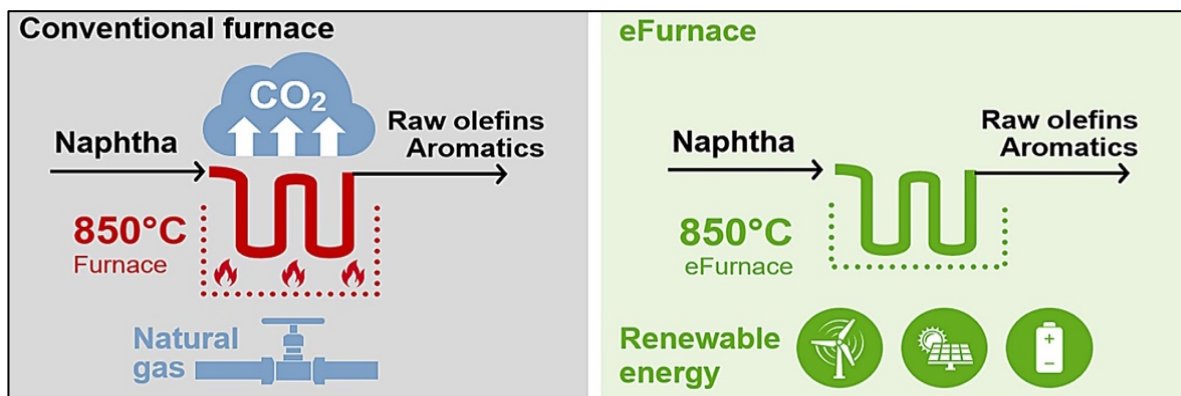
Figure 17: Conceptual representation of the conventional and e-Furnace highlighting the main difference (Nonnast, 2021, p. 1)

This transition assumes that the thermal energy requirement is equivalent to the electrical energy needed (s. additional electricity as input needed in **Figure 16** and **Table 4**). That is the reason why the electricity value had to be increased from 0.09 kWh to over 6.89 kWh: This amount is derived from 0.09 kWh needed for operating the process and 6.7988 kWh to replace the heat from CH_4 combustion with a lower heating value (LHV): LHV (CH_4) = 52.5 MJ/kg. The LHV is used to calculate the total heat input required for the radiant box in the form of electricity (24.48 MJ/kg naphtha) with an assumed 1:1 conversion into kWh and no energy losses assumed (World Nuclear Association, 2020; Ye et al., 2022). Furthermore, the AF has changed from 0.3513 to 0.3168 as the produced methane is not needed anymore for operating the radiant section and thus, accounted in the economic allocation calculation (s. **Appx. Table 5** in Appendix 6.1.1). Electrically heated steam cracker furnaces not only reduce

emissions (s. no N_2O, CO_2, $PM_{2.5}$, VOC emissions due to use of electricity instead of burning fossil fuels in radiant section in **Table 4** and **Figure 16**), but also offer several additional advantages, such as higher thermal conductivity, improved efficiency, and reduced furnace size, which translate into lower capital costs and enhanced safety (this section draws upon Gu et al., 2022).

*Table 4: LCI of Steam Cracking with e-furnace as process modification incl. all in- and outputs as well as emissions according to system boundaries defined in **Figure 16**, which have not been adjusted to the respective AF, yet. Co-products are listed in the Appendix (s. **Appx. Table 5** in Appendix 6.1.1).*

	Unit/kg ethylene	Value	Source
Allocation Factor:	[ ]	0.3168	s. Appendix 6.1.1
Product:			
Ethylene	kilogram	1.00000	Pre-defined FU
Inputs:			
Feedstock	kilogram	3.33000	Young et al., 2022
Steam	kilogram	1.40000	Yang & You, 2017; Rodriguez-Vellejo et al., 2020
Electricity	kilowatt hour	6.88875	Own calculation based on Ye et al., 2022
NaOH	kilogram	0.00070	Yang & You, 2017
Natural Gas (fuel)	cubic meter	---	Ye et al., 2022
Emissions:			
Fossil CO_2	kilogram	---	Rodriguez-Vellejo et al., 2020; Ye et al., 2022; Yang & You, 2017
$PM_{2.5}$	kilogram	---	Ye et al., 2022
VOC	kilogram	---	Ye et al., 2022
N_2O	kilogram	---	Ye et al., 2022
H_2O	cubic meter	0.00022	Ye et al., 2022
PO_4^{3-}	kilogram	0.00010	Ye et al., 2022
SO_2	kilogram	0.00800	Ye et al., 2022
NO_x	kilogram	0.00400	Ye et al., 2022

This concept has already been implemented in practice, as demonstrated by the chemical company *BASF* in collaboration with *Linde* and *SABIC* which inaugurated the first electrically powered demonstration furnace at one of its sites in 2024 (Nonnast 2021, 2024).

Low Emissions Furnace

Based on Mynko et al., 2023 and Oud, 2020, another promising emerging technology is the low-emission furnace, which focuses on enhancing thermal efficiency within the firebox by over 30% compared to the conventional design. It improves the ratio of heat absorbed by the reactor coils from the heat generated by fuel combustion. This approach aims to maintain the required heat for the cracking process while using less fuel, thereby reducing emissions. However, increasing the share of radiant heat can diminish the heat available for the

convection section reintegrated by the TLE, potentially limiting the preheating of the feed and dilution steam mixture.

This challenge is addressed by a novel heat recovery scheme, patented by the company *Technip Energies*: it involves an additional TLE downstream connected to the first TLE as well as minor adjustments to the convection section enabling greater heat recovery and eliminating the need for additional boilers. As a result, fuel consumption decreases by assumed 30%, also leading to 30% lower emissions of N_2O, CO_2, VOC and $PM_{2.5}$ compared to the baseline case as it can be seen in the LCI values in **Table 5**. Apart from reducing energy inflow and emission outflow of the mentioned chemical compounds, the other in- and output parameters remain consistent as described in **Figure 11**. Important to note, is that the AF has changed as well from 0.3513 to 0.3402 as less methane produced is needed to cover the energy demand for the radiant section, which is why excess methane is accounted for in the economic allocation (s. **Appx. Table 4** in Appendix 6.1.1).

*Table 5: LCI of Steam Cracking with low-emission-furnace as process modification incl. all in- and outputs as well as emissions according to Chapter 3.1.1.2 – Low emission Furnace, which have not been adjusted to the respective AF, yet. Co-products are listed in the Appendix (s. **Appx. Table 4** in Appendix 6.1.1).*

	Unit/kg ethylene	*Value*	*Source*
Allocation Factor:	[ ]	0.3402	s. Appendix 6.1.1
Product:			
Ethylene	kilogram	1.00000	Pre-defined FU
Inputs:			
Feedstock	kilogram	3.33000	Young et al., 2022
Steam	kilogram	1.40000	Yang & You, 2017; Rodriguez-Vellejo et al., 2020
Electricity	kilowatt hour	0.09000	Ye et al., 2022
NaOH	kilogram	0.00070	Yang & You, 2017
Natural Gas (fuel)	cubic meter	---	Ye et al., 2022
Emissions:			
Fossil CO_2	kilogram	1.27400	Rodriguez-Vellejo et al., 2020; Ye et al., 2022; Yang & You, 2017
$PM_{2.5}$	kilogram	0.00070	Ye et al., 2022
VOC	kilogram	0.00280	Ye et al., 2022
N_2O	kilogram	0.00002	Ye et al., 2022
H_2O	cubic meter	0.00022	Ye et al., 2022
PO_4^{3-}	kilogram	0.00010	Ye et al., 2022
SO_2	kilogram	0.00800	Ye et al., 2022
NO_x	kilogram	0.00400	Ye et al., 2022

Steam Cracking Plant with CCS

As discussed in the literature review, CCS as PSC can significantly improve the environmental performance (s. Chapter 2.1). In this scenario, CO_2 emissions from the Steam Cracking process are captured and stored, contributing to a reduction in the plant's carbon footprint (s. **Figure 18**). The LCI of the Steam Cracking reported in **Table 1** remains the same. However,

CO_2 emission from Steam Cracking (1.82 CO_2 as emission in **Table 2**) are captured by 90% (1.638 CO_2 as emission in **Table 6**) by the CCS plant and 10% (0.182 CO_2 as emission in **Table 6**) are re-emitted again due to technical constraints. Because no CO_2 emissions occur at the Steam Cracking process stage anymore, the amount of the CO_2 emission in the Steam Cracking process turns to zero.

The input CO_2 compression, transport and storage accounts for compression to 11 MPa, a 50 km pipeline transportation to the storage site with another 15 MPa compression at the storage site, before the CO_2 is injected into a geological reservoir through wells with a depth of 3 km (Koornneef et al., 2008). The carbon capture process itself will be described in more detail in Chapter 3.1.2.1.1.1.

Table 6: LCI of Steam Cracking with CCS as process modification incl. all in- and outputs as well as emissions according to system boundaries defined in Figure 18, which have been adjusted to capturing CO_2 from the production of 1 t of ethylene.

	Unit/kg captured & stored CO_2	Value	Sources
Product:			
Captured & stored CO_2	kilogram	1.6380	Adjusted to FU = 1 t ethylene
Inputs:			
Electricity	kilowatt hour	0.5348	Meunier et al., 2020 & Rosental et al., 2020
MEA	kilogram	0.0020	Rosental et al., 2020
CO_2 compression, transportation and storage	kilogram	1.6380	Own calculation based on Rosental et al., 2020
Emissions:			
Fossil CO_2	kilogram	0.1820	Own calculation based on Rosental et al., 2020
Ethylene diamine	kilogram	0.0033	Own Calculation on Zhou et al., 2012
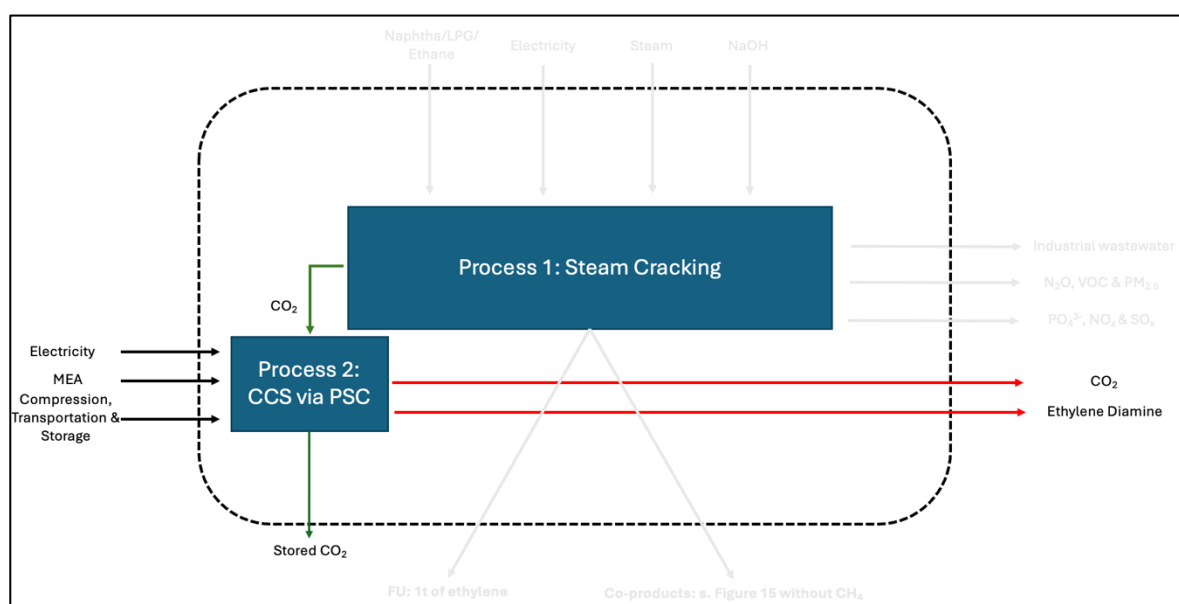
Figure 18: System Boundaries of Steam Cracking including CCS, highlighting the changes made compared to the Baseline Scenario

3.1.2 The novel route – Methanol-to-Olefins

The MTO-route is a novel approach to produce ethylene not from fossil fuels via Steam Cracking, but from MeOH. The interesting part concerning this Master Thesis is the production of MeOH, which can be conducted without any use of fossil resources by either direct hydrogenation of CO_2 with (green) H_2 (H_2+CCU-to-Olefins Route) or with post-treated (sweet) syngas from biomass gasification (Biomass-to-Olefins Route). Therefore, it is assumed that the general process set-up only differs in the production of the precursor needed to form MeOH and ultimately ethylene although some inputs and emissions may differ from process to process (s. **Figure 19**).
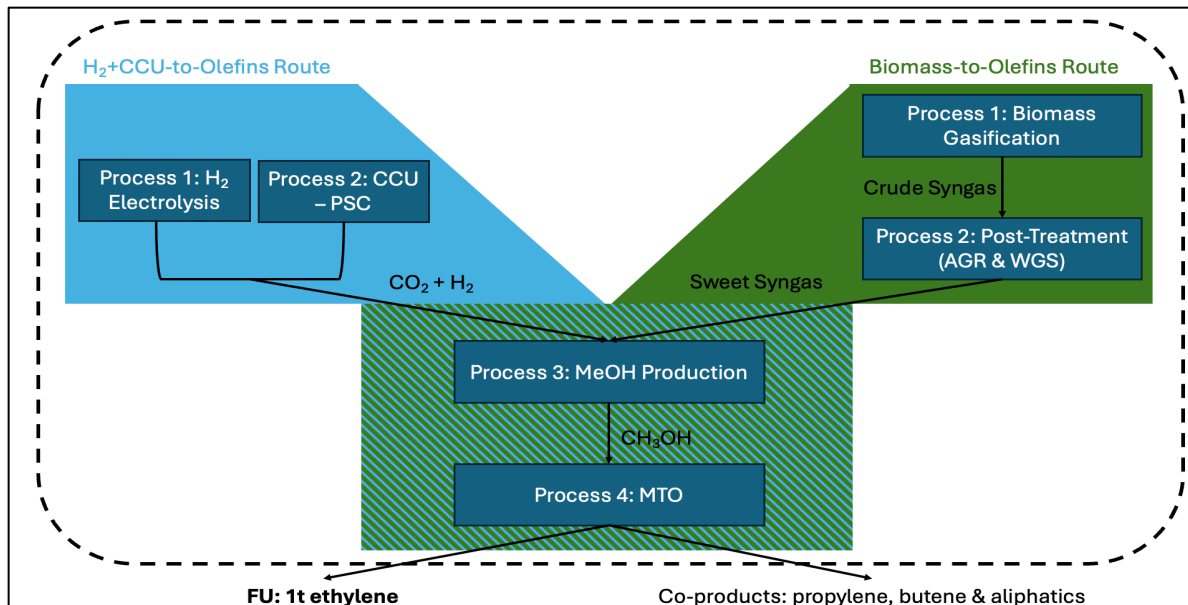
Figure 19: *System Boundaries and overview of the MTO-Route with two different approaches including the all processes and intermediate as well as end-product*

3.1.2.1 Baseline Scenario

3.1.2.1.1 Methanol Production
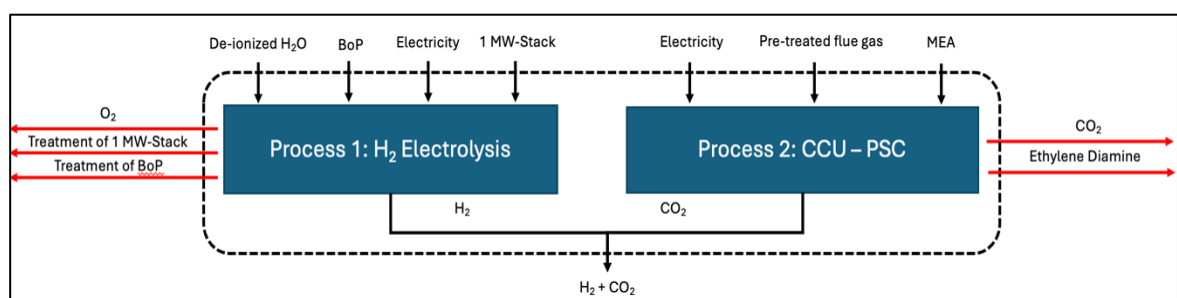
Figure 20: *System Boundaries including all in- and outflows as well as emission of the H_2 electrolysis and CCU process*

3.1.2.1.1.1 Direct Hydrogenation of CO₂ Route with electrolytic H₂

PEM-Electrolysis Plant

Based on Schropp et al., 2020, the PEMEC system is composed of two primary components: the stack and the balance of plant (BoP; s. 1 MW Stack and BoP as inputs for the H_2 electrolysis process in **Figure 20** and **Table 7**). The stack consists of a PEM electrolyzer itself, which is composed of several individual electrolyzer cells connected in series to enhance hydrogen production (s. **Figure 22**: number of cells n = 50), each equipped with a 60-200 micrometer thick Nafion® membrane made of tetrafluoroethylene, which separates the two half-cells (s.

Figure 21). Electrodes of ten micrometer thickness are placed directly on either side of this membrane (Bareiß et al., 2019). The anode where the oxygen evolution reaction (OER) occurs (s. **Equation 15**) is coated with an iridium oxide (IrO_2) electrocatalyst, while the cathode where the hydrogen evolution reaction (HER) takes place (s. **Equation 16**) is coated with a platinum catalyst (Schropp et al., 2020). The system operates at low pH and high electrical potentials (s. electricity input for the H_2 electrolysis in **Figure 20** and **Table 7**) (Como et al., 2014).
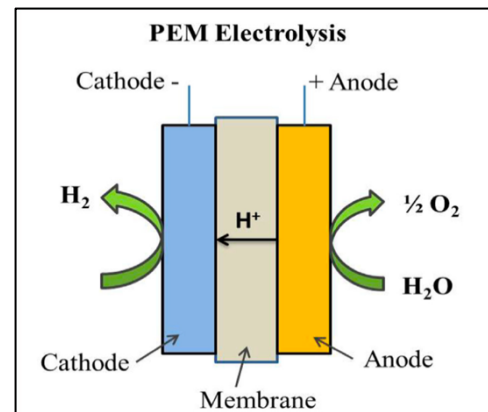
Figure 21: Schematic representation of the functioning of a PEM electrolysis cell (Shiva and Himabindu, 2019, p. 5)

Equation 15: Oxygen Evolution Reaction as Oxidation at the PEM anode

$$2H_2O \rightarrow 4H^+ + 4e^- + O_2$$
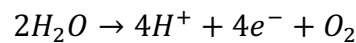
Equation 16: Hydrogen Evolution Reaction as Reduction at PEM cathode

$$4H^+ + 4e^- \rightarrow 2H_2$$
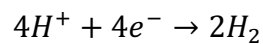
The PEM and electrodes are further supported by titanium-based gas diffusion layers, which serve as current collectors, and finally, these components are sandwiched by Ti-based bipolar plates, which usually feature channel-like structures for water and gas transport (s. **Figure 22**) (Schropp et al., 2020).
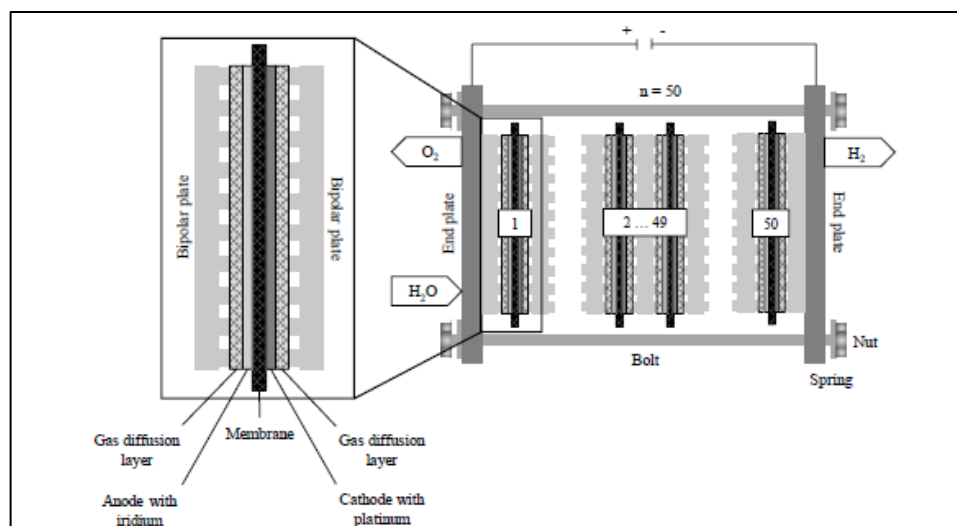
Figure 22: Representation of a PEM cell and stack structure (Schropp et al., 2020, p. 3)

According to Schropp, et al., 2020, the BoP includes systems for gas and water separation, as well as water and hydrogen purification (s. **Figure 23**). The gas/water separator isolates excess water from produced gases (either O_2 on the left side or H_2 on the right side) because not all water is consumed during electrolysis; some of it circulates through the system to cool the electrolyzer, which generates heat during operation, and is recycled back via the circulation pump and heat and ion exchanger. The produced O_2 passes on the left side of the electrolyzer through a condensation trap before exiting the system (s. O_2 emission of the H_2 electrolysis process in **Figure 20** and **Table 7**). The water purification unit step is crucial because

the electrolyzer requires ultra-pure or deionized water to function properly (s. de-ionized H_2O as input for the H_2 electrolysis process in **Figure 20** and **Table 7**). The synthesized H_2 on the right side of the stack requires several complex purification steps.
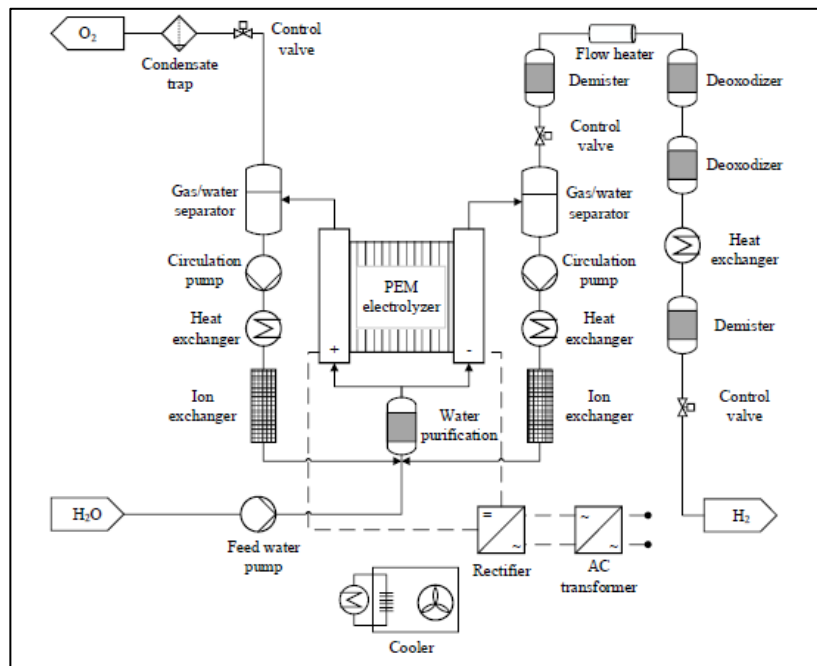
Figure 23: Representation of BoP of an electrolysis plant including its operation (Schropp et al., 2020., p. 4)

Table 7: LCI of H_2-production via PEMEC incl. all in- and outputs as well as emissions according to system boundaries defined in **Figure 20**

	Unit/kg H_2	Value	Sources
Product:			
H_2	kilogram	1.0000	Pre-defined
Inputs:			
PEM Stack (1 MW)	unit	1.04E-06	Wei et al., 2024
PEM BoP Production	unit	3.45E-07	Wei et al., 2024
De-ionized H_2O	kilogram	12.0000	Wei et al., 2024
Electricity	kilowatt hour	57.4700	Wei et al., 2024
Emissions:			
O_2	kilogram	8.0000	Wei et al., 2024
Wastes:			
Waste Treatment of PEM BoP	unit	-1.04E-06	Wei et al., 2024
Waste Treatment of PEM Stack	unit	-3.45E-07	Wei et al., 2024

Initially, a demister removes fine water droplets, after which excess oxygen is catalytically oxidized to water in two deoxidizers, which is then condensed and removed using heat exchangers and an additional demister. The whole system usually operates at 323-353 K (low temperature electrolysis) and a pressure of 40 bar producing the final product H_2 with a purity of 99.9% at a pressure of 35 bar and a temperature range of 333-353 K. (Schropp, et al.,

2020). The LCI values reported in Wei et al., 2024 were selected because they do not only provide a more comprehensive inventory than Meunier et al., 2020 and Rosental et al., 2020 including additional future inventories, but also cover SOEC, which makes it better at comparing these two technologies based on the same scientific paper (s. **Table 7**).

Carbon Capture Utilization-Plant

Based on Bisinella et al., 2021, the pretreated flue gas, assumed to be originating from a cement plant in Switzerland/China, is cooled and introduced into an absorber reactor containing a mass concentration of 30

Figure 25: LEWIS-structure of the chemical carbon capture compound MEA

wt% monoethanolamine (MEA; s. **Figure 24**) solution, maintained at a temperature of 298-323 K and 1 bar pressure (a. flue gas and CO_2 absorber in **Figure 25** as well as pre-treated flue gas as input for the CCU – PSC process in **Figure 20** and **Table**). MEA is the industrial benchmark due to its relatively low cost and high capture efficiency, capable of capturing up to 90% of CO_2 emissions whereas 10% of the captured CO_2 is emitted again (s. MEA as input and CO_2 as emission of the CCU – PSC process in **Figure 20** and **Table 8**).

Figure 24: Schematic representation of the functioning of a carbon capture plant (Øi et al., 2014, p. 2)

Based on Lv et al., 2015, the CO_2 in the flue gas is captured by the solution in the CO_2 Absorber column, forming a carbamate anion (chemical formula: RNHCOO$^-$; s. **Equation 18**). The widely accepted reaction mechanism is proposed for primary alkanolamines (formula: RNH_2 such as MEA): at first, MEA reacts with CO_2 to form a zwitterion (formula: $RNH_2^+COO^-$; s. **Equation 17**) as intermediate, which is instantaneously neutralized by a base (in this case either H_2O or RNH_2) producing a carbamate molecule (s. **Equation 18**). Subsequently, the CO_2-rich amine solution is pumped through a heat exchanger to the stripper column (s. **Figure 25**).

Equation 17: Zwitterion Formation with (Alcohol-)Amines and captured CO_2

$$RNH_2 + CO_2 \rightleftharpoons RNH_2^+COO^-$$
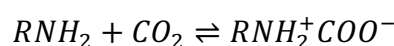
Equation 18: Carbamate Formation

$$RNH_2^+CCO^- + RNH_2 \rightleftharpoons RNHCOO^- + RNH_3^+$$
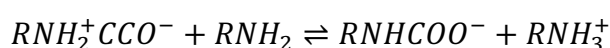
Based on Bisinella et al., 2021 and **Figure 25**, in the stripper column, the CO_2-rich amine solution is further heated to 373-413 K by the reboiler, which is assumed to be operated by an electrical heat pump (s. electricity as input for the CCU – PSC process in **Figure 20** and **Table 8**). The stripping process operates on a counter-current principle at 1-2 bar, where stripping gas separates the CO_2 from the liquid, leaving the gas saturated with water vapor at the top of the Stripper column, while the MEA solution is nearly fully recovered through the condenser. Lost MEA happens only due to degradation through formation of heat-stable salts and losses due to vapor and aerosols during stripping. The regenerated MEA solution at the bottom of the stripper column is recycled and pumped back through the heat exchanger and amin cooler to the CO_2 absorber (as lean amine).

*Table 8: LCI of CCU process as PSC-technology with MEA incl. all in- and outputs as well as emissions according to system boundaries defined in **Figure 20***

	Unit/kg captured CO_2	Value	Sources
Product:			
Captured CO_2	kilogram	1.0000	Pre-defined
Inputs:			
Electricity	kilowatt hour	0.5348	Meunier et al., 2020 & Rosental et al., 2020
MEA	kilogram	0.0020	Rosental et al., 2020
CO_2 from point sources	kilogram	1.1111	Own calculation based on Rosental et al., 2020
Emissions:			
Fossil CO_2	kilogram	0.1111	Own calculation based on Rosental et al., 2020
Ethylene diamine	kilogram	0.0020	Own Calculation based on Zhou et al., 2012

Most of the LCI values listed in **Table 8** were taken out from Rosental et al., 2020. Ethylene diamine is used as proxy data for MEA waste to complete the mass balance of this process, which is an intermediate product of MEA degradation and can be found as parameter in *ecoinvent* (Zhou et al., 2012). The values of CO_2 from point sources as well as the CO_2 as emission were calculated based on Rosental et al., 2020 with 90% of the incoming flue gas captured and utilized, while 10% of the flue gas is released again. The electricity amount is composed of two electricity values: 0.015 kWh/kg CO_2 captured is needed to operate the whole process set-up (Rosental et al., 2020), while the 0.5198 kWh are required for the heat pump (coefficient of performance (COP) = 2.9) to increase the temperature to the around 373 K. The 0.5198 kWh are based on the heat requirement for the heat reported by Meunier et al., 2020 with 3.68 MJ/kg CO_2 and converted into kWh including the conversion rate of 0.5085 retrieved from the *ecoinvent* data base by comparing these two different data sets:

- Product: carbon dioxide, captured from atmosphere; activity: carbon dioxide, captured from atmosphere and stored, with a sorbent-based direct air capture system, 100kt CO_2, with industrial steam heat, and grid electricity; location: Europe (EUR)

- Product: carbon dioxide, captured from atmosphere; activity: carbon dioxide, captured from atmosphere and stored, with a sorbent-based direct air capture system, 100kt CO_2, with heat pump heat, and grid electricity; location: EUR

3.1.2.1.1.2   Sweet Syngas from Biomass
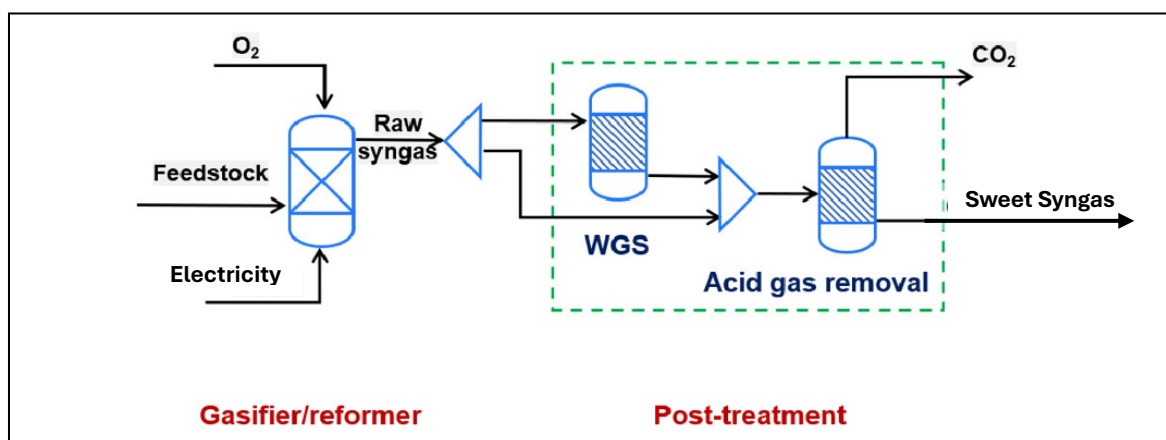
Figure 26: Schematic process structure of the Biomass-to-Olefins Route (based on Jiang et al., 2024, p. 3)
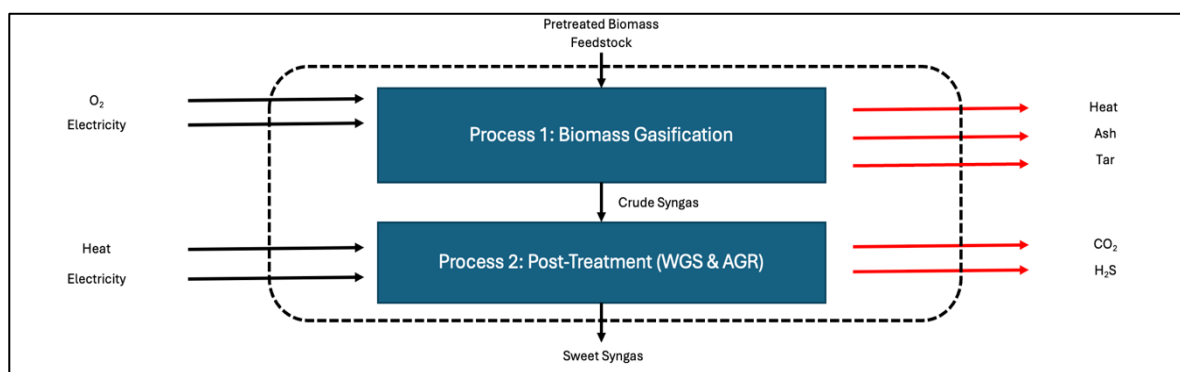
Figure 27: System Boundaries of all in- and outflows as well as respective emissions from Biomass Gasification and Post-Treatment process)

Biomass Gasification

Biomass feedstock must undergo several pretreatments such as crushing and screening (Liu et al., 2020; Liu et al., 2024). To produce crude syngas, biomass is quickly gasified with pure O_2 from an air separation unit under high pressure with energy assumed from electricity (s. O_2 and electricity as inputs for the biomass gasification in **Figures 26, 27** and **Table 9**) to CO, H_2 and CO_2 as effective components with minor amounts of N_2, CH_4, H_2O and O_2 in an entrained flow gasifier (Liu et al., 2020; Jiang et al., 2024). Various chemical reactions occur during biomass gasification making this process quite complex. In general terms, the reaction can be summarized by the following equation (s. **Equation 19**) (Jiang et al., 2024).

Equation 19: Overall Biomass Gasification Reaction

$$Biomass \rightarrow CO + CO_2 + N_2 + O_2 + H_2 + H_2O + CH_4$$
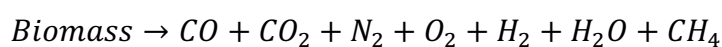
Besides these compounds listed in **Equation 19**, steam, ash and tar are also produced. While CH_4 is assumed to be reformed or oxidized according to **Equation 20-23**, while heat in the form of steam is emitted along with tar and ash (s. tar and ash as emissions for the biomass gasification process in **Figure 27** and **Table 9**) (Jiang et al., 2024).

Equation 20: CH₄ – Dry Reforming

$$CH_4 + CO_2 \rightleftharpoons 2CO + 2H_2; \; \Delta H_R^0 = +247 \frac{kJ}{mol}$$
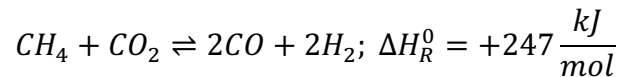
Equation 21: CH4 – Wet Reforming

$$CH_4 + H_2O \rightleftharpoons CO + 3H_2; \; \Delta H_R^0 = +206 \frac{kJ}{mol}$$
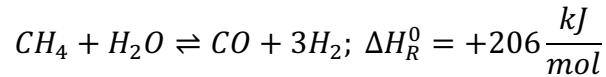
Equation 22: CH₄ Oxidation Reaction – Case 1

$$CH_4 + 2O_2 \rightleftharpoons CO_2 + 2H_2O; \; \Delta H_R^0 = -800 \frac{kJ}{mol}$$
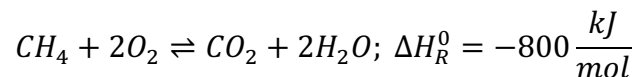
Equation 23: CH₄ Oxidation Reaction – Case 2

$$2CH_4 + 3O_2 \rightleftharpoons 2CO + 4H_2O; \; \Delta H_R^0 = -1034 \frac{kJ}{mol}$$
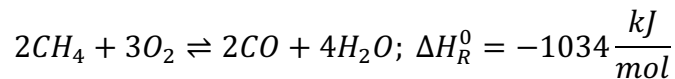
Table 9: LCI of Biomass Gasification incl. all in- and outputs as well as emissions according to system boundaries defined in Figure 27

	Unit/kg crude syngas	Value	Sources
Product:			
Crude Syngas	kilogram	1.000	Pre-defined
Inputs:			
Bark Chips	kilogram	0.654	Own Calculation based on Liu et al., 2020
O_2	kilogram	0.358	Own Calculation based on Liu et al., 2020
Electricity	kilowatt hour	0.016	Liu et al., 2020
Emissions:			
Ash	kilogram	0.009	Liu et al., 2020
Heat (in form of steam), waste	megajoule	0.820	Liu et al., 2020
Coke	kilogram	0.003	Liu et al., 2020

N_2 emissions are not accounted for, which makes sense as it does not contribute to GWP, while O_2 is assumed to be fully consumed by CH_4 oxidation reactions (s. **Equations 20-23**). Afterwards, the hot raw syngas is quenched cooling it down via nozzles spraying condensate and water. It separates inorganic smelt and entrained alkali-salts containing particles which the system does not account for due to their negligible amounts (Carvalho et al., 2017).

In the case of Biomass-to-Olefins, it was difficult to gather reliable, comprehensive data, which properly reflects the several processes needed to undergo this route. Although the paper of Liu et al., 2020 at least provides all the relevant processes with the respective parameters required, the feedstock inputs for the biomass gasification process had to be calculated

to be consistent with the overall carbon and mass balance (s. **Table 9**). The plant installation is assumed to be insignificant.

Acid Gas Removal and Water Gas Shift Reaction

Despite the fact that crude syngas contains high amounts of CO, the MeOH production also requires a high content of H_2 for an ideal ratio expressed as stoichiometric number (SN) of 2 according to **Equation 24** (Carvalho et al., 2017; Jiang et al., 2024; Liu et al., 2020). To adjust the crude syngas to this ratio, the WGS reaction (s. **Equation 26**) comes into place. The operating temperature, in a fixed-bed, multi-stage WGS reactor (s. **Figure 26**) with a shift catalyst, is set between 473 K and 723 K and thus, consumes the biggest portion of energy and releases a significant amount of CO_2 (s. heat and electricity as inflows and CO_2 as emission for the post-treatment process in **Figures 26, 27** as well as in **Table 10**) (Carvalho et al., 2017).

Equation 24: Formula for the calculation of the Stoichiometric Number of Syngas

$$SN = \frac{n_{H_2} - n_{CO_2}}{n_{CO} + n_{CO_2}}$$

Table 10: LCI of Post-treatment process with AGR and WGS incl. all in- and outputs as well as emissions according to system boundaries defined in Figure 27

	Unit/kg sweet syngas	Value	Sources
Product:			
Sweet Syngas	kilogram	1.000	Pre-defined
Inputs:			
Crude Syngas	kilogram	1.940	Own Calculation
Electricity	kilowatt hour	0.004	Liu et al., 2020
Heat	megajoule	1.320	Liu et al., 2020
Emissions:			
Non-fossil CO_2	kilogram	0.940	Own Calculation
H_2S	kilogram	0.0005	Liu et al., 2020

In the next syngas post-treatment step, acid gases are removed via the Rectisol® system developed independently from the companies *Linde* and *Lurgi*, which is a widely used acid gas removal method (AGR) in industry (US Department of Energy, n.d.). It employs cold MeOH as solvent, which efficiently removes CO_2 and H_2S from the gas in one tower (s. CO_2 and H_2S emission of the post-treatment process in **Figures 26, 27** as well **Table 10**) to avoid catalyst poisoning and deactivation and can be fully recovered (Carvalho et al., 2017; US Department of Energy, n.d.). CO_2 does not need to be removed in terms of catalyst deactivation, but a higher CO_2 content means also a higher requirement of H_2 to maintain the ratio of SN = 2 (Keller et al., 2020). Once again, the crude syngas value was calculated to align with the mass and carbon balance whereas all the other values were retrieved from Liu et al., 2020 (s. **Table 10**). The plant installation is assumed to be insignificant, once again.

3.1.2.1.1.3 Methanol Synthesis
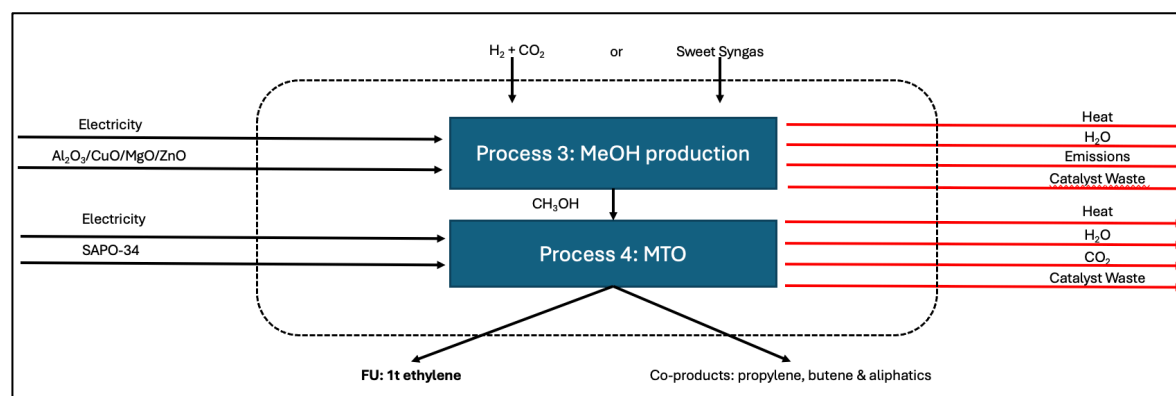
Figure 28: System Boundaries including all in- and outflows as well as emissions of the MeOH production and MTO process

The exothermic MeOH synthesis occurs in commercial *Lurgi Methanol Synthesis Reactor* (s. **Figure 29**), which is filled with a packed-bed state-of-the-art $Al_2O_3/CuO/MgO/ZnO$ catalyst (s. $Al_2O_3/CuO/MgO/ZnO$ catalyst as input for the MeOH production process in **Figure 28** and **Tables 11, 12**) and a counter-current coolant jacket to avoid overheating of the reactor, which would lead to deterrence of reactor, reaction product and catalyst (Kansy, et al., 2023; Markowitsch et al., 2023; Santos et al., 2018). It operates at 503-523 K and 50-80 bar, which is provided via electricity (s. electricity as input for the MeOH production process in **Figure 28** and **Tables 11, 12**) (Kansy, et al., 2023; Markowitsch et al., 2023).

Equation 25 is linked to **Equation 27** over the reversed WGS reaction (s. **Equation 26**). Therefore, a ratio between H_2 and CO_2 of 3:1 (H_2: CO_2) in the direct hydrogenation of CO_2 case or a ratio of SN = 2 for the biomass case according to **Equation 24** must be adjusted (s. sweet syngas or $CO_2 + H_2$ as inputs for the MeOH production process in **Figure 28** and **Tables 11, 12**). Next, these compounds are pressurized to match the operating conditions and getting mixed by a mixer with the recycled stream while the required heat is provided by the pre-reactor heater (s. **Figure 29**). The catalytic zone the reactions according to **Equations 25-27** occur releasing a lot of heat due to the exothermic nature of MeOH production (s. heat as emission of the MeOH production process in **Figure 28** and **Tables 11, 12**). After the reaction, the product stream, initially at 588 K, gets cooled down to 313 K through multiple heat exchangers to liquefy and separate the mix from H_2O and MeOH from unreacted gases mainly containing CO, CO_2 and H_2 (s. flash cooler and separator in **Figure 29**) (Markowitsch et al., 2023; Meunier et al., 2020). The unreacted gas stream is partially recycled, while the remainder is purged to avoid the accumulation of inert gas and unwanted by-products, which is assumed to be solely CO_2 (s. purge in **Figure 29** and CO_2 as emission of the MeOH production process in **Figure 28** and **Tables 11, 12**) (Meunier et al., 2020).

Equation 25: MeOH-Synthesis via Direct Hydrogenation of CO_2 with H_2

$$3H_2 + CO_2 \rightleftharpoons CH_3OH + H_2O; \ \Delta H_R^0 = -49.5 \ kJ/mol$$
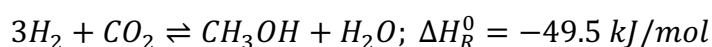
Equation 26: Reversed WGS Reaction

$$CO_2 + H_2 \rightleftharpoons CO + H_2O; \Delta H_R^0 = +41.2 \ kJ/mol$$
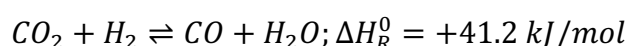
Equation 27: MeOH-Synthesis via Syngas

$$CO + 2H_2 \rightleftharpoons CH_3OH; \ \Delta H_R^0 = -94 \ kJ/mol$$
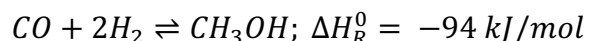
In the case of direct hydrogenation of CO_2, the water-MeOH mix is further separated in a distillation column, from which high-purity MeOH (>99%) at 1 bar and 293 K is obtained at the head of distillation column while pure water is recovered at the bottom (s. H_2O emission of the MeOH production process in **Figure 28** and **Tables 11, 12**) (Meunier et al., 2020). This makes the process operation set-up simpler, more efficient and at lower cost compared to the complex purification steps in the sweet syngas case. In the syngas case, there are several additional impurities and by-products to be filtered out such as VOC in measurable amounts (s. VOC and CO emissions of the MeOH production process in **Figure 28** and **Table 12**) (Marlin et al., 2018).
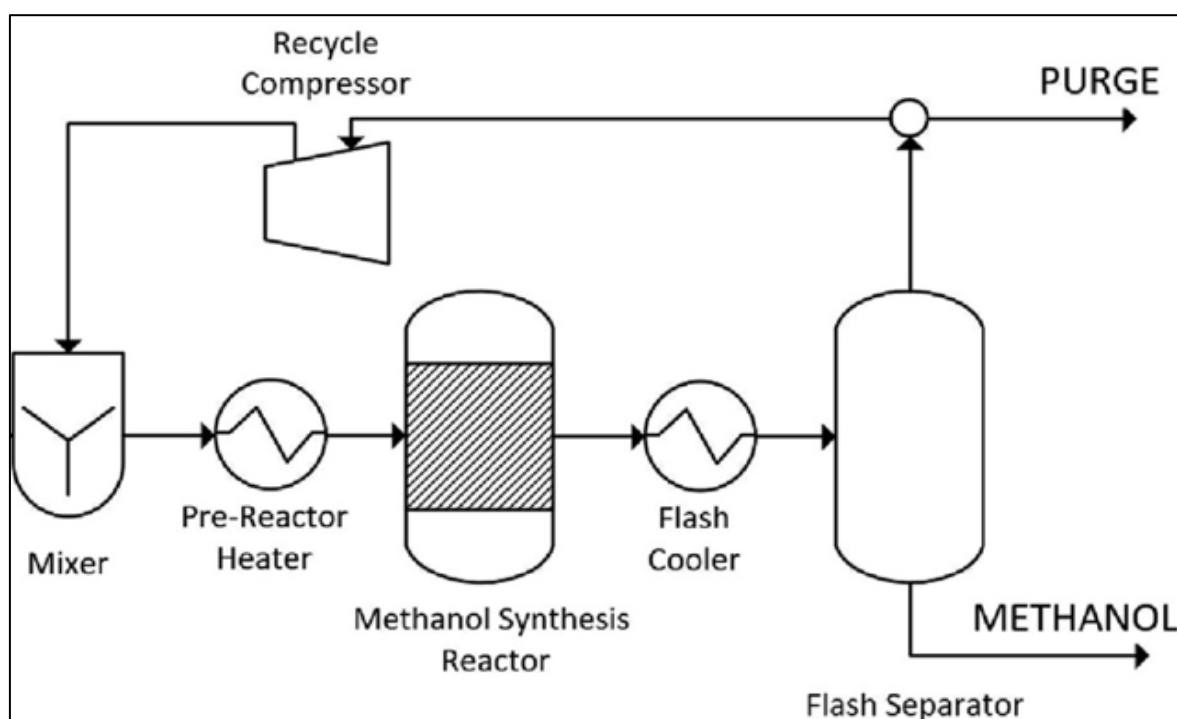
Figure 29: A schematic representation of MeOH production process (Santos et al., 2018, p.3)

The reaction is both pressure- and temperature-dependent, with high pressures and lower temperatures favoring MeOH production in accordance with Le Chatelier's principle (Markowitsch et al., 2023). However, the reactor operating conditions represent a compromise between reaction kinetics, thermodynamic equilibrium and catalyst activity, given that MeOH is the least thermodynamically favored product of syngas conversion (Arvidsson et al., 2016).

Rosental et al., 2020 provides an extensive LCI for the direct hydrogenation of CO_2 with H_2 including a differentiation of the various catalyst components as outlined in **Table 11**. The material inputs stem from Meunier et al., 2020. Zeolite waste is regarded as a good proxy for a degraded catalyst and thus, is included to complete the mass balance of this process. The amount of electricity is composed of two different values under the assumption that all energy stems from electricity. To operate this process 0.33 kWh/kg MeOH is needed, while the

required heat of 3.47 MJ/kg MeOH to separate MeOH from H_2O also is assumed come from electricity and thus, is converted into 0.97 kWh/kg MeOH (Hank et al., 2019).

*Table 11: LCI of MeOH production via direct hydrogenation of CO_2 with green H_2 incl. all in- and outputs as well as emissions according to system boundaries defined in **Figure 28***

	Unit/kg MeOH	Value	Sources
Product:			
MeOH	kilogram	1.0000	Pre-defined
Inputs:			
CO_2	kilogram	1.4410	Meunier et al., 2020
H_2	kilogram	0.2030	Meunier et al., 2020
Electricity	kilowatt hour	1.3000	Rosental et al., 2020, Hank et al., 2019
MgO	kilogram	0.0002	Rosental et al., 2020
ZnO	kilogram	0.0024	Rosental et al., 2020
CuO	kilogram	0.0064	Rosental et al., 2020
Al_2O_3	kilogram	0.0010	Rosental et al., 2020
Emissions:			
H_2O	cubic meter	0.0006	Rosental et al., 2020
Fossil CO_2	kilogram	0.0660	Rosental et al., 2020
Heat, waste	megajoule	1.4000	Rosental et al., 2020
Waste:			
Zeolite waste	kilogram	0.0100	Own Calculation based on Rosental et al., 2020

Since the MeOH production via sweet syngas does not differ from direct hydrogenation of CO_2 with H_2 in terms of their process set-up, the catalyst reported in Rosental et al., 2020 is also included while zeolite waste is used as proxy like in the case above. The heat as waste is calculated based on **Equation 27** as it will be important for process integration later (s. Chapter 3.1.2.3.1 – Process Integration). All other values are retrieved from Liu et al., 2020. However, the electricity value also needs further clarification: Liu et al., 2020 reported an electricity value of 0.01 kWh/kg MeOH, while 5.51 MJ/kg MeOH was required assumed for purification steps. According to Rosental et al., 2020, it is assumed that all energy comes from electricity, which is why the heat from Liu et al., 2020 in the form of steam is also converted into electricity with a final value of 1.53 kWh (total value of 1.54 kWh/kg MeOH). Although both MeOH production processes require a production plant with the respective pipes, etc., it is assumed that the whole plant installation can be neglected in both cases. All data discussed in this section is summarized in **Table 12**.

Table 12: LCI of MeOH production via post-treated syngas from biomass incl. all in- and outputs as well as emissions according to system boundaries defined in Figure 28

	Unit/kg MeOH	Value	Sources
Product:			
MeOH	kilogram	1.000	Pre-defined
Inputs:			
Sweet Syngas	kilogram	1.080	Liu et al., 2020
Electricity	kilowatt hour	1.540	Liu et al., 2020; Rosental et al., 2020
MgO	kilogram	0.000	Rosental et al., 2020
ZnO	kilogram	0.002	Rosental et al., 2020
CuO	kilogram	0.006	Rosental et al., 2020
Al_2O_3	kilogram	0.001	Rosental et al., 2020
Emissions:			
H_2O	cubic meter	0.0001	Liu et al., 2020
CO	kilogram	0.0006	Liu et al., 2020
Non-fossil CO_2	kilogram	0.0030	Liu et al., 2020
VOC	kilogram	0.0100	Liu et al., 2020
Heat, waste	megajoule	2.658	Own Calculation based on **Equation 27**
Waste:			
Zeolite waste	kilogram	-0.010	Own Calculation based on Rosental et al., 2020

3.1.2.1.2 Methanol-to-Olefins Process

Although the MTO process was discovered by *Mobile Oil Corporation* (now *EXXON Mobile*) in the US as a response to the energy crisis of the 1970s, marked by the oil embargo and accompanied by volatile gasoline prices and uncertain supply chains, it has only been recently implemented on a large industrial scale. Currently, four technologies exist of which all of them are used in China`s ongoing coal-to-olefins industry (Gogate, 2019). By 2019, over 25% of global MeOH production was already being utilized in the MTO process (Abuagela and Ahmed, 2022).

In a fluidized-bed reactor operating at medium pressures of 2.2-3.5 bar and high temperatures of 723-803 K with the help of electricity, MeOH is converted to light olefins, primarily ethylene and propylene (s. **Figure 30** and electricity as well as MeOH as input for the MTO process in **Figure 28** and **Table 13**) (Kansy et al., 2023). A more advanced silicon-aluminophosphate (SAPO-34) catalyst is utilized replacing traditional acid zeolite (Gogate, 2019). SAPO-34 was found by researchers of *Union Carbide*, which displaces spacious cages connected by small 8-ring windows (s. **Figure 30** and SAPO-34 as input for the MTO process in **Figure 28**) (Cnudde et al., 2020).

Due to SAPO-34's unique pore size of 3.5 Å and geometry restricting the diffusion of heavy or branched hydrocarbons, it offers a high selectivity towards light olefins as it can be depicted in **Figure 30** (Cnudde et al., 2020; Gogate et al., 2019). Additionally, its milder acidity compared to zeolite reduces the extent of hydrogen transfer reactions, thereby minimizing

the production of paraffinic by-products although it is susceptible to rapid deactivation (Gogate et al., 2019).
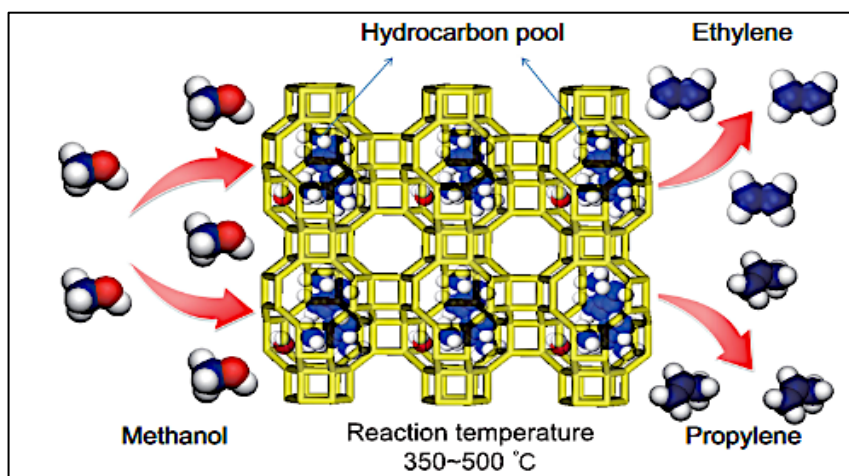
Figure 30: Schematic representation of MTO conversion process over the SAPO-34 catalyst (Sun et al., 2018, p. 2)

The conversion and diffusion of light olefins through SAPO-34's pores is a highly complex process influenced by various factors, including process conditions, catalyst loading, acid strength and acid site density (Cnudde et al., 2020). Moreover, the MTO process itself involves multiple reactions and exhibits a complex reaction scheme, making the whole process difficult to describe in mechanistic terms (Arvidsson et al., 2016). According to **Equation 28-30**, it is generally believed that dimethyl ether (DME; formula: CH_3OCH_3) forms as an intermediate product, which further reacts to produce light olefins, releasing water at each step (s. H_2O emission of MTO process in **Figure 28** and **Table 13**). The water must be separated from the mixture by cooling the mixture down to 303 K (s. heat as emission of the MTO process in **Figure 28** and **Table 13**) because it inhibits the ongoing process (Gogate, 2019; Kansy et al., 2023). Finally, the separation of light olefins happens at cryogenic temperatures (Kansy et al., 2023).

Equation 28: DME Synthesis with MeOH

$$2CH_3OH \rightleftharpoons CH_3OCH_3 + H_2O; \; \Delta H_R^\circ = -39 \frac{kJ}{mol}$$
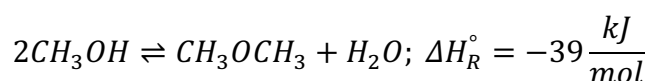
Equation 29: Olefin Production via DME – Case 1

$$CH_3OCH_3 \rightleftharpoons C_2H_4 + H_2O; \; \Delta H_R^\circ = -93 \frac{kJ}{mol}$$
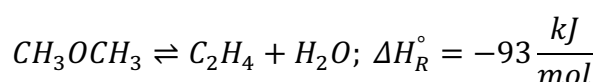
Equation 30: Olefin Production via DME – Case 2

$$CH_3OCH_3 + CH_3OH \rightleftharpoons C_3H_6 + 2H_2O; \; \Delta H_R^\circ = -129 \frac{kJ}{mol}$$
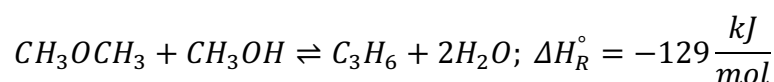
Compared to other well-known synthesis methods, such as the FT-process, the MTO process offers significant advantages. It ensures high yields of light olefins of over 90%, particularly ethylene, with almost complete conversion, allows flexibility in adjusting the propylene-to-

ethylene ratio, produces a narrower range of by-products, and compared to Steam Cracking, operates at more moderate temperatures (Abuagela and Ahmed 2022; Gogate, 2019; Kanys et al., 2023).

Rosental et al., 2020 also provides for this process a comprehensive LCI, which is really challenging to find from literature sources. Since the SAPO-34 catalyst contains silicon, aluminum and phosphorous all connected via oxygen bridges, it is assumed that metallurgical Al_2O_3, Na_4SiO_4 production and PO_4^{3-}-rock beneficiation with equal mass shares are good proxies to model this zeolite catalyst in the LCI due to lack of SAPO-34 data sets availability in *ecoinvent*. Zeolite waste is assumed to be a good proxy for the degradation of the SAPO-34 catalyst and is calculated to align with the mass balance of this process. The plant installation is assumed to be neglected like in the MeOH production processes while all other discussed data is condensed in **Table 13**.

*Table 13: LCI of MTO-process incl. all in- and outputs as well as emissions according to system boundaries defined in **Figure 28**, which have not been adjusted to the respective AF, yet. Co-products are listed in the Appendix (s. **Appx. Table 8** in the Appendix 6.1.2)*

	Unit/kg ethylene	*Value*	*Sources*
Allocation Factor:	[]	0.4338	s. Appendix 6.1.2
Product:			
Ethylene	kilogram	1.0000	
Inputs:			
MeOH	kilogram	5.4370	Rosental et al., 2020
Electricity	kilowatt hour	1.5100	Rosental et al., 2020
Metallurgical Al₂O₃	kilogram	0.4653	Rosental et al., 2020
PO₄³⁻- rock beneficiation	kilogram	0.4653	Rosental et al., 2020
Na₄SiO₄ production	kilogram	0.4653	Rosental et al., 2020
Emissions:			Rosental et al., 2020
Heat, waste	megajoule	4.4610	Rosental et al., 2020
H₂O	cubic meter	0.0000	
CO₂	kilogram	0.1450	Rosental et al., 2020
Waste:			
Zeolite waste	kilogram	-1.3959	Own calculation based on Rosental et al., 2020

3.1.2.2   Process Modifications

3.1.2.2.1   Direct Hydrogenation of CO_2

Direct Air Capture as alternative Carbon Capture Utilization Technology
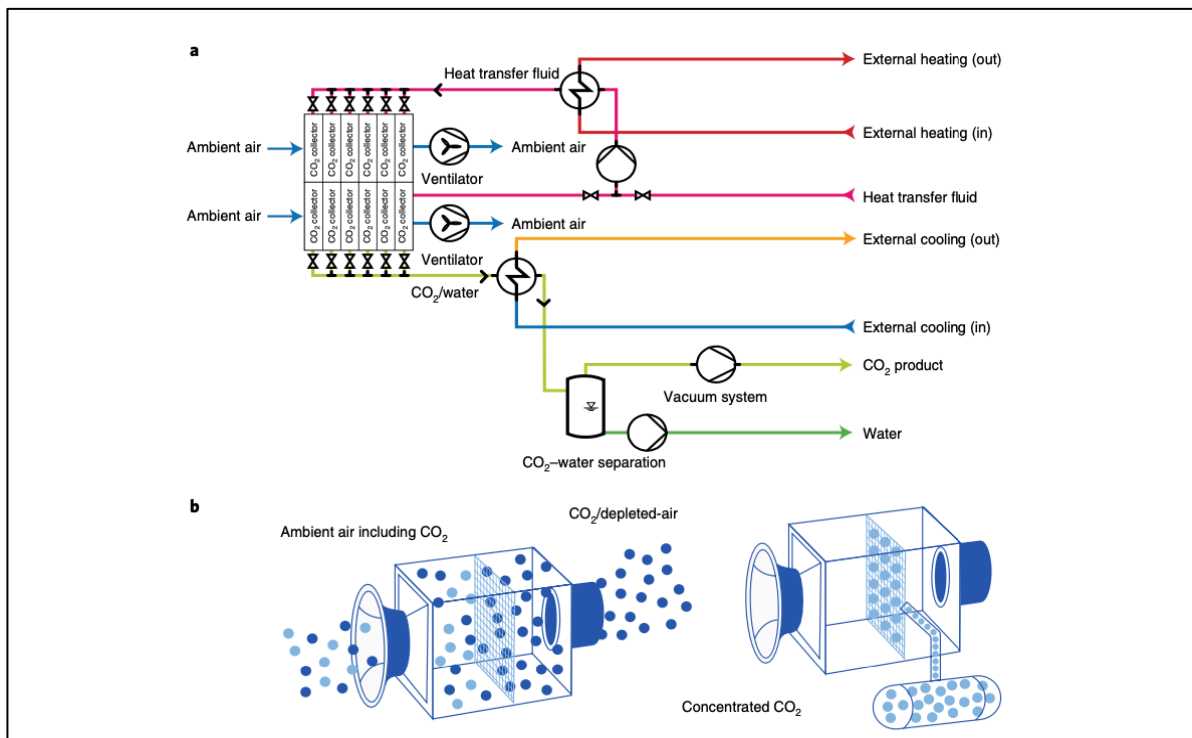
Figure 31: Technical flowchart (a) and adsorption (left)-desorption (right) phase (b) of the DAC process by Climeworks (Deutz and Bardow, 2021, p. 2)

An alternative method for carbon capture is DAC, which differs from amine scrubbing by capturing CO_2 directly from the atmosphere rather than from point-source emissions (Deutz & Bardow, 2021; Meunier et al; 2020). The CCU-DAC process establishes a closed CO_2 loop by capturing non-fossil CO_2 already present in the atmosphere, incorporating it into ethylene, and eventually releasing it back into the air at the end of the product's life cycle. In contrast, the CCU-PSC process follows a linear CO_2 pathway: Fossil carbon is extracted as fuel from underground, combusted, captured and stored temporarily in the ethylene product and ultimately released as fossil CO_2 into the atmosphere at the end of the product's lifecycle.

Moreover, the capture process must be done at ambient conditions because it is uneconomical to pressurize, heat or cool large quantities of air and its energy must be sourced carbon-free (Sodiq et al., 2023). As a consequence, the energy consumption is shifted to a more favorable stage in the process where higher concentrations of CO_2 can be removed from the sorbent (Shi et al., 2020).

Several performance criteria are critical for DAC systems, including high selectivity, high capacity, fast transport and kinetic properties, thermal and chemical stability and mechanical properties. Other considerations encompass ease of loading, resistance to fouling, ease of regeneration and low cost (Sodiq et al., 2023). There are mainly two types of materials: liquid or solid sorbents, although solids are used most of time as they exhibit the better kinetics and can be regenerated at lower temperatures. Solid sorbents can be further divided into physi-, chemi- and moisture swing-sorption materials. Even though these different sorption types display advantages and drawbacks, the chemisorption materials are examined in this Master Thesis because it is used in the already commercially available *Climeworks* DAC system

employing amine-based solid sorbents (s. **Figure 32**) to capture CO_2 (Deutz and Bardow, 2021; Shi et al., 2020).

Based on Deutz and Bardow, 2021, the *Climeworks* system includes multiple CO_2 collectors, heat exchangers, a vacuum pump, and a water separation unit (s. **Figure 31a**). During operation, air is driven through a CO_2 collector, where CO_2 chemically binds to the adsorbent (s. **Figure 32**), which follows the reaction (s. **Equation 17-18**) propagated in Chapter 3.1.2.1.1.1 – Carbon Capture Utilization Plant under dry conditions in principal. Depending on weather and humidity conditions, some adsorbents may also co-adsorb water.
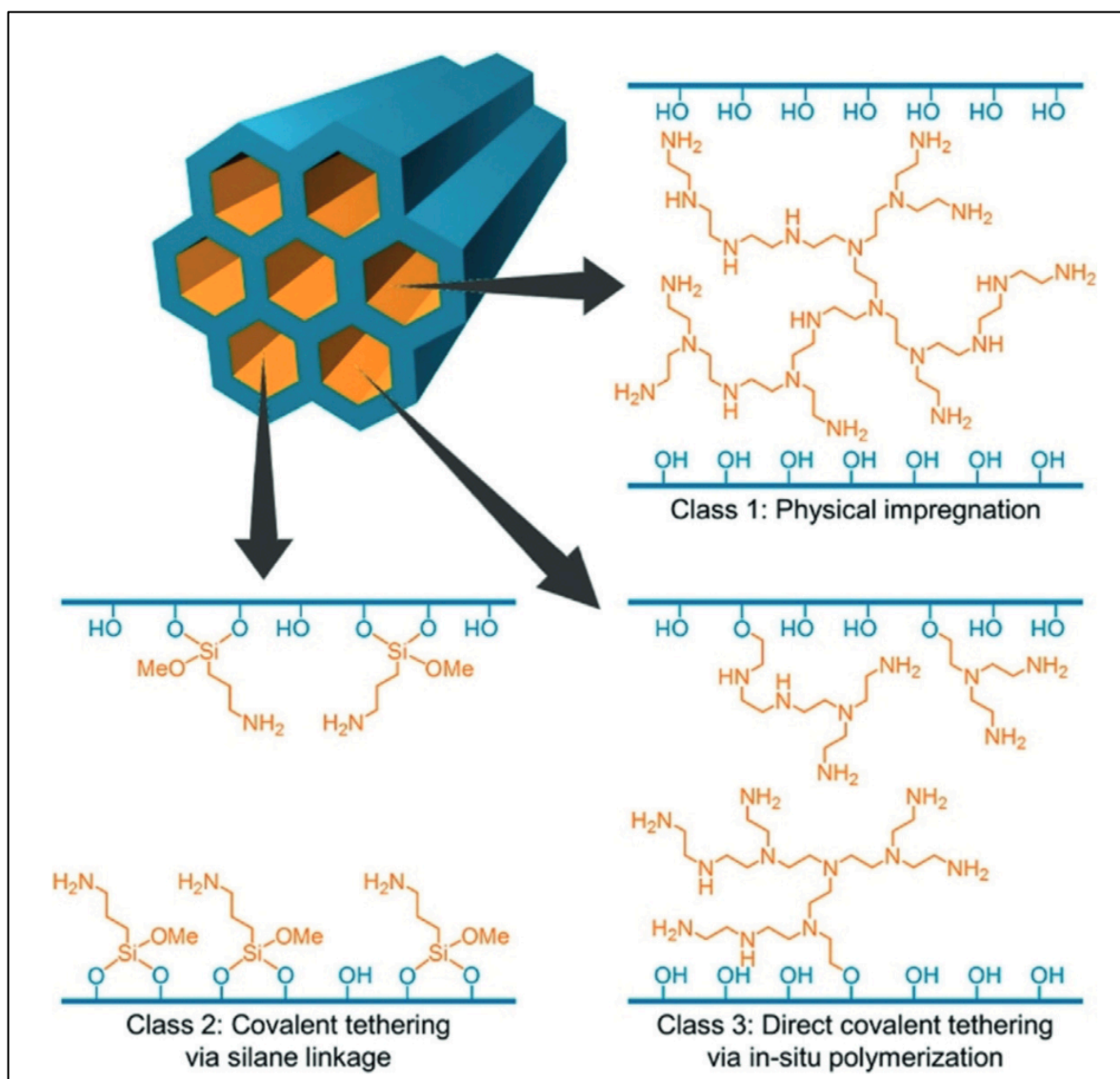
Figure 32: Type of amine-modified sorbents: class 1 sorbent: in porose materials impregnated polyethyleneimine; class 2 sorbent: covalent bonded amines over silane; class 3: in-situ-Aziridine-polymerization on solid material (Shi et al., 2020, p.8)

Once the adsorption phase is complete, the compartment is closed, and desorption is initiated by heating the adsorbent to approximately 373 K in a semi-batch process, using an electric heat pump. The CO_2 is then released and collected via a vacuum system, while water is separated by cooling and condensing it (s. **Figure 31b**). The resulting CO_2 is 99% pure and can be stored or utilized (Deutz and Bardow, 2021).
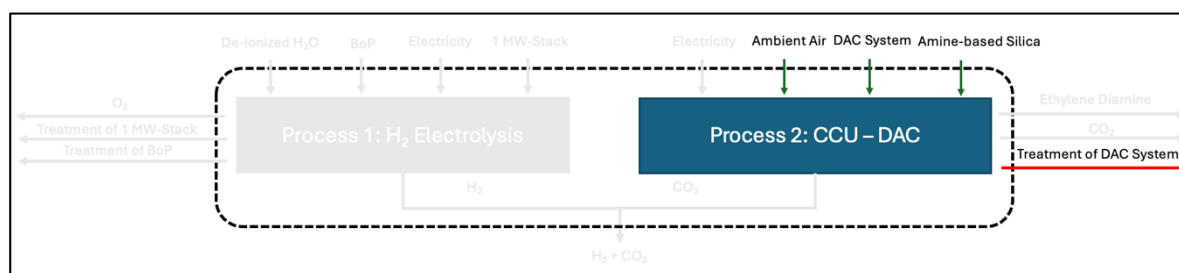
Figure 33: *System Boundaries including all in- and outflows as well as emissions, highlighting the changes made compared to the baseline scenario*

Other than in PSC, DAC also includes the DAC system and its corresponding waste in the system boundaries (s. DAC system as an input and waste treatment of the CCU – DAC process in **Figure 33** and **Table 14**), solely for the sake of completeness as these two items have also been reported in the *ecoinvent* data base, whereas for PSC as CCU technology none of these two items were listed. These two parameters do not have a significant impact on the overall results, though. Additionally, it is assumed that ethylene diamine is a good proxy to describe the degradation product of amine-based silica, since it also does contain derivatives of amines (s. ethylene diamine as emission for the CCU – DAC process in **Figure 33** and **Table 14**). All other values are retrieved from the *ecoinvent* database of the data set (product: carbon dioxide, captured from atmosphere; activity: carbon dioxide, captured from atmosphere and stored, with a sorbent-based direct air capture system, 100 kt CO_2, with heat pump heat, and grid electricity; location: EUR), which refers to the paper of Deutz & Bardow, 2021 (s. **Table 14**).

Table 14: *LCI of CCS process with DAC technology incl. all in- and outputs as well as emissions according to system boundaries defined in* **Figure 33**

	Unit/kg captured CO_2	Value	Sources
Product:			
Captured CO_2	kilogram	1.000	Pre-defined FU
Inputs:			
Electricity	kilowatt hour	1.0172	*Ecoinvent* 3.9 based on Deutz & Bardow, 2021
Sorbent based DAC System	unit	5E-10	*Ecoinvent* 3.9 based on Deutz & Bardow, 2021
Amine-based silica	kilogram	0.003	*Ecoinvent* 3.9 based on Deutz & Bardow, 2021
CO_2 captured from air	kilogram	1.111	*Ecoinvent* 3.9 based on Deutz & Bardow, 2021
Emissions:			
Non-fossil CO_2	kilogram	0.111	*Ecoinvent* 3.9 based on Deutz & Bardow, 2021
Ethylene diamine	kilogram	0.003	Own Calculation based on Zhou et al. 2012
Waste:			
Waste Treatment of DAC system	unit	-5E-10	*Ecoinvent* 3.9 based on Deutz & Bardow, 2021

Solid Oxide Electrolysis

As outlined in the Literature Review (s. Chapter 2.1), the electricity demand for operating electrolysis significantly impacts the LCA of H_2 production (Bareiß et al., 2019). Consequently, improving the energy efficiency of the electrolyzer stack is crucial for reducing this burden. SOEC remains under research especially because SOEC still lacks in stability and is prone to degradation (Shiva & Himabindu, 2019). However, SOECs present a promising solution as they offer higher efficiencies compared to other electrolysis technologies by using a solid electrolyte membrane (typically yttria-stabilized zirconia: ZrO_2 doped with Y_2O_3) through which, as shown

Figure 34: Schematic Representation of the functioning of a SOEC-cell (Shiva and Himabindu, 2019, p. 5)

in **Figure 34**, O^{2-} instead of H^+ (PEMEC) or OH^- ions (AEC) diffuse (Ahabi et al., 2024; Shiva & Himabindu, 2019; Vilbergsson et al., 2023). The cell operates at high temperatures (773 K-1123 K) and high pressures, with the following reactions (s. **Equations 31-32**) occurring at the electrodes (Shiva & Himabindu, 2019):

Equation 31: Hydrogen Evolution Reaction as Reduction at the SOEC cathode

$$2H_2O + 4e^- \rightarrow 2H_2 + 2O^{2-}$$
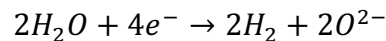
Equation 32: Oxygen Evolution Reaction as Oxidation at the SOEC anode

$$2O^{2-} \rightarrow O_2 + 4e^-$$
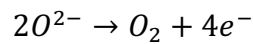
Table 15: LCI of H_2 production via SOEC incl. all in- and outputs as well as emissions according to system boundaries defined in Chapter 3.1.2.3.1 – Solid Oxide Electrolysis

	Unit/kg H_2	Value	Sources
Product:			
H_2	kilogram	1.00	Pre-defined FU
Inputs:			
SOEC Stack (1 MW)	unit	2.31E-06	Wei et al., 2024
SOEC BoP Production	unit	2.57E-07	Wei et al., 2024
De-ionized H_2O	kilogram	12.00	Wei et al., 2024
Electricity	kilowatt hour	42.73	Wei et al., 2024
Heat	megajoule	18.86	Wei et al., 2024
Emissions:			
O_2	kilogram	8.00	Wei et al., 2024
Wastes:			
Waste Treatment of SOEC BoP	unit	-2.31E-06	Wei et al., 2024
Waste Treatment of SOEC Stack	unit	-2.57E-07	Wei et al., 2024

While the system set-up with its boundaries, in- and outputs remain the same, SOEC requires less electricity for H_2 production (42.73 compared to 57.47 kWh/kg H_2) and the BoP as well as the 1 MW stack are changed from PEMEC to SOEC (s. **Table 15**). Furthermore, SOEC is categorized as high temperature electrolysis, which is why additional heat is required as input to operate the SOEC efficiently (s. heat as input for the H_2 electrolysis in **Table 15**). The values for the respective parameters are collected from Wei et al., 2024 like already in the PEMEC case.

Novel Carbon Capture Compounds

Based on Vega et al., 2020, solvent regeneration accounts for nearly 50-80% of the total energy requirement in post-combustion CCS technologies based on chemical absorption, which makes it crucial to optimize the solvents' performance. The energy demand for solvent regeneration and the kinetics of CO_2 capture are primarily determined by the chemical structure of the solvent, which exhibits a linear relationship with CO_2 reactivity. Balancing high CO_2 absorption performance with low regeneration energy costs remains a key challenge, tough.

According to Vega et al., 2020, the total heat required for solvent regeneration includes the heat of water vaporization, the sensible heat necessary to raise the temperature of the CO_2-rich solvent to the stripper conditions, and the heat needed to break the CO_2-solvent bond. Therefore, the ideal CCS solvent should have high CO_2 capacity, fast reaction kinetics, stability, low energy demands, and low volatility, viscosity, and toxicity. It must also minimize environmental impacts, degradation, and manufacturing costs, while maintaining operational efficiency, cyclic capacity, and suitable flow and stripping conditions.
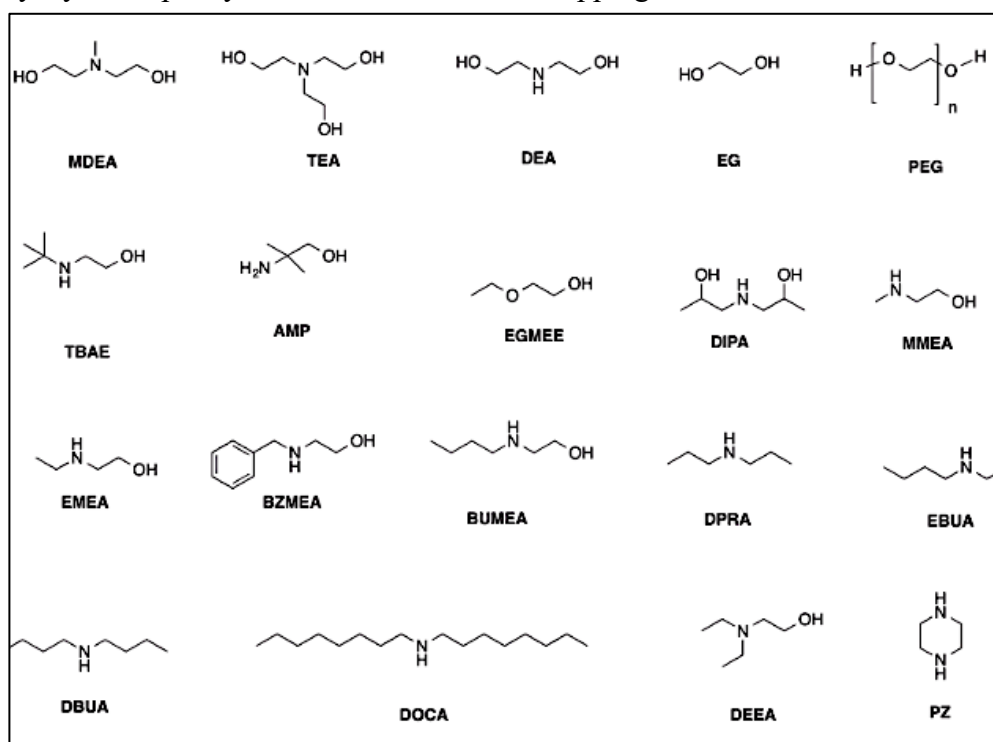
Figure 35: Different possible carbon capture compounds (Heldebrant et al., 2017, p. 3)

Several companies are currently developing commercial absorption processes focused on CCS. For example, under a license from the companies *DOW* and *ALSTOM*, the *URCA-SOL™* technology has achieved a 23% reduction in energy consumption during solvent

regeneration compared to MEA. *Fluor Corporation's Econoamine FG Plus™* process has demonstrated an even greater overall energy reduction potential of 30% compared to conventional MEA configurations by using different amine blends (Vega et al., 2020). Especially MEA in combination with piperazine (PZ) and 2-amino-2-methyl-1-propanol (AMP) showed promising results in energy reductions (s. **Figure 35**) (Vega et al., 2020).

It is assumed that the amine blends can still be represented by the MEA as input and ethylene diamine as emission. However, due to the specifics of the new blends, as mentioned above, 30% less electricity for the heat pump value is needed. Apart from that, the system boundaries, the LCI of CCU according to **Table 8** as well as in- and outflows do not change.

Process Integration
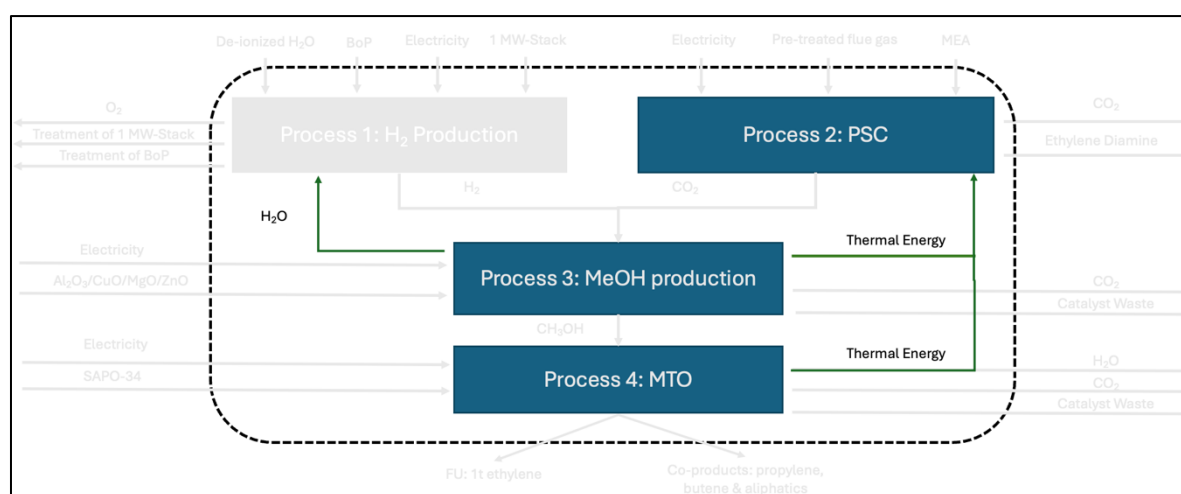
Figure 36: System Boundaries including all in- and outflows as well as emissions, highlighting the changes made compared to the baseline scenario

Based on Meunier et al., 2020, integration of exothermic reactions within industrial processes offers opportunities to improve energy efficiency. For instance, the gained energy from additional combustion of inert and purged gases as well as due to the exothermic nature of the MeOH production and MTO-process, can be harnessed for the CCU process, which would lower the required energy input, particularly for the heat pump (s. **Figure 36**) by -41% assuming all heat generated can be recycled without any losses. Furthermore, the water produced along the MeOH-production and MTO process can fuel the electrolysis so that -47% less external water for the electrolysis is needed (s. **Figure 36**). The complete LCI of the integrated H_2+CCU-to-Olefins route is not listed here due to clarity reasons but it can be viewed in the Appendix (s. **Appx. Table 12** in Appendix 6.3.2.2).

3.1.2.2.2   Syngas from Biomass

Different Feedstocks

The goal is to assess how the environmental footprint of the biomass cultivation and preparation stage influences the overall result of this Biomass-to-Olefins route via MeOH under the assumption that apart from the change of feedstock input all in- and outflows stay the same throughout the whole LCA model. The carbon content however is adjusted to the respective biomass feedstock: miscanthus and wood chips have a reported carbon content of approximately 45% whereas bark chips consist of 50% of carbon (Bilandžja, et al., 2022; Hrbek, et al., 2021; Sinan et al., 2024). Due to these circumstances, the LCIs, as reported in **Tables 9, 10, 12** and **13** for bark chips are the same for miscanthus and wood chips feedstocks.

Only the biomass input and the oxygen required in the Biomass Gasification process is changed to 0.7265 kg of biomass and 0.2855 kg of oxygen for both, miscanthus and wood chips.

Process Integration

Like in the process integration of H_2+CCU-to-Olefins case, produced heat from the MTO- and MeOH-process can be redirected to the post treatment process of crude syngas. It can be also accompanied by heat generated during the biomass gasification process making external heat requirement obsolete (s. **Figure 37**). In the baseline case scenario, 3.349 MJ/kg ethylene was externally required to operate the post-treatment process, which is replaced by 3.349 MJ/kg ethylene of the total 4.01 MJ/kg ethylene from the biomass gasification process. The rest heat of the biomass gasification process (0.661 MJ/kg ethylene), the heat from the MTO process (1.927 MJ/kg ethylene) as well as the heat from the MeOH synthesis (6.244 MJ/kg ethylene) can now be used to reduce the energy demand for the MeOH distillation process reducing the overall electricity demand of MeOH production (incl. its distillation) by -67.8%. It is assumed that all heat generated can be back integrated without any losses. The complete LCI of the integrated Biomass-to-Olefins route can be accessed in the Appendix (s. **Appx. Table 10** in Appendix 6.3.2.2) and is not shown here due to clarity reasons.
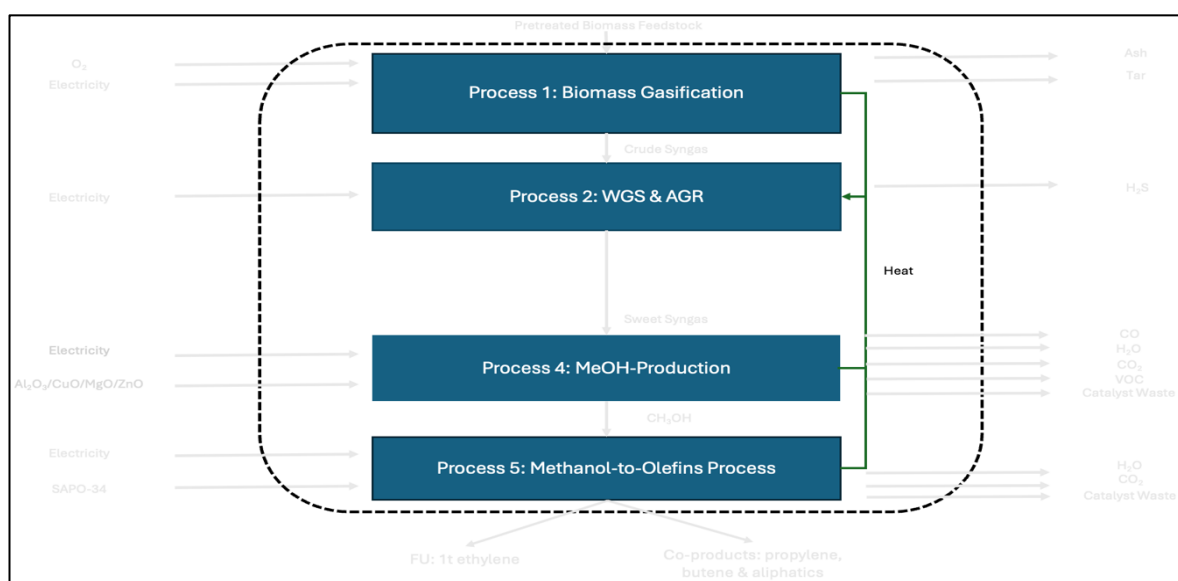
Figure 37: System Boundaries including all in- and outflows, highlighting the changes made compared to the baseline scenario

Post-Treatment Process integrating CCS

Since the Rectisol® process is already employed, which separates CO_2 from syngas and H_2S, the filtered CO_2 only has to be transported and stored at appropriate sites instead of releasing it into the air (s. Compression, Transportation & Storage in **Figure 38**) with the same data set reported in chapter 3.1.1.2 – Steam Cracking Plant with CCS.
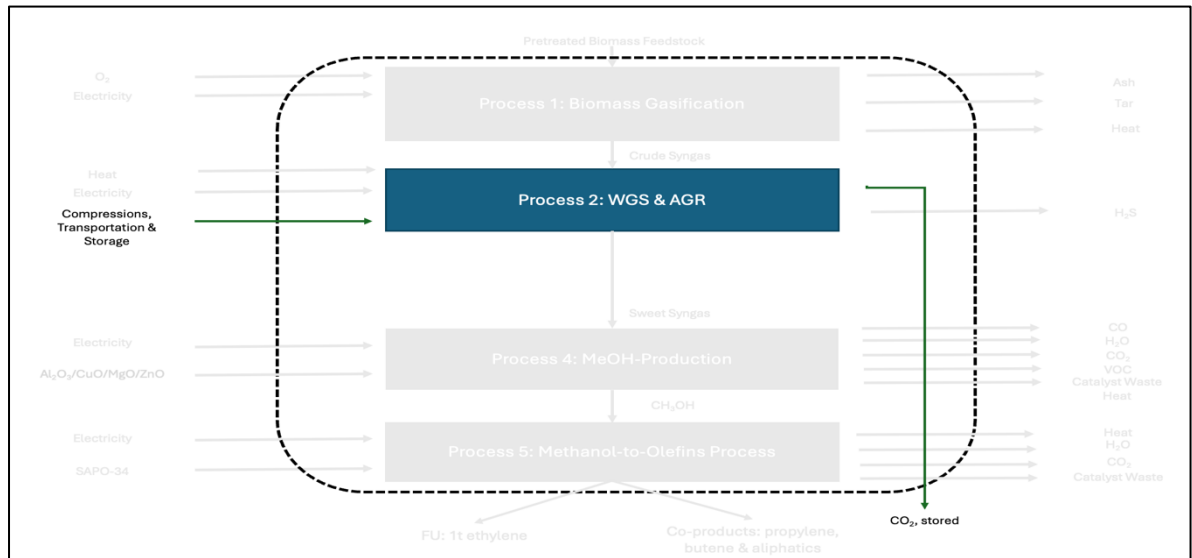
Figure 38: *System Boundaries including all in- and outflows, highlighting the changes made compared to the baseline scenario*

3.2 Future Scenarios

To account for potential future scenarios, two main inputs are considered. The first input is based on IAMs discussed in Chapter 2.2.2, which project energy mixes in future scenarios. For both Switzerland and China, these IAMs anticipate an increased share of renewable energy sources in electricity generation (s. **Figure 39**).
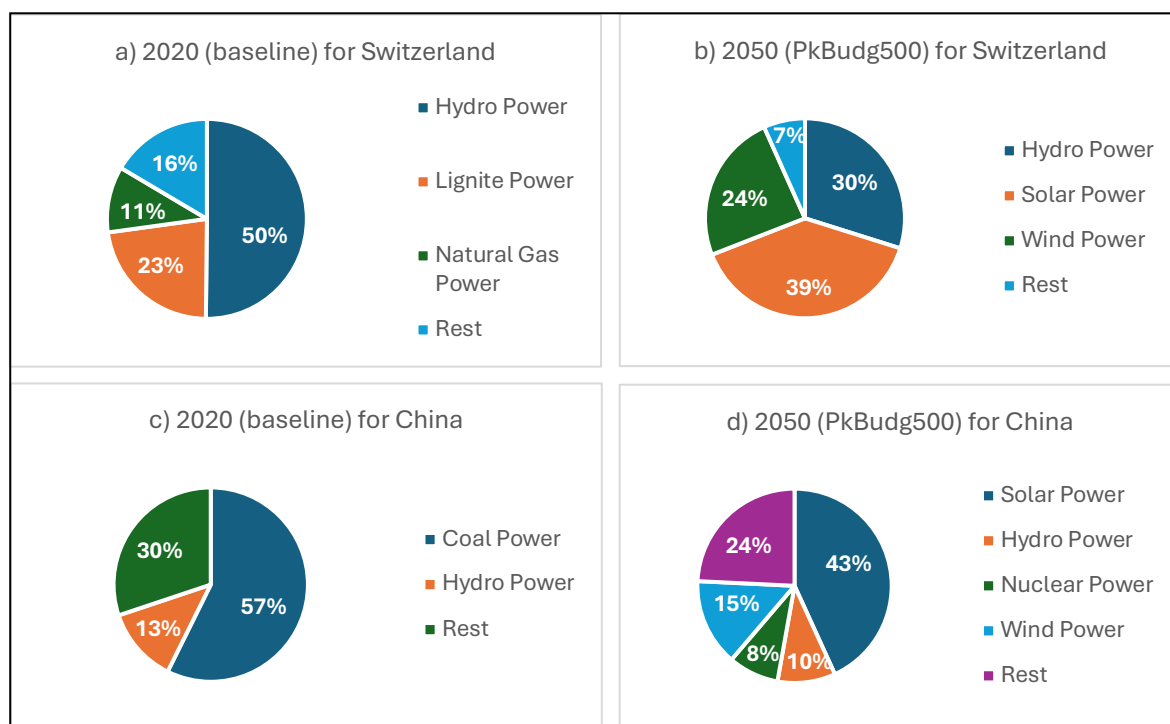
Figure 39: *Electricity mix of China and Switzerland, both for the year 2020 as baseline scenario (s. letter a and c) and for the year 2050 as PkBudg500 scenario (s. letter d and d). Data sets retrieved from ecoinvent (product: electricity, high voltage; activity: market (group) for electricity; location: CHA/CH). All values with a contribution >1% of the overall electricity mix are considered in the calculation, while only aggregated electricity sources exceeding 5% are reported in this pie chart diagram. Electricity medium and low voltage have the same underlying data and only include minor transformation losses*

The second input involves assumptions about impacts associated with technological advancements and process improvements over time as summarized in **Table 16**. For the Steam Cracking process, minimal improvements in efficiency are expected due to its high level of technological maturity and limited remaining efficiency gains (Mynko et al., 2023; Symoens et al., 2018). Consequently, it is assumed that electricity and fuel inputs can be decreased by 2.5% in both 2030 and 2050. If fuel input is reduced, more methane is produced as product, which means that the AF must change, as well (s. **Appx. Tables 6, 7** in Appendix 6.1.1). Hydrogen production data is sourced primarily from literature (Bareiß et al., 2019; Wei et al., 2024) and supplemented specifically with the following data set (product: hydrogen, gaseous, 30 bar; activity: hydrogen production, gaseous, 30 bar, from PEM electrolysis, from grid electricity; location: Europe) from *ecoinvent*. While the current carbon capture efficiency is already high at over 90%, further improvements are anticipated in the efficiency of electricity and MEA usage. These reductions are projected at 2.5% in 2030 and 5% in 2050 for input requirements and associated ethylenediamine output. Nonetheless, significant efficiency gains in CO_2 capture are limited, given the technology's maturity with MEA as carbon capture solvent and the trade-offs between CO_2 capture and solvent regeneration (Vega et al., 2020; Cruz et al., 2021). MeOH production processes, already achieving over 95% conversion yields, are assumed to have limited potential for yield improvement (Meunier et al., 2020;

Rosenthal et al., 2020). However, catalyst and electricity requirements could be reduced by 15% and 20% for catalysts, and by 2.5% and 5% for electricity in 2030 and 2050, respectively, due to assumed potential efficiency gains. For the MTO process, though it has been extensively studied, the reaction mechanisms remain complex and partially understood (Arvidsson et al., 2016). It is assumed that continued research will lead to a fuller understanding of the reaction mechanisms, resulting in incremental energy improvements of 5% in the near term, followed by a larger 15% reduction in energy and catalyst deployment by 2050. The biomass gasification process is expected to see only gradual improvements, following the trends for Steam Cracking and CCU processes. Due to the advanced nature of this technology, a reduction of 5% in energy usage is anticipated by both 2030 and 2050 (Babu, 2005; Vaithyanathan et al., 2023).

Finally, the AGR technology, using Rectisol®, is an advanced process, thus with limited improvement potential (US Department of Energy, n.d.). Accordingly, a modest 5% in reduction of energy usage is projected for 2030 and 2050, with the WGS process expected to follow the same trend. For the Biomass-to-Olefins route, the MeOH and MTO processes are assumed to follow the same trends as those observed for the H_2+CCU-to-Olefins route. All LCIs of future scenarios can be found in the Appendix (s. **Appx. Table 9** in Appendix 6.3.1.1 and **Appx. Table 11** in Appendix 6.3.2.1).

Table 16: Presentation of assumptions implemented for future scenarios 2030 and 2050 for all 3 ethylene production routes

	2030	**2050**	**Comments**
Conventional Route			
Steam Cracking	-2.5%	-2.5%	Accounting for electricity & fuel
H_2+CCU-to-Olefins			
H_2-Electrolysis	s. *ecoinvent* 3.9 & literature	s. *ecoinvent* 3.9 & literature	*Ecoinvent* 3.9 data set: *hydrogen production, gaseous, 30 bar, from PEM electrolysis, from grid electricity* & literature data: Bareiß et al., 2019 & Wei et al., 2024
CCU-Process	-2.5%	-5%	Accounting only for MEA & electricity inflow as well as ethylene diamine outflow
MeOH-Production	-10% -2.5%	-15% -5%	catalyst electricity
MTO-Process	-5%	-15%	Accounting for electricity & catalyst
Biomass-to-Olefins			
Biomass Gasification	-5%	-5%	Accounting for electricity
Post-Treatment (WGS & AGR)	-5%	-5%	Accounting for energy input
MeOH-Production	-10% -2.5%	-15% -5%	Same assumptions made as for the direct hydrogenation case
MTO-Process	-5%	-15%	Same assumptions made as for the direct hydrogenation case

3.3   Life Cycle Impact Assessment

This LCIA, as stated in Chapter 1.1.4, is a cradle-to-gate analysis and only calculates the climate-related GWP scores for the 2020 (BASE), 2030 (BASE), 2050 (BASE) and 2050 (Pk-Budg500) scenarios for the three different ethylene production routes (Steam Cracking, Biomass- and H_2+CCU-to-Olefins) in Switzerland and China (s. Chapter 3.3.1) and in several process modifications (s. Chapter 3.3.2) in accordance to the LCA-standard (s. Chapter 2.2). This means that no impacts related to the use and end of life phase are accounted for.

3.3.1   Comparison of different ethylene production processes including future scenarios and different locations

This section evaluates and compares the GWP impacts of the three baseline ethylene production routes - Biomass-to-Olefins, H_2+CCU-to-Olefins and Steam Cracking - as previously outlined in Chapter 3.1, across two geographic locations (China and Switzerland) and under four temporal scenarios (2020 (BASE), 2030 (BASE), 2050 (BASE) and 2050 (PkBudg500)).

3.3.1.1   *Ethylene production processes located in Switzerland*

The Biomass-to-Olefins route consistently exhibits the lowest GWP across all scenarios. GWP values remain below -1000 kg CO_2-eq./t ethylene and reach as low as -2911.1 kg CO_2-eq./t ethylene in the 2050 (PkBudg500) scenario. The negative numbers can only originate due to the cradle-to-gate analysis without taking into account further impacts after the ethylene production. In fact, during photosynthesis, CO_2 is sequestered into biomass, which contributes a negative impact to the overall GWP, which is subsequently converted into ethylene with minimal carbon losses. Because all other downstream stages including the use and incineration at the end of life are not considered, these values can display negative values at the gate.

Table 17: GWP values (kg CO_2-eq./t ethylene) of the LCIA results of the baseline cases from Switzerland including 2030 (BASE), 2050 (BASE) and 2050 (PkBudg500) projections

	2020 (BASE) *[kg CO_2-eq.]*	*2030 (BASE)* *[kg CO_2-eq.]*	*2050 (BASE)* *[kg CO_2-eq.]*	*2050 (PkBudg500)* *[kg CO_2-eq.]*
H_2+CCU-to-Olefins	9324.7	4364.1	121.38	-2528.3
Biomass-to-Olefins	-1149.2	-1700.5	-2357.5	-2911.1
Steam Cracking	1648.8	1597	1549.1	1465.4

Conversely, the H_2+CCU-to-Olefins route initially demonstrates the highest GWP, peaking at +9324.7 kg CO_2-eq./t ethylene in the 2020 (BASE) and even +4364.1 kg CO_2-eq./t ethylene in the 2030 (BASE) scenario. It stays above the values calculated for the Steam Cracking route ranging from +1648.8 in the 2020 (BASE) and +1597.0 kg CO_2-eq./t ethylene in the 2030 (BASE) scenario. From the 2050 (BASE) scenario onward however, the GWP value of H_2+CCU-to-Olefins drops to +121.38 kg CO_2-eq./t ethylene and even further to -2528.3 kg CO_2-eq./t ethylene in the 2050 (PkBudg500) scenario surpassing the Steam Cracking route. The GWP value of Steam Cracking stays positive at +1549.1 kg CO_2-eq./t ethylene in the 2050 (BASE) scenario and +1465.4 kg CO_2-eq./t ethylene in the 2050 (PkBudg500) scenario. The negative value of the H_2+CCU-to-Olefins route in the 2050 (PkBudg500) scenario

can only happen because it is assumed that captured CO_2 during the CCU-PSC process is assigned to ethylene.

Showing a steady but modest reduction in GWP over time, the Steam Cracking route remains the least improved pathway of all three routes, with values declining by only -11.1% between 2020 (BASE) and 2050 (PkBudg500). Relative reductions in GWP for the other two pathways are more pronounced: Biomass-to-Olefins achieves a -153.3% reduction with a decline of -1761.9 kg CO_2-eq./t ethylene, while H_2+CCU-to-Olefins shows a -127.1% reduction, a decline of -11853.0 kg CO_2-eq./t ethylene for the same two scenarios. All these observations are represented in **Figure 40** from data retrieved from **Table 17**.
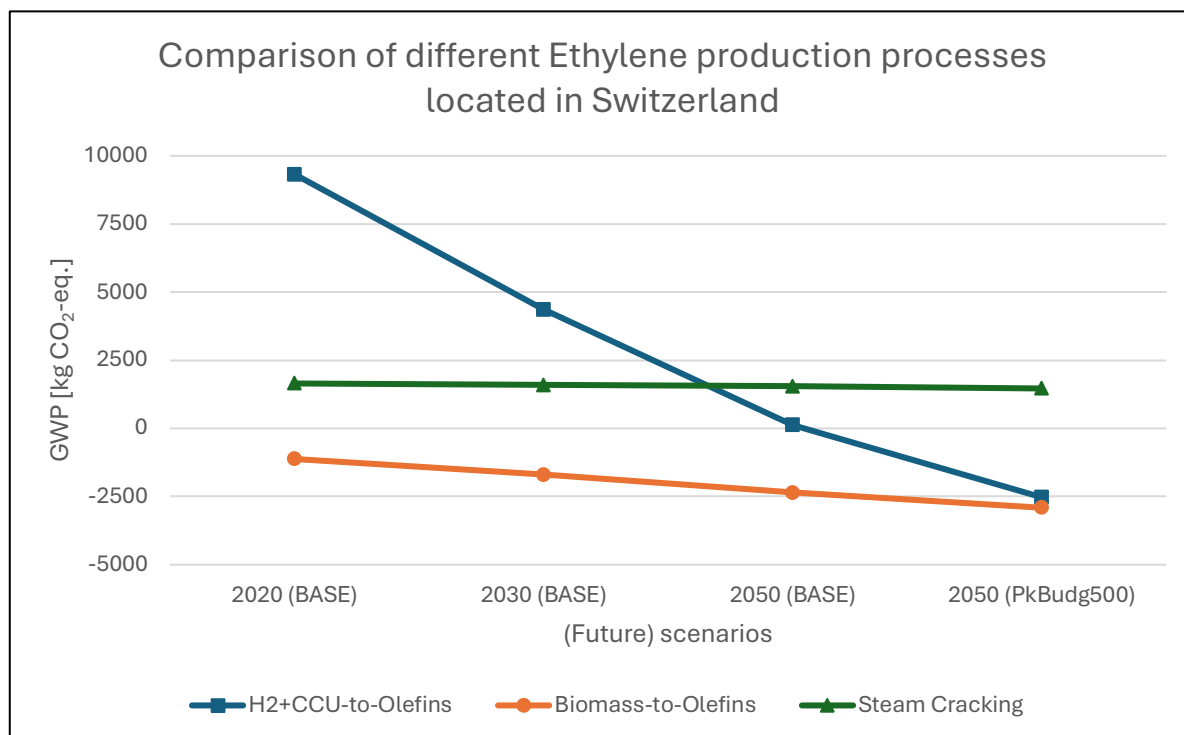
Figure 40: *Line chart of results from p-LCA in Switzerland of Steam Cracking, Biomass-to-Olefins and H_2+CCU-to-Olefins routes for 2020, 2030, 2050 and 2050 (PkBudg500) scenarios expressed in (kg CO_2-eq./t ethylene) showed in **Table 17***

In summary, Biomass-to-Olefins emerges as the most environmentally advantageous process in Switzerland across all scenarios from a GWP perspective while the H_2+CCU-to-Olefins routes performs the worst in the first two scenarios before it almost achieves parity with Biomass-to-Olefins under the 2050 (PkBudg500) scenario.

3.3.1.2   *Ethylene production processes located in China*

According to **Table 18** and **Figure 41**, a similar pattern appears when modeled for China assuming identical operating parameters, yet with different location: the Biomass-to-Olefins route demonstrates the lowest GWP across all scenarios, with values ranging from +1280.3 kg CO_2-eq./t ethylene in the 2020 (BASE) to -2910.5 kg CO_2-eq./t ethylene in the 2050 (PkBudg500) scenario. On the other end, the H_2+CCU-to-Olefins route exhibits the highest GWP in early scenarios, with values of +27758.0 kg CO_2-eq./t ethylene in the 2020 (BASE), +12854.0 kg CO_2-eq./t ethylene in the 2030 (BASE) and +3432.6 kg CO_2-eq./t ethylene in the 2050 (Base) scenario. Although this pathway improves significantly outperforming the Steam Cracking route by achieving -2486.2 kg CO_2-eq./t ethylene in the 2050 (PkBudg500) scenario, it still lags behind the Biomass-to-Olefins route.

The Steam Cracking route in China shows negligible GWP reductions over time, with a decline of only -232.3 kg CO_2-eq./t ethylene between 2020 (BASE) and 2050 (PkBudg500). Notably, the absolute GWP reduction is highest for H_2+CCU-to-Olefins route (-30244.2 kg CO_2-eq.), followed by Biomass-to-Olefins (-4190.8 kg CO_2-eq.).

Table 18: *GWP values (kg CO_2-eq./t ethylene) of the LCIA results of the baseline cases from China including 2030 (BASE), 2050 (BASE) and 2050 (PkBudg500) projections*

	2020 (BASE) [kg CO_2-eq.]	2030 (BASE) [kg CO_2-eq.]	2050 (BASE) [kg CO_2-eq.]	2050 (PkBudg500) [kg CO_2-eq.]
H_2+CCU-to-Olefins	27758.0	12854.0	3432.6	-2486.2
Biomass-to-Olefins	1280.3	-459.40	-1840.8	-2910.5
Steam Cracking	1776.4	1702.90	1652.2	1544.1

Overall, while Biomass-to-Olefins remains the top GWP performer in China, H_2+CCU-to-Olefins achieves substantial improvements in later scenarios in contrast to the Steam Cracking route.
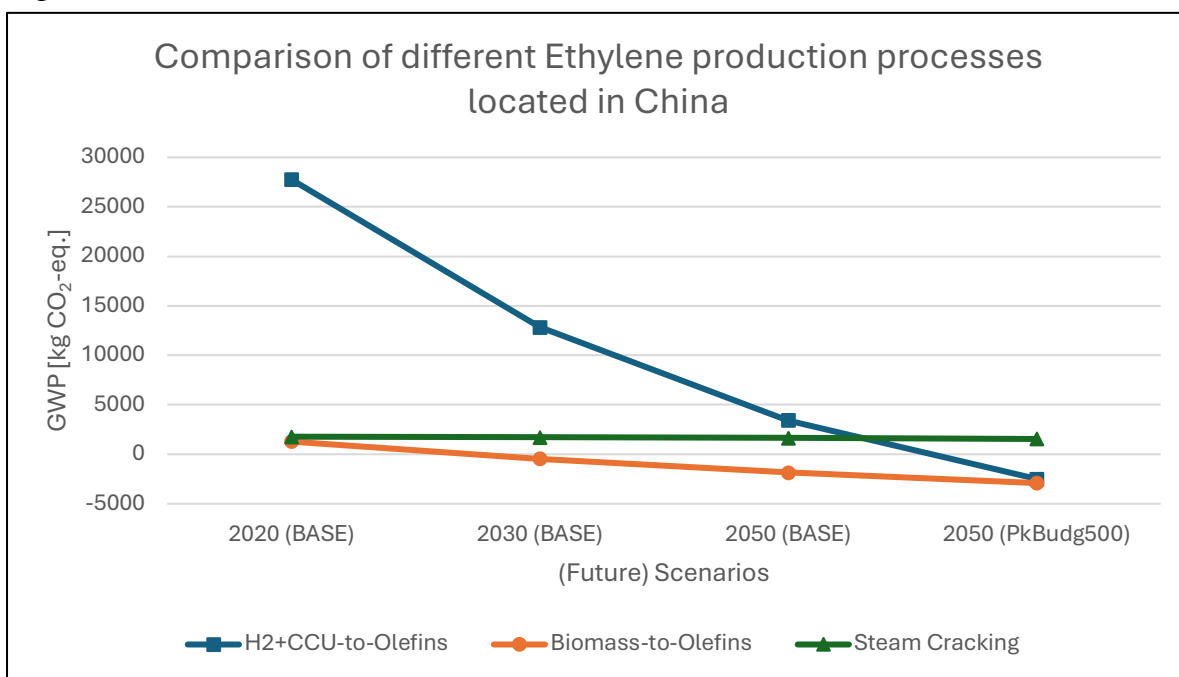
Figure 41: *Line chart of results from p-LCA in China of Steam Cracking, Biomass-to-Olefins and H_2+CCU-to-Olefins routes for 2020, 2030, 2050 and 2050 (PkBudg500) scenarios expressed in (kg CO_2-eq./t ethylene) showed in* **Table 18**

3.3.1.3   Comparative Analysis: Switzerland vs. China

Based on **Figure 42**, the GWP trends across Switzerland and China are broadly similar as mentioned in Chapter 3.3.1.2, with Biomass-to-Olefins consistently outperforming the other processes in both regions. However, significant differences emerge in absolute GWP values between the two locations.

For instance, in 2020, Biomass-to-Olefins in China has a GWP of +1280.3 kg CO_2-eq./t ethylene, while in Switzerland, the value is at -1149.2 kg CO_2-eq./t ethylene. A more striking disparity is observed for the H_2+CCU-to-Olefins route where China records +27758.0 CO_2-eq./t ethylene (an increase of +18433.3 kg CO_2-eq.), nearly three times the GWP in Switzerland for the same year and route. By the 2050 (PkBudg500) scenario, the GWP values for

both Biomass-to-Olefins and H_2+CCU-to-Olefins converge across the two regions. The Steam Cracking route, meanwhile, shows minimal geographic variation, with differences not exceeding 127.6 kg CO_2-eq./t ethylene across scenarios.
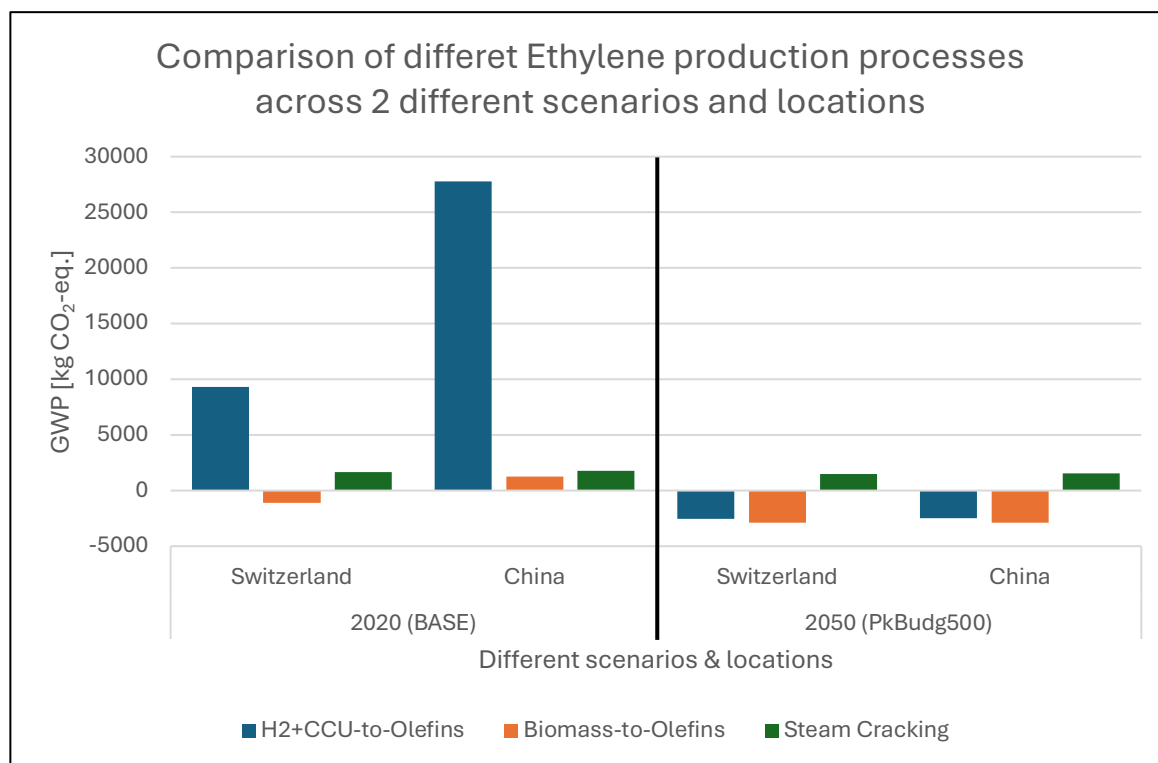
Figure 42: Column chart of the comparison of the GWP results (expressed in kg CO_2-eq./t ethylene) of the 3 baseline routes under study (H_2+CCU-to-Olefins, Biomass-to-Olefins and Steam Cracking) in China and Switzerland across the 2020 and 2050 (PkBudg500) scenario

3.3.2 Process Modifications

In this section, the three distinct ethylene production pathways are analyzed individually within the context of the 2020 (BASE) scenario for Switzerland. Each pathway's baseline case is modified, following the guidelines outlined in Chapter 3.1.2.2, to assess how these adjustments affect the resulting GWP outcomes. Besides these modifications, a best case for each ethylene production route is formulated, which contains a combination of different process configurations, and is further explained for each production route individually.

3.3.2.1 *Steam Cracking Route*

Presented in **Figure 43**, modifications of the Steam Cracking process result in mixed GWP outcomes. Substituting feedstocks with LPG or ethane increases GWP by +83.8% to +3030.1 kg CO_2-eq./t ethylene and +25.4% to +2067.8 CO_2-eq/t ethylene, respectively. Conversely, technological upgrades, such as implementing e- (-0.4%) or a low-emission furnace (-14.5%), achieve moderate GWP reductions of -6.3 and -238.6 kg CO_2-eq., respectively, while CCS has substantial decrease potential by -38.8%, resulting in a GWP score of +1009.4 kg CO_2-eq./t ethylene. The best-case, combining CCS technology with a low-emission furnace, yields the highest GWP reduction (-40.9%) compared to the baseline case, reducing emissions to +976.8 kg CO_2-eq./t ethylene.
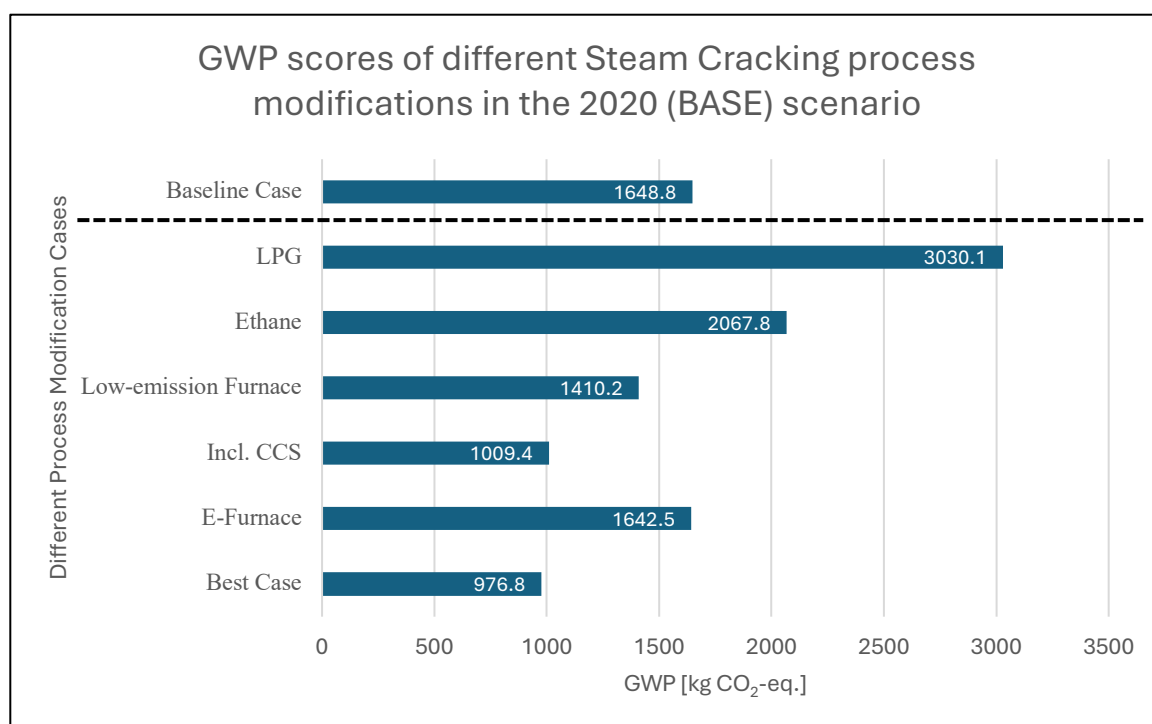
Figure 43: *Bar chart of results from c-LCA of different configurations of the Steam Cracking process (baseline, LGP and ethane as feedstocks, low emission- and e-furnace, incl. CCS and best case as a combination of CCS and low emission furnace) showed in **Table 19** (expressed in kg CO₂-eq./t ethylene) for the 2020 (BASE) scenario*

3.3.2.2   Biomass-to-Olefins Route
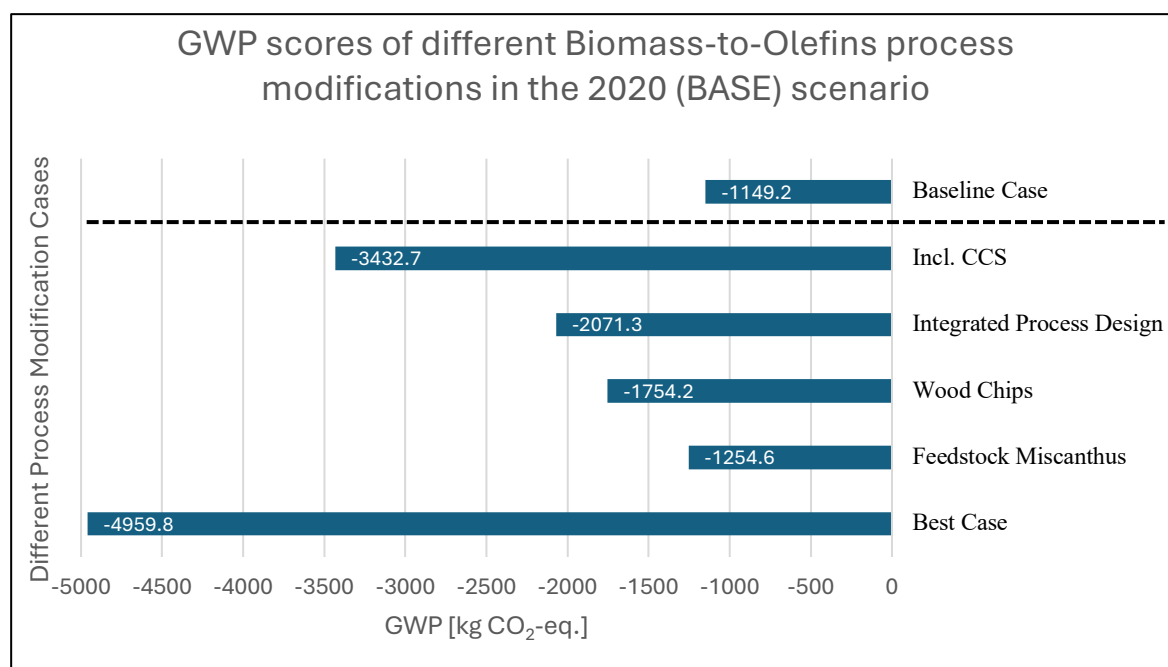
Figure 44: *Bar chart of results from c-LCA of different configurations of the Biomass-to-Olefins process (baseline, miscanthus and wood chips as feedstocks, incl. CCS, integrated process design and best case as a combination of CCS, wood chips and integrated process design) showed in **Table 20** (expressed in kg CO₂-eq./t ethylene) for the 2020 (BASE) scenario*

Feedstock changes from bark chips to wood chips or miscanthus reduce GWP by -52.7% to -1754.2 kg CO_2-eq./t ethylene and -9.2% to -1254.6 kg CO_2-eq./t ethylene, respectively which is the opposite development shown in the Steam Cracking case with ethane and LPG (s. Chapter 3.3.2.1). Greater reductions are achieved through process integration (-80.2%)

and CCS implementation (-198.7%) bringing the GWP down from -1149.2 to -2071.3 and -3432.7 kg CO_2-eq./t ethylene, respectively. Combining CCS, process integration, and wood chips, which performed from a GWP stance best across the three feedstocks selected, in a best-case yield a remarkable GWP of -4959.8 kg CO_2-eq./t ethylene, a reduction of -331.6% from baseline. All these changes are graphically represented in **Figure 44**.

3.3.2.3   *H_2+CCU-to-Olefins Route*
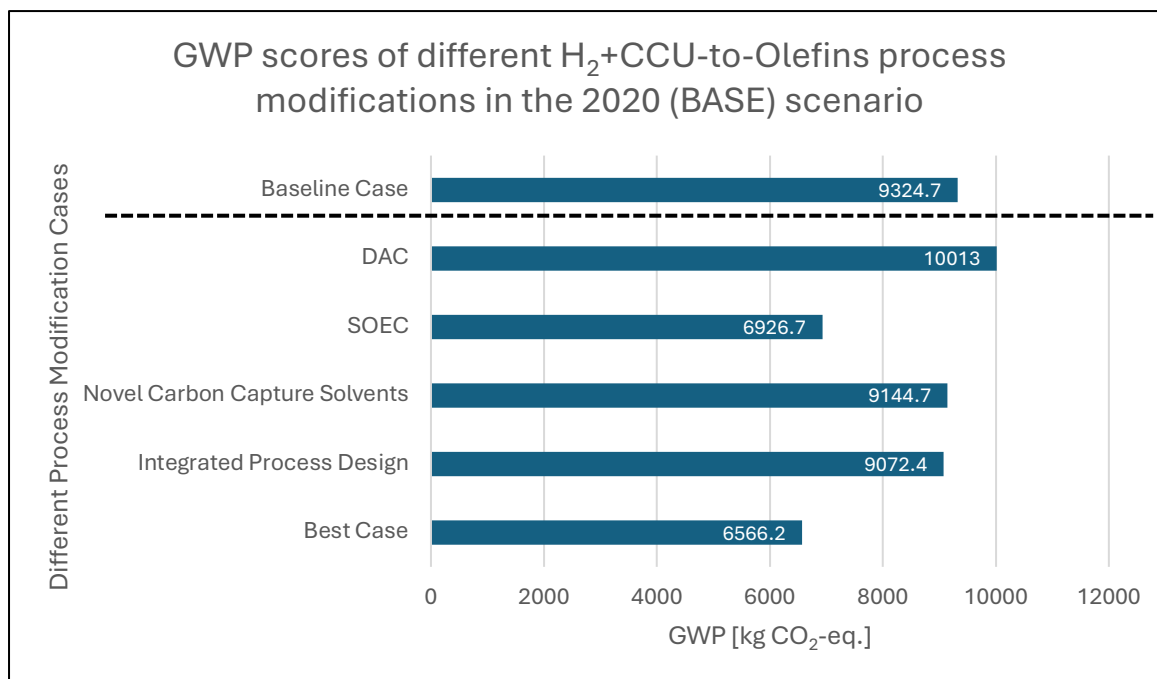
Figure 45: *Bar chart of results from c-LCA of different configurations of the H_2+CCU-to-Olefins process (baseline, DAC, SOEC, integrated process design, novel solvents for carbon capture and best case as a combination of SOEC, integrated process design and novel solvents) showed in **Table 21** (expressed in kg CO_2-eq./t ethylene) for the 2020 (BASE) scenario*

The impact of process modifications on H_2+CCU-to-Olefins, as seen in **Figure 45**, is in comparison to the other two ethylene production routes minor yet lying in a range of up to 30%. While DAC increases GWP (+7.4%) from +9324.7 to +10013.0 kg CO_2-eq./t ethylene, novel carbon capture solvents (-2.7%) and integrated process design (-19.3%) achieve modest reductions from +9324.7 to +9144.7 kg CO_2-eq./t ethylene and from +9324.7 to +9072.4 kg CO_2-eq./t ethylene. Combining these optimizations in a best-case reduces GWP by -29.6% to +6566.2 kg CO_2-eq./t ethylene, which is intuitively the lowest GWP of all process modifications under study.

3.3.2.4   *Comparison of best-cases for the 2020 (BASE) scenario with the baseline cases for the 2020 (BASE) and 2050 (PkBudg550) scenarios*

Among the three pathways, Biomass-to-Olefins achieves the most significant GWP reductions in both relative and absolute terms according to **Figure 46**. Its best-case scenario reaches -4959.8 kg CO_2-eq./t ethylene, representing a -331.6% improvement over the baseline case for the 2020 (BASE) scenario. Steam Cracking achieves a higher relative reduction by -40.8% compared to the H_2+CCU-to-Olefins route with a reduction potential of -29.6% although the absolute decrease is higher at the H_2+CCU-to-Olefins route with -2758.5 kg CO_2-eq. compared -672 kg CO_2-eq. in the Steam Cracking route for the 2020 (BASE) scenario. Ultimately, Biomass-to-Olefins emerges as the most sustainable option from a GWP perspective, while H_2+CCU-to-Olefins performs worst compared to the other ethylene production processes in the 2020 (BASE) scenario.

When comparing the results to the baseline cases in the 2050 (PkBudg500) scenario for Switzerland (s. **Figure 46**), it becomes evident that the best-case scenarios for Steam Cracking and the Biomass-to-Olefins route in 2020 (BASE) also outperform their respective baseline cases even in the 2050 (PkBudg500) scenario. Steam Cracking shows an impact of +976.8 kg CO_2-eq./t ethylene as best-case configuration in the 2020 (BASE) scenario compared to +1465.4 kg CO_2-eq./t ethylene as baseline configuration in the 2050 (PkBudg500) scenario; the Biomass-to-Olefins route achieves -4959.8 kg CO_2-eq./t ethylene as best-case in the 2020 (BASE) scenario, surpassing baseline case of -2911.1 kg CO_2-eq./t ethylene in the 2050 (PkBudg500) scenario. In contrast, the best-case for the H₂+CCU-to-Olefins route in 2020 (+6566.2 kg CO_2-eq./t ethylene) does not outperform baseline case in the 2050 (PkBudg500) scenario, which has a significantly lower impact of -2528.3 kg CO_2-eq./t ethylene.
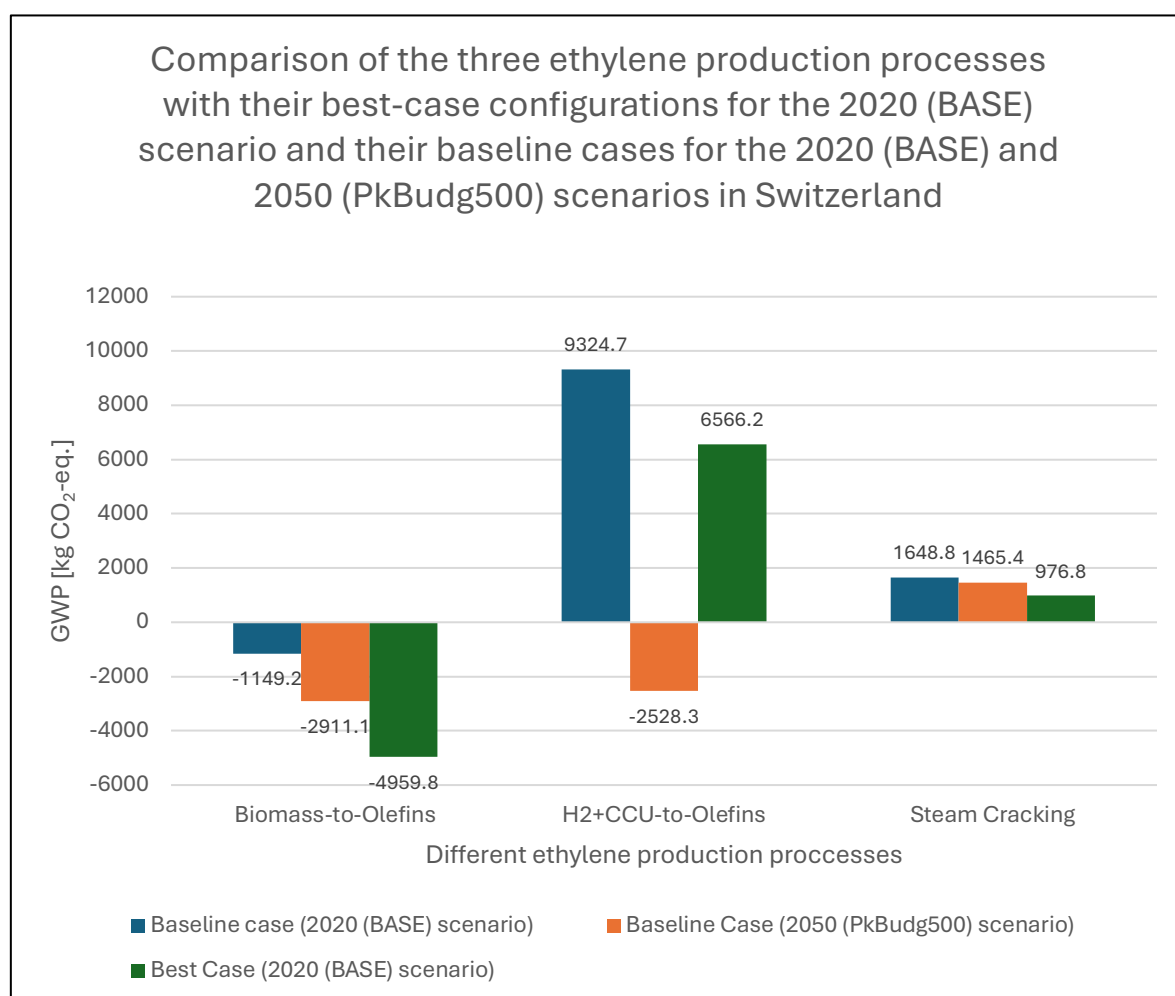
Figure 46: *Column chart of the comparison of the GWP results (expressed in kg CO_2-eq./t ethylene) of the three ethylene production routes under study (H₂+CCU-to-Olefins, Biomass-to-Olefins and Steam Cracking) in Switzerland as baseline case for the 2020 (BASE) and 2050 (PkBudg500) scenarios with their best-case counterparts for the 2020 (BASE) scenario*

3.4 Life Cycle Interpretation

To analyze the composition of the results reported in the LICA (s. Chapter 3.3), a life cycle interpretation was conducted using process contribution analysis for all processes outlined in Chapter 3.1. For clarity reasons, only the five largest contributors with their individual, not accumulated GWP impact to the overall results for each process are listed separately. All other impacts with smaller GWP contributions are aggregated into a "Rest" category to enhance comprehensibility.

This "Rest" category warrants further explanation:

- If the "Rest" category is negative, it indicates that the processes with negative GWP impacts offset the processes with positive GWP impacts.
- Conversely, if the "Rest" category is positive, it reflects the predominance of processes with positive GWP impacts.

Since the "Rest" category encompasses a wide array of minor contributing factors, it is beyond the scope of this analysis to provide a detailed discussion of its composition unless a specific and significant impact within this category can be identified.

The analysis begins with a comparison of the GWP composition across the three distinct ethylene production processes located in Switzerland, evaluated across the scenarios for 2020 (BASE), 2030 (BASE), 2050 (BASE), and 2050 (PkBudg500) in Chapter 3.4.1.1. These results are then juxtaposed with corresponding data for ethylene production in China in Chapter 3.4.1.2. Subsequently, a detailed examination of GWP composition for each ethylene production route with their different possible process modifications is presented in Chapter 3.4.2.

3.4.1 Comparison of different ethylene production processes including future scenarios

3.4.1.1 Switzerland as production location

Steam Cracking

The analysis of the Steam Cracking process reveals that the process itself is consistently the largest contributor to the overall GWP across all scenarios. It accounts for 38.8% of total GWP in the 2020 (BASE) scenario and 41.4% in the 2050 (PkBudg500) scenario. Processes related to naphtha production – including global natural gas venting during gas production, global sweet gas combustion in gas turbines for electricity generation, the production of naphtha itself in Europe without Switzerland (CH) and global waste natural gas flaring during crude oil production – contribute to a cumulative share of 42.6% in the 2020 (BASE), increasing to 47.3% in the 2050 (PkBudg500) scenario. The natural gas venting observed originates from exploration processes, while the burning of sweet gas in gas turbines generates on-site electricity. Waste natural gas flaring is an intentional release of gas during crude oil and natural gas production. The remaining impacts are aggregated into the "Rest" category, which decreases from 18.5% in 2020 (BASE) to 11.3% in 2050 (PkBudg500).

Notably, no processes exhibit a negative GWP contribution in this pathway, although all parameters show a decline in impact from the 2020 (BASE) sceanrio onward, albeit at varying rates. Significant reductions between the 2020 (BASE) and 2050 (PkBudg500) scenarios include a -138.4 kg CO_2-eq. decrease in the "Rest" category and a -35 kg CO_2-eq.

decrease in the Steam Cracking process itself. In contrast, the remaining parameters decline by only 0.6–6 kg CO_2-eq. over the same two scenarios.

Table 19: The values listed of the top 5 biggest GWP contributors of the Steam Cracking route expressed in CO_2-eq./t ethylene for the scenarios 2020 (BASE), 2030 (BASE), 2050 (BASE) and 2050 (Pk Budg500)

	2020 (BASE) [kg CO_2-eq.]	2030 (BASE) [kg CO_2-eq.]	2050 (BASE) [kg CO_2-eq.]	2050 (PkBudg500) [kg CO_2-eq.]
Waste natural gas, burned in production flare (GLO)	86.8	86.4	85.7	85.5
Naphtha production (Europe without CH)	106.8	106.5	106.2	106.2
Natural gas venting from natural gas production (GLO)	396.7	394.9	391.7	390.7
Steam Cracking Process (CH)	641.9	624.0	606.9	606.9
Sweet gas burned in gas turbine (GLO)	112.3	111.8	110.7	110.3
Rest	304.2	273.4	248.0	165.8
SUM	1648.8	1597.0	1549.1	1465.4
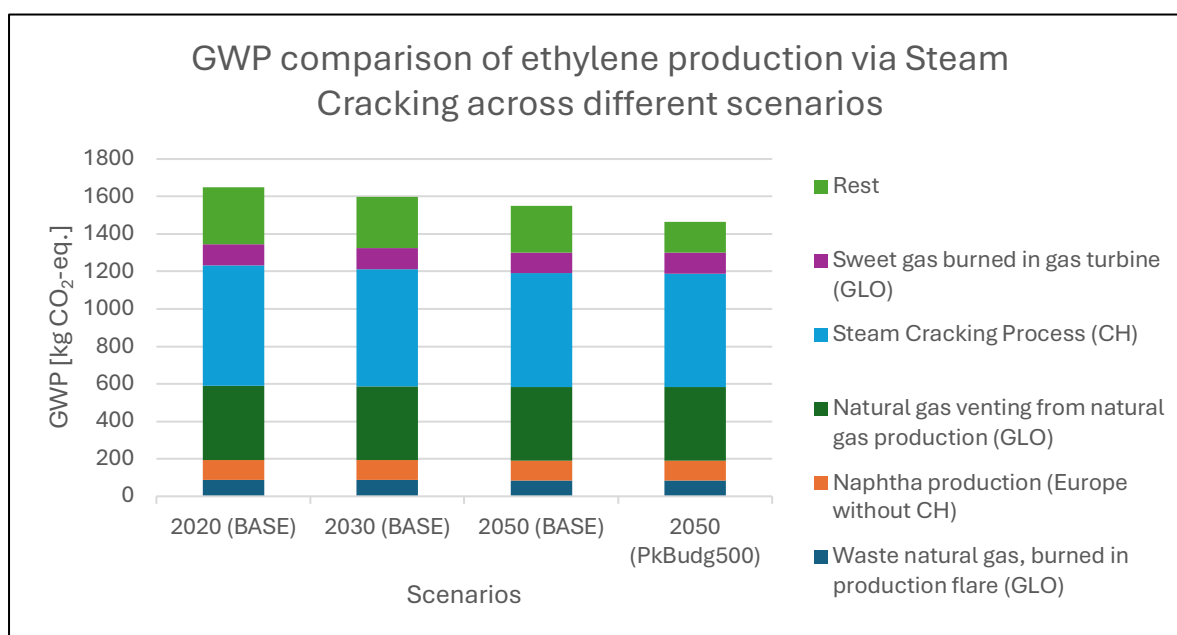
Figure 47: Bar chart of the GWP results expressed in CO_2-eq./t ethylene of the Steam Cracking route located in Switzerland for the 2020 (BASE), 2030 (BASE), 2050 (BASE) and 2050 (PkBudg500) scenarios, incl. the top 5 GWP contributors for each scenario based on Table 19

These reductions align with efficiency improvements, particularly in reduced electricity and fuel demand. Lower electricity consumption and decreased fuel requirements, lowering upstream and combustion-related emissions, results in lower GWP impacts of the Steam Cracking process. The increasing share of renewable energy in electricity production further supports these trends. Additionally, less fuel use increases the production of methane as a co-product, which lowers the AF of ethylene from 0.3513 in the 2020 (BASE) to 0.3494 in the 2050 (PkBudg500) scenario (s. **Appx. Tables 1, 6, 7** in the Appendix 6.1.1). The demand for naphtha, however, remains unchanged across scenarios, resulting in almost consistent

contributions from the biggest GWP naphtha production-related processes. The data presented in this paragraph can be view in **Table 19** and **Figure 47**.

H₂+CCU-to-Olefins
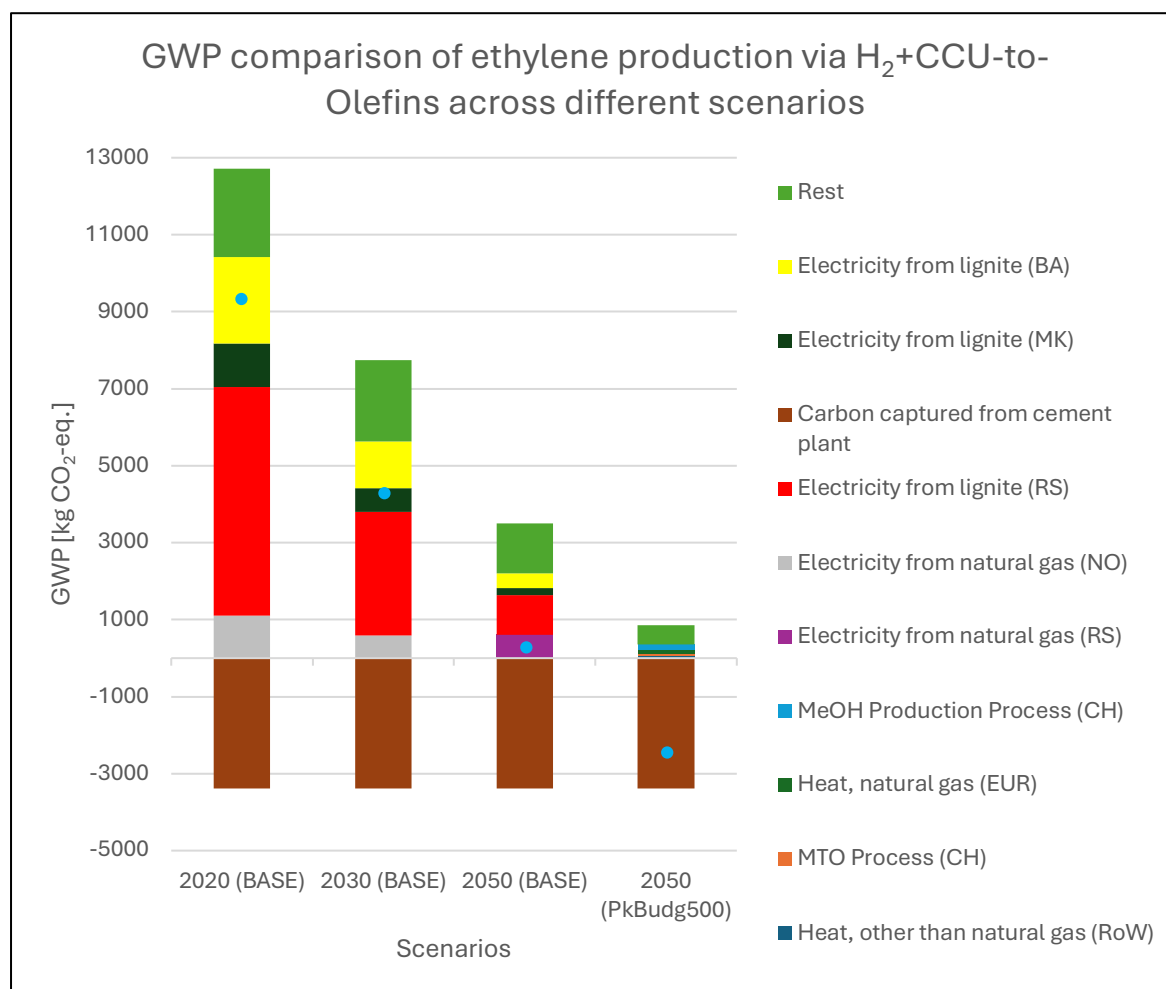
*Figure 48: Bar chart of the GWP results expressed in CO₂-eq./t ethylene of the H₂+CCU-to-Olefins route located in Switzerland for the 2020 (BASE), 2030 (BASE), 2050 (BASE) and 2050 (PkBudg500) scenarios, incl. the top 5 GWP contributors for each scenario based on **Table 20**. The blue dots show the net GWP result for each scenario.*

As it can be viewed in **Figure 48** and **Table 20**, it is interesting to notice, that most of the different steps for ethylene production within this route (PEM electrolysis, MeOH- and MTO-process) do not play a significant role in the first three scenarios. The route's overall GWP in the first three scenarios is mainly composed by positively contributing different electricity sources within the Swiss electricity mix and the CCU – PSC process, contributing negatively to the GWP result. The Swiss electricity mix comprises electricity available in Switzerland and is composed by various electricity sources from all over Europe (s. **Appx. Figure 3** in Appendix 6.2.3), which is more suitable as there is no future electricity mix specifically for Switzerland, but for Europe. The major electricity-related contributors include electricity from lignite in Serbia (RS), Bosnia-Herzegovina (BA) and in North Macedonia (MK) as well as in the first two scenarios (2020 BASE) and 2030 (BASE)) electricity from natural gas in Norway (NO), which will be overtaken in the 2050 (BASE) scenario by electricity from natural gas in RS. In the final 2050 (PkBudg500) scenario, however, the composition shifts: although the PSC – CCU process remains in the top 5 GWP contributors, MTO- and MeOH-production processes, along with heat sources from natural gas in EUR and

alternative sources in the Rest of the World (RoW), emerge as major contributors, while electricity-related impacts diminish.

The absence of GWP impact from the hydrogen production process itself (via PEM electrolysis) is intuitive, as no emissions occur aside from oxygen production. The electricity-intensive nature of the route explains why the GWP impacts of electricity sources not only superimpose GWP impacts of the MTO- and MeOH-processes in the first three scenarios, but also drop significantly across scenarios, driven by greener electricity mixes and reduced electricity demand due to technological efficiencies (s. Chapter 3.2). For instance, the GWP of electricity from lignite in RS decreases from +5936.73 kg CO_2-eq. in the 2020 (BASE) to +1020.97 kg CO_2-eq. in the 2050 (BASE), ultimately falling out of the top five contributors by the 2050 (PkBudg500) scenario. The negative GWP effect of the carbon capture of point sources from cement plant emissions remains identical throughout the different future scenarios at -3384.8 kg CO_2-eq., which makes sense as during the CCU – PSC process, the CO_2 up-take and the CO_2 emissions of the not captured CO_2 do not change over different future scenarios. The -3384.8 kg CO_2-eq. is composed by -3760.9 kg CO_2-eq. through CO_2 up-take and +376.1 kg CO_2-eq. due to re-emission of not captured CO_2.

Heat contributions from alternative sources in RoW and natural gas in EUR, related to catalyst production for MTO- and MeOH production processes, are minor but appear in the 2050 (PkBudg500) scenario due to the significant reduction of other impacts. Additionally, the "Rest" category decreases markedly from +2297.4 kg CO_2-eq. in 2020 to +580.4 kg CO_2-eq. in 2050 (PkBudg500).

Table 20: The values listed of the top 5 biggest GWP contributors of the H_2-to-Olefins route expressed in CO_2-eq./t ethylene for the scenarios 2020 (BASE), 2030 (BASE), 2050 (BASE) and 2050 (Pk Budg500)

	2020 (BASE) [kg CO_2-eq.]	2030 (BASE) [kg CO_2-eq.]	2050 (BASE) [kg CO_2-eq.]	2050 (PkBudg500) [kg CO_2-eq.]
Heat, other than natural gas (RoW)	---	---	---	63.2
MTO Process (CH)	---	---	---	62.6
Heat, natural gas (EUR)	---	---	---	74.9
MeOH Production Process (CH)	---	---	---	150.3
Electricity from natural gas (RS)	---	---	609.3	---
Electricity from natural gas (NO)	1102.4	582.4	---	---
Electricity from lignite (RS)	5936.7	3218.1	1021.0	---
CCU-Process	-3384.8	-3384.8	-3384.8	-3384.8
Electricity from lignite (MK)	1130.7	612.9	194.4	---
Electricity from lignite (BA)	2242.2	1215.4	385.6	---
Rest	2297.4	2120.1	1295.9	505.5
SUM	9324.7	4364.1	121.4	-2528.3

Overall, the GWP trend in the H_2+CCU-to-Olefins process aligns with Steam Cracking but exhibits a greater magnitude of reduction due to the increasing reliance on low-carbon electricity in the future acknowledging the results in the papers of Weidner et al., 2022 and Krishnan et al., 2024.

Biomass-to-Olefins

The main contributors to the GWP composition of the Biomass-to-Olefins route are biomass inputs such as bark from sawing (softwood and hardwood) in Europe without CH and RoW as well as sulfate pulp production in CH, all of which contribute negatively due to CO_2 sequestration during photosynthesis (s. **Equation 1**). Conversely, the post-treatment process in Switzerland contributes positively to the route's GWP, which is the only positive parameter listed for this route throughout the different scenarios. Among the most significant contributors to GWP, only the electricity sourced from lignite in RS is replaced by bark from sawing softwood in Europe without CH between the 2020 (BASE) and 2030 (BASE) scenarios. This change is consistently maintained in the subsequent scenarios, while all other parameters remain unchanged.

The GWP impacts of the biomass inputs remain constant across all scenarios, with bark from sawing (softwood and hardwood) in RoW and in Europe without CH as well as sulfate pulp production in CH contributing -1378.3, -586.9, -886.8, and -1439.3 kg CO_2-eq./t ethylene, respectively. The post-treatment process, which adjusts the crude syngas ratio (s. **Equation 24**) and removes acid gases, does also exhibit a consistent, but positive contribution of +2381.1 kg CO_2-eq./t ethylene stemming mainly from CO_2 removal released into air. This is true since only energy efficiency improvements are anticipated in the future (s. Chapter 3.2) and the amount of CO_2 removed from the crude syngas and released into the air does not change in future scenarios (s. Chapter 3.2).
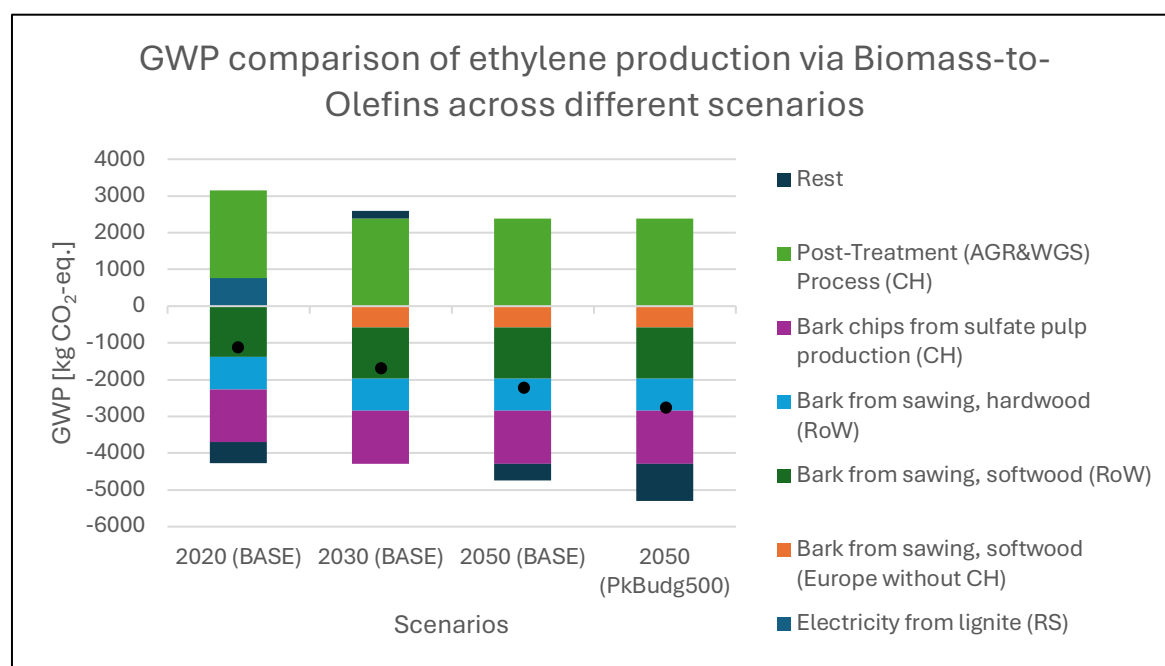
Figure 49: *Bar chart of the GWP results expressed in CO₂-eq./t ethylene of the Biomass-to-Olefins route located in Switzerland for the 2020 (BASE), 2030 (BASE), 2050 (BASE) and 2050 (PkBudg500) scenarios, incl. the top 5 GWP contributors based on **Table 21**. The black dots show the net GWP result of each scenario.*

The parameter bark from sawing, softwood in Europe without CH with a constant value of -586.9 kg CO_2-eq./t ethylene only appears from the 2030 (BASE) scenario onwards, because

in the 2020 (BASE) scenario, the GWP impact of the electricity mix, in particular the electricity source from lignite in RS, is more severe with +767.0 kg of CO_2-eq., before its impact drops under the magnitude of (-) 586.9 kg of CO_2-eq. in the 2030 (BASE) scenario.

This also explains, why the "Rest" category fluctuates between the 2020 (BASE), 2030 (BASE) and 2050 (BASE) scenario from -565.7 to +209.8 and back to -447.2 kg of CO_2-eq., respectively before it reaches its all-time low at -1000.9 kg of CO_2-eq./t ethylene in the 2050 (PkBudg500) scenario. In the 2020 (BASE) scenario, the bark from sawing, softwood in Europe without CH was included in the "Rest" contributing negatively to the "Rest's" value, while the part of the Swiss electricity mix in the form of electricity from lignite in RS was listed separately. In the 2030 (BASE) scenario, however, the electricity parameter gets replaced by the bark from sawing, softwood in Europe without CH. Under this situation, the GWP impact of electricity from lignite in RS now adds to the "Rest" value making the "Rest's" GWP value positive before it continues to decrease in future scenarios making the "Rest's" GWP value negative again. Consequently, the electricity usage is a notable positive contributor to GWP in early scenarios but diminishes over time due to greener electricity sources and reduced demand. This trend mirrors that Biomass-to-Olefins requires less amount of electricity compared to the production of captured CO_2 and electrolytic H_2, still influences the GWP result distinctively (the data and trends described in this paragraph, is also presented in **Table 21** and **Figure 49**).

Table 21: The values listed of the top 5 biggest GWP contributors of the Biomass-to-Olefins route expressed in CO_2-eq./t ethylene for the scenarios 2020 (BASE), 2030 (BASE), 2050 (BASE) and 2050 (Pk Budg500)

	2020 (BASE) [kg CO₂-eq.]	*2030 (BASE) [kg CO₂-eq.]*	*2050 (BASE) [kg CO₂-eq.]*	*2050 (PkBudg500) [kg CO₂-eq.]*
Electricity from lignite (RS)	753.4	---	---	---
Bark from sawing, softwood (Europe without CH)	---	-586.9	-586.9	-586.9
Bark from sawing, softwood (RoW)	-1378.3	-1378.3	-1378.3	-1378.3
Bark from sawing, hardwood (RoW)	-886.8	-886.8	-886.8	-886.8
Bark chips from sulfate pulp production (CH)	-1439.3	-1439.3	-1439.3	-1439.3
Post-Treatment (AGR&WGS) Process (CH)	2381.1	2381.1	2381.1	2381.1
Rest	-579.2	209.8	-447.2	-1000.9
SUM	-1149.2	-1700.5	-2357.5	-2911.1

In the 2050 (PkBudg500) scenario, the cradle-to-gate GWP results for Biomass-to-Olefins and H_2+CCU-to-Olefins are exceptionally low, at -2911.1 and -2804.4 kg CO_2-eq./t ethylene, respectively, which is why it would be interesting to look at the combustion (end-of-life) of ethylene because the results reported so far only reflect cradle-to-gate impacts. The combustion of 1 t of ethylene releases +3142.9 kg CO_2-eq. under the assumption that it will be incinerated completely at the end of life-phase (s. **Equation 33**).

Equation 33: Combustion of Ethylene

$$C_2H_4 + 3O_2 \rightarrow 2CO_2 + 2H_2O$$
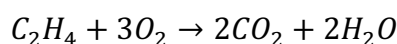
This means that the production of 1 t of ethylene by using the two novel routes Biomass-to-Olefins and H₂+CCU-to-Olefins would yield up to +231.8 and +388.5 kg of CO_2-eq./t of ethylene, respectively if the whole cradle-to-grave LCA is implemented with the supposition of no emissions occurring during the use- and end-of-life phase.

This sounds reasonable as most of the energy supplied comes from fossil-free resources in their best scenario in 2050 (PkBudg500) and carbon as feedstock is either sourced from biogenic matter as syngas or from capturing fossil CO_2 assigned to ethylene and splitting water for H_2 synthesis.

3.4.1.2   China as production location

This subchapter explains the differences of the three ethylene production processes located in China compared to the identical processes located in Switzerland.

The LCIA (s. Chapter 3.3) has shown, that the differences between ethylene production routes in Switzerland and China are most pronounced in earlier scenarios for H₂+CCU-to-Olefins and Biomass-to-Olefins routes, with GWP values converging by the 2050 (PkBudg500) scenario. Nevertheless, the Steam Cracking route between China and Switzerland does not differ significantly throughout different scenarios compared to the other two routes. That is why only the 2020 (BASE) and the 2050 (PkBudg500) scenarios of these two locations are set into contrast to one another.

Steam Cracking Route

As presented in **Figure 50** and **Table 22**, the Steam Cracking route exhibits the least variation between Switzerland and China (CN) in the 2020 (BASE) scenario: the GWP values for Switzerland and China are +1649.8 kg CO_2-eq./t ethylene and +1776.4 kg CO_2-eq./t ethylene, respectively. This slight difference persists in the 2050 (PkBudg500) scenario, with GWP values of +1465.4 kg CO_2-eq./t ethylene for Switzerland and 1544.1 kg CO_2-eq./t ethylene for China. Despite these differences, both locations share the same top five contributors to GWP with almost the same GWP amounts across scenarios, including the Steam Cracking process itself and upstream parameters affiliated to naphtha production.

Table 22: The values listed of the top 5 biggest GWP contributors of the Steam Cracking route in China expressed in CO_2-eq./t ethylene for the scenarios 2020 (BASE)and 2050 (Pk Budg500)

	2020 (BASE) [kg CO₂-eq.]	2050 (PkBudg500) [kg CO₂-eq.]
Waste natural gas, burned in production flare (GLO)	65.6	64.3
Naphtha production (IN)	164.9	164.0
Natural gas venting from natural gas production (GLO)	366.6	359.9
Steam Cracking Process (CN)	641.9	606.9
Sweet gas burned in gas turbine (GLO)	93.9	91.8
Rest	443.6	257.2
SUM	1776.4	1544.1

Yet, the location of naphtha production (India (IN) instead of Europe without CH) and the Steam Cracking process itself (CN instead of CH) are different from each other. For example, in the 2020 (BASE) scenario, these combined impacts for naphtha production amount to +702.6 kg CO_2-eq./t ethylene in Switzerland and +691.0 kg CO_2-eq./t ethylene in China, and this similarity holds in the 2050 (PkBudg500) scenario with values of +692.7 and +680.1 kg CO_2-eq./t ethylene, respectively.

This alignment reflects the GWP independence of location when it comes to ethylene production via Steam Cracking. The minor differences arise from regional variations in the "Rest" category, which is mainly composed of GWP impacts from electricity sources in the China case. As it was already observed above, the electricity mix from Switzerland has a minor GWP impact than the electricity mix from China, yet diminishes in future scenarios. Thus, the general trend of decreasing GWP values across future scenarios is observed in both locations, but at moderately different GWP levels.
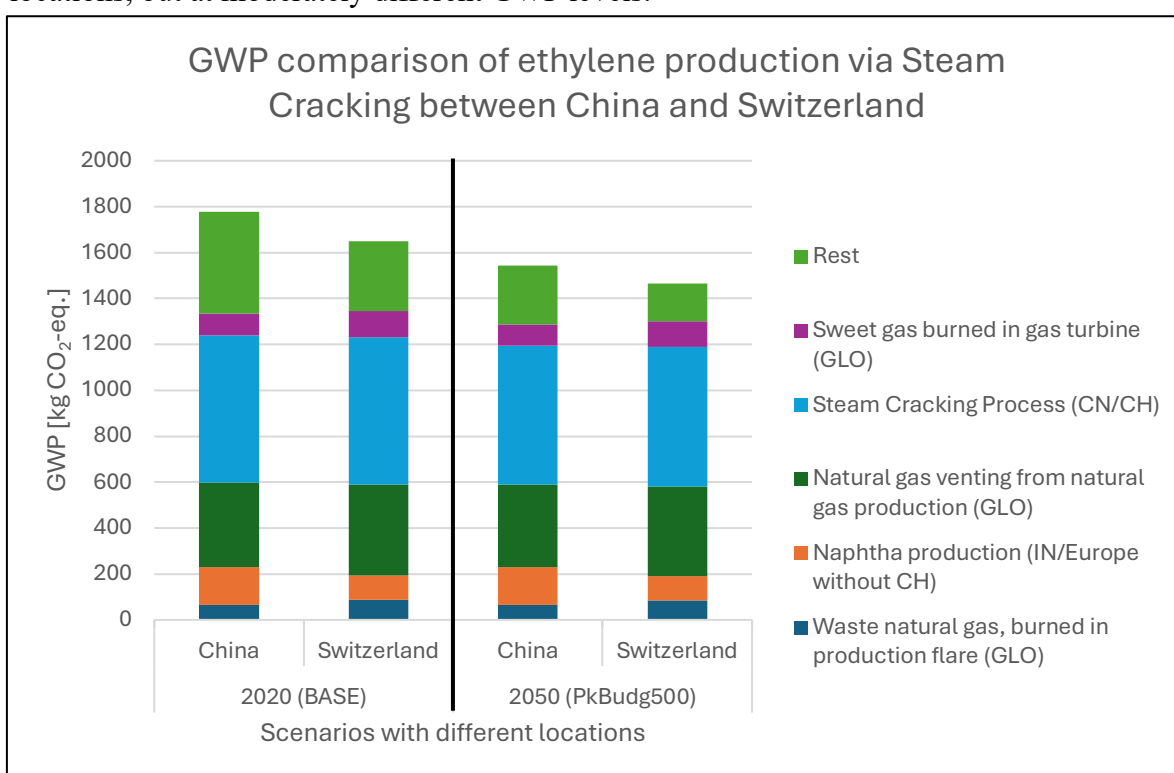
*Figure 50: Bar chart representing GWP results expressed in kg CO_2-eq./t ethylene of the Steam Cracking route for the location China and Switzerland across the 2020 (BASE) and the 2050 (PkBudg500) scenario based on **Tables 19, 22***

H₂+CCU-to-Olefins Route

Based on **Table 23** and **Figure 51**, the five biggest GWP contributors in both locations stem from different electricity sources as part of their overall electricity mix. Though in Switzerland, the top GWP contributors for this route include electricity from lignite in countries such as RS, MK and BA as well as natural gas-based electricity from NO in earlier scenarios. By contrast, in China, coal dominates the electricity mix, with the highest impacts stemming from parameters such as hard coal mine operation and preparation in CN and electricity production from hard coal in regions like Taiwan (TW), China Shangdong Sheng (CN-SD) and China Inner Mongolia (CN-NM), which contribute +4630.2, +2029.3, and +1841.0 kg CO_2-eq./t ethylene, respectively. The aggregate "Rest" category is particularly large for China in the 2020 (BASE) scenario, reaching +19313.6 kg CO_2-eq., which is more than twice as much and +740.67% higher than Switzerland's value. This is attributed to the fragmented and coal-

heavy composition of China's electricity mix (s. **Appx. Figure 1** in Appendix 6.2.1). This means that there are several impacts of coal-based electricity adding up to the "Rest" from different locations within China, which have a substantial GWP impact, but are not as influential as the top five GWP contributors.

GWP compariosn of ethylene production via H_2+CCU-to-Olefins route between China and Switzerland

Legend:
- Rest
- CO2 captured from cement plant
- Electricity from hard coal (TW)
- Electricity production from hard coal (CN-NM)
- Electricity production from hard coal (CN-SD)
- Hard Coal mine operation and preparation (CN)
- Electricity from lignite (BA)
- Electricity from lignite (MK)
- Electricity from lignite (RS)
- Electricity from natural gas (NO)
- MTO Process (CH/CN)
- MeOH Production Process (CH/CN)
- Heat, other than natural gas (RoW)

Y-axis: GWP [kg CO_2-eq.]

X-axis: Scenarios with different locations
China / Switzerland — 2020 (BASE)
China / Switzerland — 2050 (PkBudg500)

*Figure 51: Bar chart representing GWP results expressed in kg CO_2-eq./t ethylene of the H_2+CCU-to-Olefins route for the location China and Switzerland across the 2020 (BASE) and the 2050 (PkBudg500) scenario based on **Tables 20, 23**. The blue dots represent the net GWP result of each scenario with its respective location.*

Despite these stark differences in early scenarios, the GWP values for both countries converge by 2050 in the (PkBudg500) scenario. In this scenario, China's GWP is -2453.4 kg CO_2-eq./t ethylene, compared to -2386.2 kg CO_2-eq./t ethylene in Switzerland. The near parity reflects both countries' transition to greener electricity sources with higher shares of renewable energy (s. **Figure 39b, d**). There are only minor differences in their lists of biggest GWP impact contributors: while China has electricity from Biomass in China (CHA) in the list, Switzerland keeps heat, natural gas in EUR in its list in the 2050 (PkBudg500) scenario, instead. The CCU process shows consistent GWP values of -3384.8 kg CO_2-eq./t ethylene across both locations and scenarios. This uniformity is expected since the individual process's emissions, the re-emission of 10% of captured CO_2, are independent of geographic or energy-related factors.

Overall, the H₂+CCU-to-Olefins route demonstrates the greatest initial differences between Switzerland and China due to the electricity mix's significant role in this electricity-intensive route. In the 2020 (BASE) scenario, China's GWP result is significantly higher, driven by its reliance on coal-based electricity, while Switzerland benefits from an already cleaner electricity mix (s. **Figure 39a, c**). Nevertheless, this discrepancy gets vanished throughout the different scenarios, as their electricity sources align more and more with each other from a GWP perspective.

Table 23: The values listed of the top 5 biggest GWP contributors of the H₂+CCU-to-Olefins route in China expressed in CO_2-eq./t ethylene for the scenarios 2020 (BASE)and 2050 (Pk Budg500)

	2020 (BASE) [kg CO₂-eq.]	*2050 (PkBudg500) [kg CO₂-eq.]*
Electricity from Biomass (CHA)	---	88.1
Heat, other than natural gas (RoW)	---	100.3
MeOH Production Process (CN)	---	150.3
MTO Process (CH/CN)	---	62.6
Hard Coal mine operation and preparation (CN)	3328.7	---
Electricity production from hard coal (CN-SD)	2029.3	---
Electricity production from hard coal (CN-NM)	1841.0	---
Electricity from hard coal (TW)	4630.2	---
CCU-Process	-3384.8	-3384.8
Rest	19313.6	497.3
SUM	27757.9	-2486.2

Biomass-to-Olefins Route

As outlined in **Table 24** and **Figure 52**, the Biomass-to-Olefins route reveals a similar pattern of variation, with GWP differences stemming from electricity sources. The composition of the negative contributors, such as bark chips from biomass, is largely similar between the two locations but is allocated differently. For instance, in Switzerland, bark chips from sulfate pulp production in CH is prominent, while in China, the allocation shifts more to bark from sawing, softwood in RoW. This allocation difference, however, does not alter the overall GWP impact of biomass sourcing.

Table 24: The values listed of the top 5 biggest GWP contributors of the Biomass-to-Olefins route in China expressed in CO_2-eq./t ethylene for the scenarios 2020 (BASE)and 2050 (Pk Budg500)

	2020 (BASE) [kg CO₂-eq.]	*2050 (PkBudg500) [kg CO₂-eq.]*
Bark chips from sulfate pulp production (RoW)	---	-363.8
Electricity from hard coal (TW)	614.6	---
Post-treatment (WGS&AGR) process (CN)	2381.1	2381.1
Bark from sawing, softwood (RoW)	-1952.1	-1952.1
Bark from sawing, softwood (Europe without CH)	-831.3	-831.3
Bark from sawing, hardwood (RoW)	-1256.0	-1256.0
Rest	2324.1	-888.1
SUM	1280.3	-2910.3

The post-treatment process required for adjusting crude syngas composition and removing acid gases contributes identically across both locations, with a consistent GWP value of

+2381.1 kg CO_2-eq./t ethylene across all scenarios. This consistency mirrors the behavior of the CCU process in the H_2+CCU-to-Olefins route.

In the 2020 (BASE) scenario, the GWP of the "Rest" category for China is significantly higher at +2325.1 kg CO_2-eq./t ethylene, a +510.8% increase compared to Switzerland. This discrepancy arises from China's reliance on coal-based electricity. Although both locations have one electricity source individually exhibited in the 2020 (BASE) scenario (China: electricity from hard coal in TW and Switzerland: electricity from lignite in RS), the "Rest" category of China comprises more parameters of different regional electricity sources from coal, as it is the case with the H_2+CCU-to-Olefins route. These parameters have higher GWP impacts than the different electricity sources from the Swiss electricity mix.

As with the other routes, the 2050 (PkBudg500) scenario shows nearly identical GWP values for Switzerland and China, attributed to the convergence of electricity mixes (s. **Figure 39b, d**). Both countries achieve significantly lower overall GWP impacts, driven by reduced reliance on high-emission electricity and the incorporation of more sustainable energy sources.
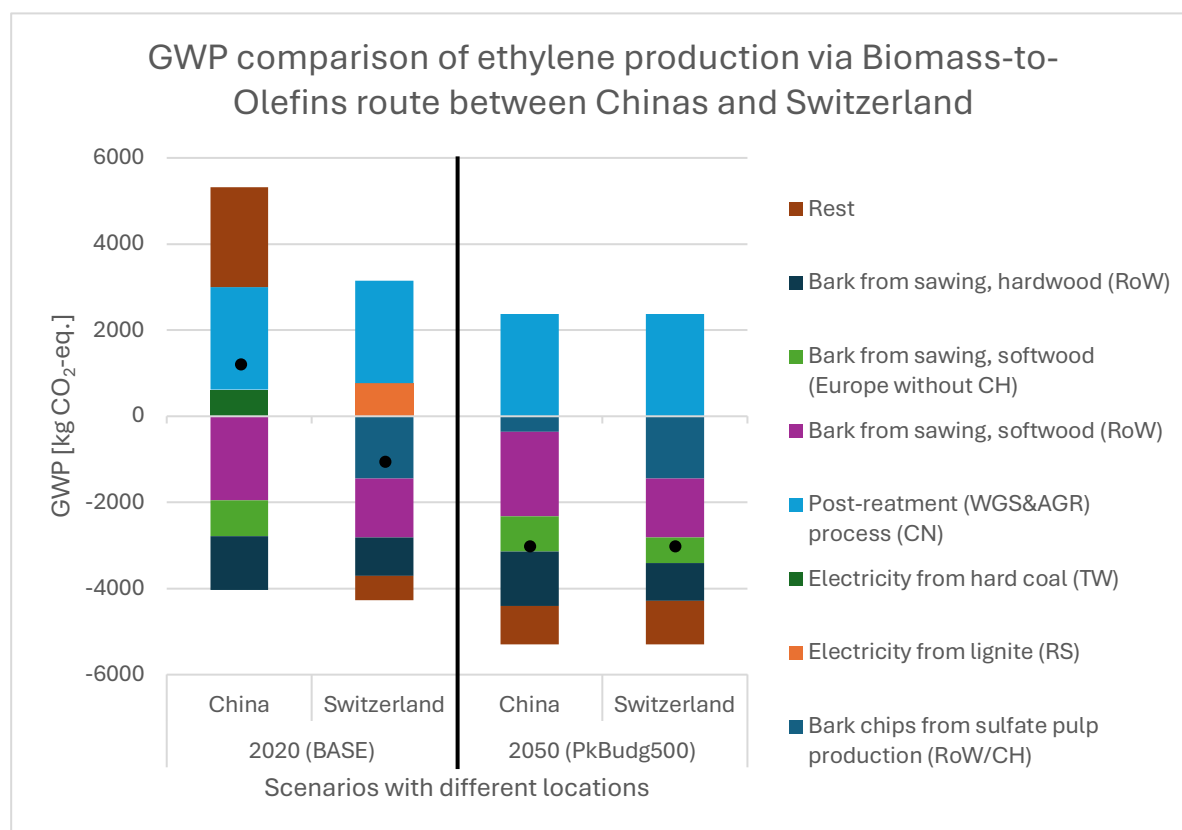
*Figure 52: Bar chart representing GWP results expressed in kg CO₂-eq./t ethylene of the Steam Cracking route for the location China and Switzerland across the 2020 (BASE) and the 2050 (PkBudg500) scenario based on **Tables 21, 24**. The black dots represent the net GWP results of each scenario with its respective location.*

Bottom line, the differences between the Swiss and Chinese ethylene production routes are most evident in the early scenarios, driven by China's dependence on coal-dominated electricity. These differences diminish in the 2050 (PkBudg500) scenario as both countries adopt similar greener electricity mixes. While the Steam Cracking route shows the smallest variation between the two locations, the H_2+CCU-to-Olefins route highlights the significant impact of electricity composition, particularly die electricity-intensive nature. The Biomass-to-Olefins route, although less dependent on electricity, still reflects regional disparities in electricity mix between these two locations. Overall, electricity emerges as the dominant driver

of GWP differences, underscoring the importance of transitioning to renewable energy sources to achieve consistent and sustainable production outcomes globally.

3.4.2 Process Modifications
Steam Cracking Modifications
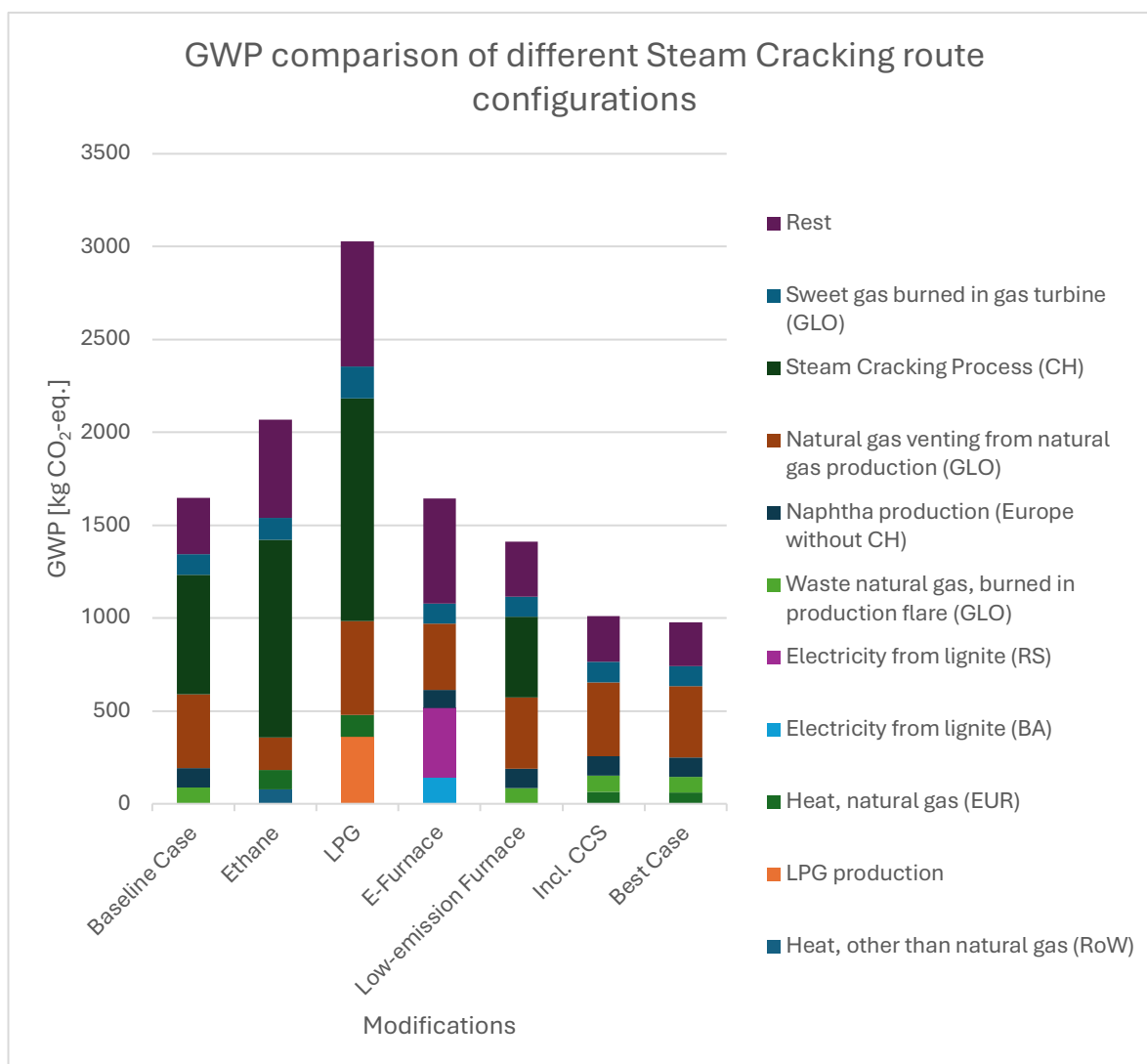
*Figure 53: Bar chart representing GWP results expressed in kg CO₂-eq./t ethylene of the different Steam Cracking route configurations for Switzerland in the 2020 (BASE) scenario based on **Table 25***

According to **Figure 53** and **Table 25**, Steam cracking with LPG as feedstock demonstrates the highest GWP impact among the modifications, with a value of +3030.1 kg CO₂-eq./t ethylene. In contrast, the best-performing scenario involves a combination of naphtha as feedstock, CCS and a low-emission furnace, achieving a GWP of +976.9 kg CO₂-eq./t ethylene, which is a reduction of -40.8% compared to the baseline case. This stark contrast highlights the role of process modifications and feedstock choices in mitigating emissions.

The GWP impact for the Steam Cracking process is higher in the LPG and ethane modifications with +2067.8 and +3030.1 kg CO₂/t ethylene, respectively compared to the baseline scenario with naphtha as feedstock. Differences in product distribution influencing AFs drive these variations. The allocation factor for LPG (0.6552) and ethane (0.5827) are significantly higher than for naphtha (0.3513) (s. **Appx. Table 2, 3** in Appendix 6.1.1). This means that a

larger proportion of the emissions generated during the Steam Cracking process is attributed to ethylene production in LPG and ethane cases, leading to higher GWP values.

Table 25: The values listed of the top 5 biggest GWP contributors of the Steam Cracking route including different configurations in Switzerland expressed in CO$_2$-eq./t ethylene for the scenario 2020 (BASE)

	Baseline [kg CO$_2$-eq.]	Ethane [kg CO$_2$-eq.]	LPG [kg CO$_2$-eq.]	e-furnace [kg CO$_2$-eq.]	Low-emission furnace [kg CO$_2$-eq.]	CCS [kg CO$_2$-eq.]	Best Case [kg CO$_2$-eq.]
Heat, other than natural gas (RoW)	---	76.0	---	---	---	---	---
LPG production			360.0	---	---	---	
Heat, natural gas (EUR)	---	105.1	118.0	---	---	63.5	61.4
Electricity from lignite (BA)	---	---	---	141.4	---		---
Electricity from Ignite (RS)	---	---	---	374.4	---	---	---
Waste natural gas, burned in production flare (GLO)	86.8	---	---	---	84.0	86.8	84.0
Naphtha production (Europe without CH)	106.8	---	---	96.3	103.4	106.8	103.4
Natural gas venting from natural gas production (GLO)	396.7	177.4	507.4	359.7	384.2	396.7	384.2
Steam Cracking Process (CH)	641.9	1064.6	1197.1	---	435.1	---	---
Sweet gas burned in gas turbine (GLO)	112.3	118.0	170.5	105.0	108.8	112.3	108.8
Rest	304.2	526.6	677.1	565.7	294.6	243.3	234.9
SUM	1648.8	2067.8	3030.1	1642.5	1410.2	1009.4	976.8

Across different feedstocks, notable variations also emerge in upstream production processes. For example, LPG production has a significantly higher GWP impact with +360.0 kg CO$_2$-eq. compared to naphtha with +106.8 kg CO$_2$-eq., while ethane production does not appear in the top five contributors, at all. Upstream processes such as global natural gas venting, global sweet gas combustion in gas turbines or heat from natural gas in EUR and other sources in RoW also vary in their impact depending on the feedstock. Among the feedstocks, it can be concluded that ethane production demonstrates the lowest GWP, followed by naphtha, with LPG exhibiting the highest GWP.

In the low-emission furnace modification, the GWP impact of the Steam Cracking process is reduced relative to the baseline scenario due to improved fuel efficiency by -14.5% to +1410.2 kg CO$_2$-eq./t ethylene. This efficiency minimizes fuel consumption and reduces

combustion-related emissions, including CO_2, N_2O, $PM_{2.5}$, and VOCs. Consequently, the emissions footprint of the process is notably lower. Additionally, if less methane as fuel is required, then more methane serves as co-product, which in turn lowers the AF of this process to 0.3402 (s. **Appx. Table 4** in Appendix 6.1.1). Hence, less of the emission are allocated to this process.

When considering the modification with CCS and the best case, the Steam Cracking process is not featured in the top five GWP contributors. This is because most emissions, predominantly CO_2, are captured and stored underground, declining their contribution to the GWP to negligible. Indeed, CCS exhibits the biggest single GWP decrease by -38.9% to +1009.4 kg CO_2-eq./t ethylene across all other modifications although if combined with low-emission furnace, an even greater reduction can be accomplished of -40.8% to 976.8 kg CO_2-eq./t ethylene, which goes along with the outcomes in the paper of Bisinella et al., 2021.

The e-furnace modification is unique across all configurations as it eliminates the GWP impact of the Steam Cracking process related to the fuel combustion entirely. Instead of fuel combustion, which generates emissions such as CO_2, N_2O, $PM_{2.5}$, and VOCs, this modification uses external electricity as the energy source. This burden shift is evident in the contribution diagram, where the GWP impact of specific shares of Switzerland's electricity mix – such as electricity from lignite in BA/RS – appears in the top five GWP contributors, while the Steam Cracking processes disappears. In addition, the AF of ethylene is with 0.3168 smaller, because all methane is accounted as co-product instead of fueling the firebox (s. **Appx. Table 5** in Appendix 6.1.1). Still, the GWP impact of the e-furnace remains almost the same as the baseline case with +1642.5 CO_2-eq./t ethylene because the avoidance of emissions is offset by the additional carbon-intensive electricity.

Finally, variations in the "Rest" category across the modifications reflect differences in residual contributions from secondary sources not explicitly categorized within the top contributors.

Biomass-to-Olefins Modifications

The GWP of the baseline Biomass-to-Olefins case, which uses bark chips as feedstock, can be reduced significantly through process integration by -80.2% to -2071.3 kg CO_2-eq./t ethylene. Integration leads to the elimination of impacts such as electricity from lignite in RS from the top five contributors. This outcome is intuitive, as waste heat generated during the process is reintegrated into the system, reducing the need for external heat supplied by electricity.

When CCS is applied to the baseline biomass scenario, the GWP impact of the post-treatment process is even more reduced by -198.7% to -3432.7 kg CO_2-eq./t ethylene than in the integrated process design case, which substantiates the findings in the paper of Sammarchi et al., 2021. The CO_2 emissions separated from the product stream via the Rectisol® process can now be compressed and stored underground rather than released into the atmosphere. This modification lowers the overall GWP substantially.

Feedstocks such as wood chips and miscanthus perform better than bark chips in terms of GWP with impacts of -1754.2 and -1254.7 kg CO_2-eq./t ethylene, respectively. This improvement arises because these feedstocks require a larger quantity to produce the same amount of syngas necessary for MeOH production.

The best-case configuration, which combines wood chips with CCS and process integration, achieves the lowest GWP value of -4959.8 kg CO_2-eq./t ethylene – an extraordinary reduction

of -331.6% compared to the baseline case. This quite negative GWP score is observed due to the biogenic carbon sequestration effects of CCS, while sawlogs and veneer logs in CH appear as one of the five biggest contributor parameters, replacing the post-treatment process parameter eliminated by CCS. Furthermore, the integration process reduces electricity consumption, as evidenced by the reduced GWP impact of electricity from lignite in RS, which is not listed und er the top five parameters anymore (the whole section is graphically expressed in **Figure 54** and based on data from **Table 26**).
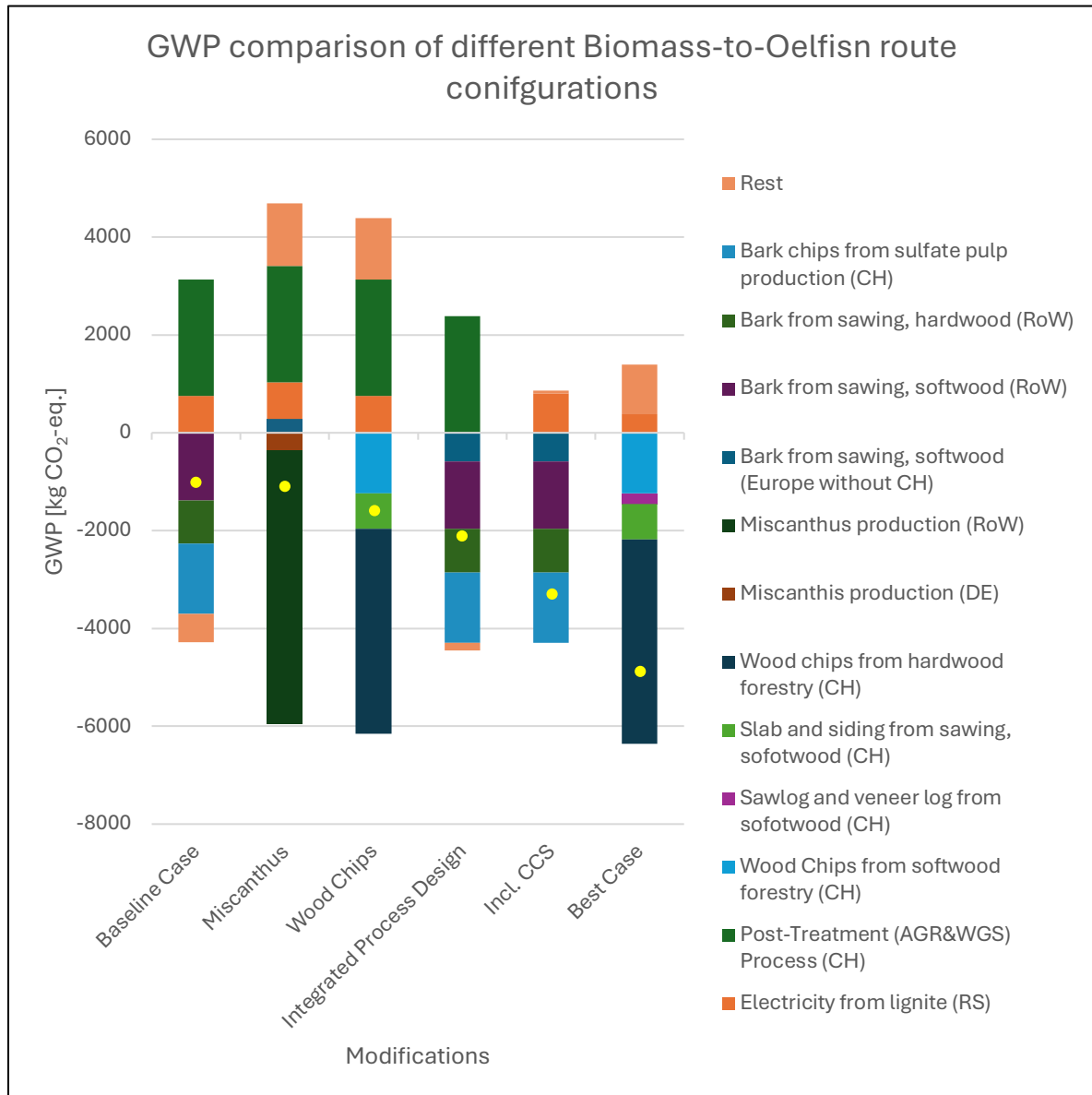
***Figure 54:** Bar chart representing GWP results expressed in kg CO₂-eq./t ethylene of the different Biomass-to-Olefins route configurations for Switzerland in the 2020 (BASE) scenario based on **Table 26**. The yellow dots represent the net GWP result for each Biomass-to-Olefin case.*

Table 26: The values listed of the top 5 biggest GWP contributors of the Biomass-to-Olefins route including different configurations in Switzerland expressed in CO₂-eq./t ethylene for the scenario 2020 (BASE)

	Baseline [kg CO₂-eq.]	Miscanthus [kg CO₂-eq.]	Wood Chips [kg CO₂-eq.]	Integrated Process Design [kg CO₂-eq.]	CCS [kg CO₂-eq.]	Best Case [kg CO₂-eq.]
Electricity from lignite (BA)	---	281.9	---	---	---	---
Electricity from lignite (RS)	753.4	746.4	749.7	---	801.5	377.7
Post-Treatment (AGR&WGS) Process (CH)	2381.1	2381.1	2381.1	2381.1	---	---
Wood Chips from softwood forestry (CH)	---	---	-1242.5	---	---	---
Sawlog and veneer log from softwood (CH)	---	---	---	---	---	-208.8
Wood Chips from softwood forestry (CH)	---	---	---	---	---	-1242.5
Slab and siding from sawing, softwood (CH)	---	---	-725.6	---	---	-725.6
Wood chips from hardwood forestry (CH)	---	---	-4180.4	---	---	-4180.4
Miscanthus production (DE)	---	-359.9		---	---	---
Miscanthus production (RoW)	---	-5587.4	---	---	---	---
Bark from sawing, softwood (Europe without CH)	---	---	---	-586.9	-586.9	---
Bark from sawing, softwood (RoW)	-1378.3	---	---	-1378.3	-1378.3	---
Bark from sawing, hardwood (RoW)	-886.8	---	---	-886.8	-886.8	---
Bark chips from sulfate pulp production (CH)	-1439.4	---	---	-1439.4	-1439.4	---
Rest	-579.2	1283.2	1263.5	-161.1	57.2	1019.7
SUM	-1149.2	-1254.7	-1754.2	-2071.3	-3432.7	-4959.8

H$_2$+CCU-to-Olefins Modifications

As it can be observed in **Figure 55** and **Table 27**, the modifications to the H$_2$+CCU-to-Olefins process are relatively straightforward, as the top five parameters contributing the most to the GWP remain consistent across all process modifications. A key observation is that the amount of carbon captured from the cement plant remains constant across different configurations at -3384.8 kg CO$_2$-eq. This is logical, as the volume of emissions captured is independent of process-specific variations.

Among the modifications, the DAC case stands out as, with a GWP impact of +10013.3 kg CO$_2$-eq./t ethylene, the only one with a higher GWP than the baseline case. This increase is primarily attributed to the significantly higher electricity demand of the DAC plant compared to the PSC plant from 0.5348 kWh/kg captured CO$_2$ to 1.0172 kWh/kg captured CO$_2$). This trend is supported by higher GWP contributions across all types of electricity sources in the DAC scenario.
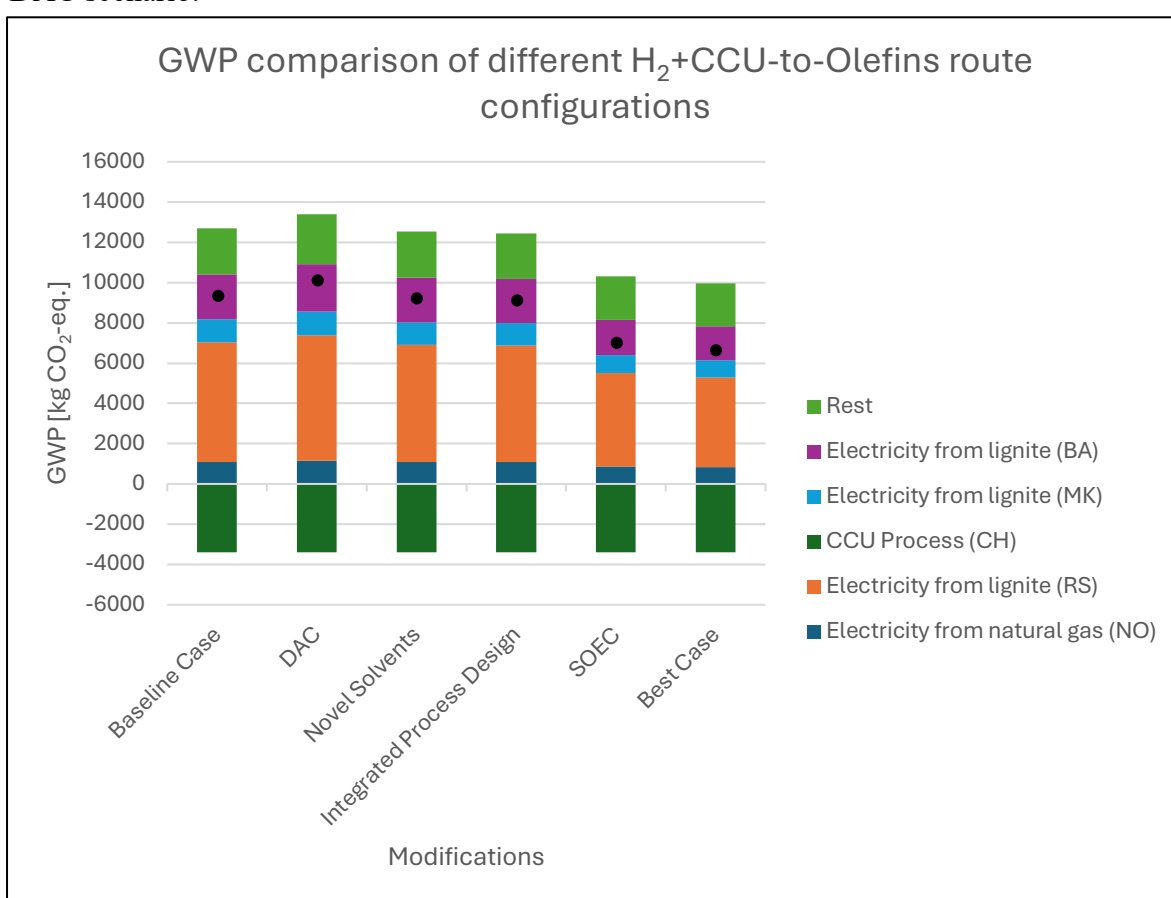
Figure 55: *Bar chart representing GWP results expressed in kg CO$_2$-eq./t ethylene of the different H$_2$+CCU-to-Olefins route configurations for Switzerland in the 2020 (BASE) scenario based on **Table 27**. The black dots represent the net GWP result of each H$_2$+CCU-to-Olefins case.*

In contrast, the novel solvents, integrated process design, and SOEC cases exhibit the opposite trend, reducing GWP relative to the baseline to +9144.7, +9072.4 and +6926.7 kg CO$_2$-eq./t ethylene, respectively. The reductions for the novel solvent and integrated process design case are similarly linked to improvements in the electricity consumption of the CCU-PSC system. The novel solvents decrease the electricity needed for MEA solvent regeneration due to their chemical properties and the integrated process supplies waste heat from other processes lowering the external electricity input. However, the Integrated Process Design modification achieves greater GWP reductions than the Novel Solvents case: While the Novel

Solvents configuration reduces the GWP impact by approximately -1.9%, the Integrated Process Design modification achieves even greater reduction of -2.7%.

The SOEC case demonstrates the greatest GWP reduction potential of -25.7% among all other single modifications. This is true because SOEC technology significantly decreases the electricity burden associated with hydrogen production, a finding that aligns with Chapter 3.4.1 and corroborates evidence reported in the paper of Bareiß et al., 2019 (s. Chapter 2.1). When these three modifications – novel solvents, integrated process design, and SOEC – are combined as best-case configuration, they synergistically achieve the lowest GWP score with +6566.2 kg CO_2-eq./t ethylene of all scenarios, a reduction of -29.6%. This outcome is both intuitive and expected, as the combined effects of these modifications address multiple emissions sources and inefficiencies, leading to a substantial overall reduction in environmental impact.

Table 27: The values listed of the top 5 biggest GWP contributors of the H₂+CCU-to-Olefins route including different configurations in Switzerland expressed in CO₂-eq./t ethylene for the scenario 2020 (BASE)

	Base [kg CO₂-eq.]	DAC [kg CO₂-eq.]	Novel Solvents [kg CO₂-eq.]	Integrated Process Design [kg CO₂-eq.]	SOEC [kg CO₂-eq.]	Best [kg CO₂-eq.]
Electricity from natural gas (NO)	1102.4	1154.4	1083.9	1079.0	863.4	830.3
Electricity from lignite (RS)	5936.7	6216.5	5837.0	5810.6	4649.6	4471.0
CCU Process (CH)	-3384.8	-3384.8	-3384.8	-3384.8	-3384.8	-3384.8
Electricity from lignite (MK)	1130.7	1183.9	1111.7	1106.6	885.5	851.5
Electricity from lignite (BA)	2242.2	2347.9	2204.6	2194.6	1756.1	1688.6
Rest	2297.4	2495.5	2292.4	2266.4	2156.9	2109.7
Sum	9324.7	10013.3	9144.7	9072.4	6926.7	6566.2

3.5   Sensitivity Analysis

This chapter identifies key parameters that, when altered, significantly impact the GWP of different olefin production routes. For each of the three processes examined, specific data sets are applied to individual stages while other parameters remain constant.

3.5.1 Steam Cracking Route

The life cycle interpretation reveals that variations in Steam Cracking's location have minimal influence on the GWP of the Steam Cracking route (s. Chapter 3.4.1). Neither the sourcing of naphtha nor electricity use plays a substantial role in this pathway's GWP. As a result, the analysis focuses on the source of steam used in the process, as shown in the Sankey Diagram in the Appendix (s. **Appx. Figure 2** in Appendix 6.2.2). Three alternative steam sources are considered:

- Product: steam, in chemical industry; activity: polyethylene production, low density, granulate; location: Europe
- Product: steam, in chemical industry; activity: maleic anhydride production by catalytic oxidation of benzene; location: Europe
- Product: steam, in chemical industry; activity: market for steam, in chemical industry; location: Europe

The results show that even changing the steam source only reduces GWP marginally (s. **Figure 56**). Using steam from maleic anhydride production decreases GWP by -6.8% to +1537.5 kg CO_2-eq./t ethylene, while steam from polyethylene production lowers it by -8.3% to +1511.7 kg CO_2-eq./t ethylene (s. **Figure 56**).

In conclusion, the Steam Cracking route is robust against changes in steam sources. Even though feedstock, steam and energy contribute significantly to the overall GWP, their variations do not substantially affect the results, regardless of geographical location.
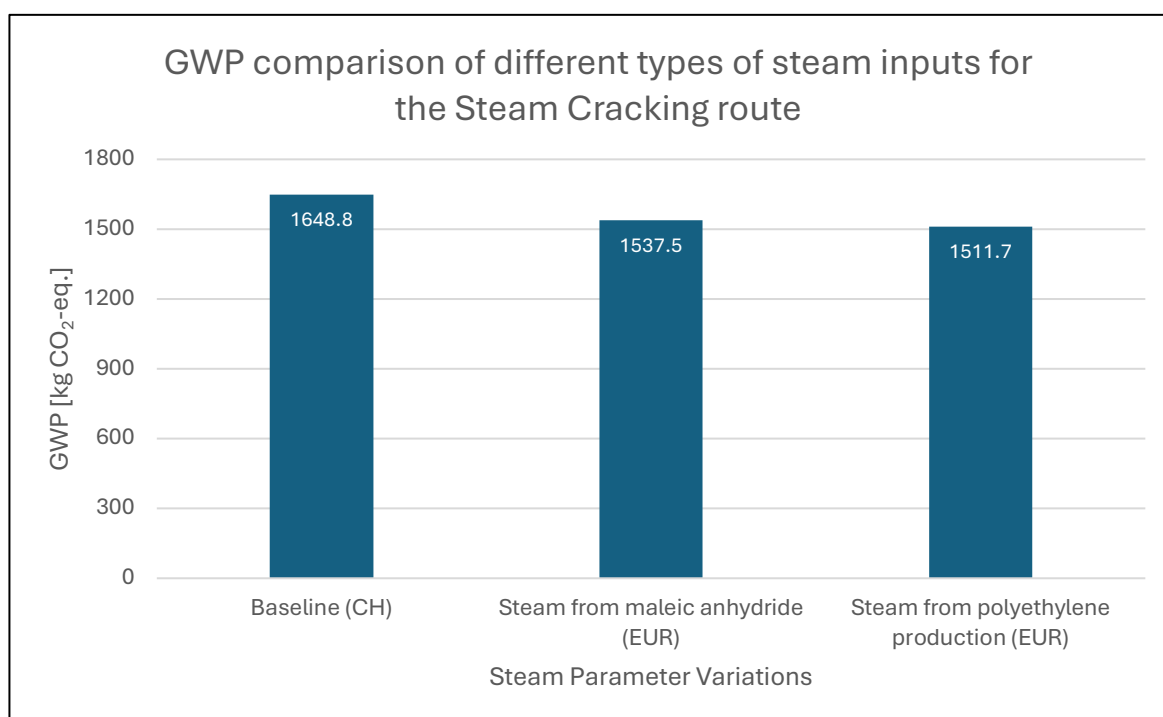
Figure 56: Bar chart of GWP comparison of the Steam Cracking route with different types of Steam expressed in CO_2-eq./t ethylene for Switzerland in the 2020 (BASE) scenario

3.5.2 H_2+CCU-to-Olefins Route

The H_2+CCU-to-Olefins route demonstrates high sensitivity to the electricity source, as highlighted in the life cycle interpretation (s. Chapter 3.4.1). This sensitivity stems from the significant electricity demand required to operate processes like hydrogen production and CO_2 capture. For this analysis, three electricity mixes are evaluated:

- Product: electricity, high voltage; activity: electricity production, hard coal; location: Germany (DE)
- Product: electricity, low/medium voltage; activity: market group for electricity, low/medium voltage; location: CH
- Product: electricity, medium/low voltage; activity: electricity, medium/low voltage, residual mix; location: CH

Although high-voltage electricity from Germany is the only available data set for coal electricity, the difference in GWP between voltage levels is minimal, as only transformation losses are excluded.
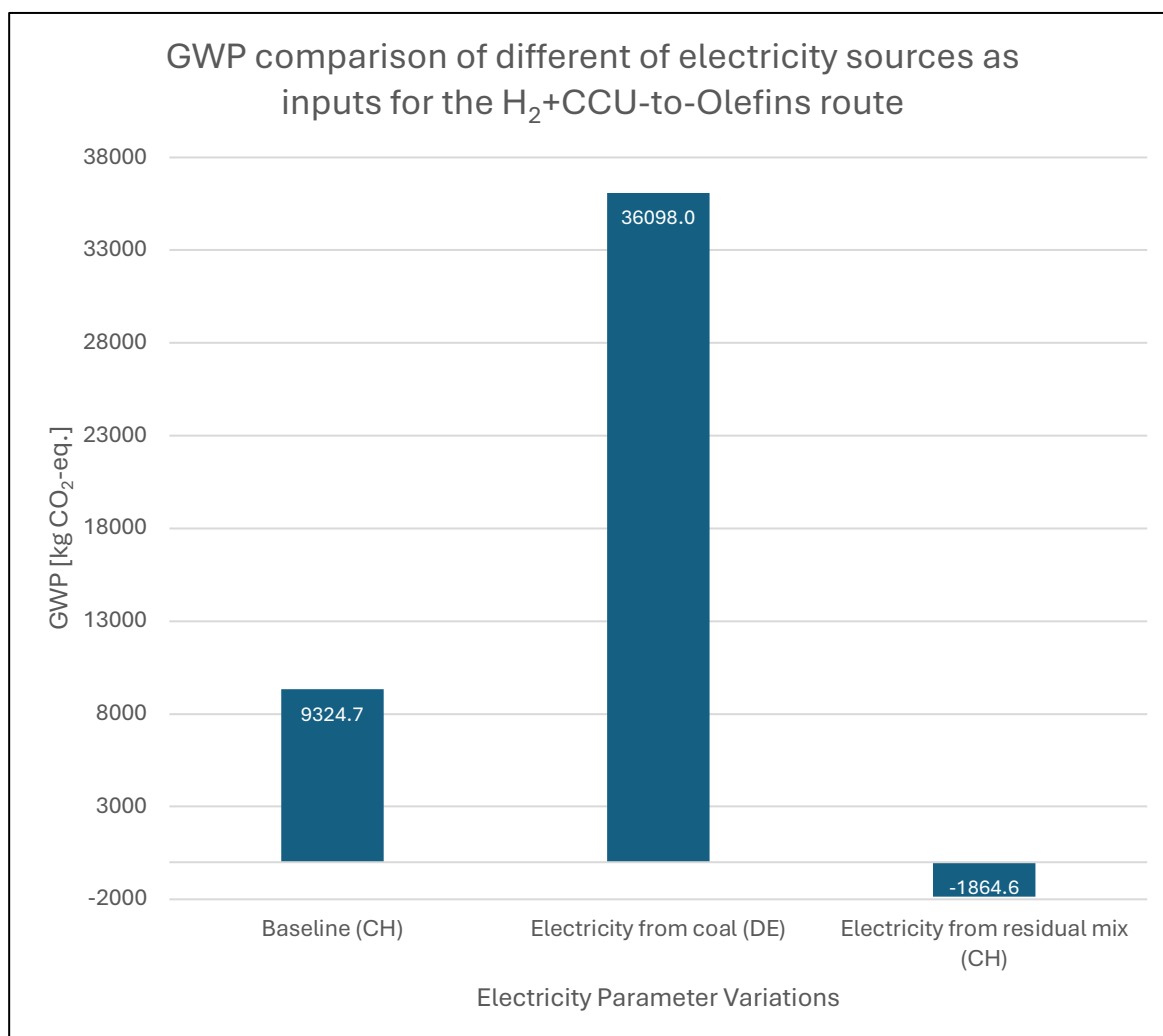
Figure 57: Bar chart of GWP comparison of the H_2+CCU-to-Olefins route with different electricity sources expressed in CO_2-eq./t ethylene for Switzerland in the 2020 (BASE) scenario

The results reveal stark contrasts in GWP outcomes based on electricity source. Switching to Switzerland's residual electricity mix results in a significant -120.0% reduction, lowering GWP from +9324.7 to -1864.6 kg CO_2-eq./t ethylene (s. **Figure 57**). Conversely, adopting coal-based electricity from Germany leads to a +287.1% increase in GWP, from +9324.7 to

+36098 kg CO_2-eq./t ethylene (s. **Figure 57**). These findings underscore the substantial influence of electricity sourcing on the overall environmental performance of this route.

3.5.3 Biomass-to-Olefins Route

The Biomass-to-Olefins route follows a similar trend to the H_2+CCU-to-Olefins pathway, as both are electricity-intensive processes. While the Biomass-to-Olefins route requires less electricity due to reduced demand in sweet syngas production compared to hydrogen production and CO_2 capture, the electricity source still significantly impacts GWP outcomes. The same three electricity mixes analyzed in Chapter 3.5.2 are applied here, as well:

- Product: electricity, high voltage; activity: electricity production, hard coal; location: DE
- Product: electricity, low/medium voltage; activity: market group for electricity, low/medium voltage; location: CH
- Product: electricity, medium/low voltage; activity: electricity, medium/low voltage, residual mix; location: CH

The results align with those observed for the H_2+CCU-to-Olefins route. Using Switzerland's residual electricity mix further reduces the GWP of this route by -62.3%, from -1149.2 to -1864.6 kg CO_2-eq./t ethylene (s. **Figure 58**). Conversely, coal-based electricity from Germany dramatically increases the GWP by +316.5%, rising from -1149.2 to +2487.6 kg CO_2-eq./t ethylene (s. **Figure 58**).
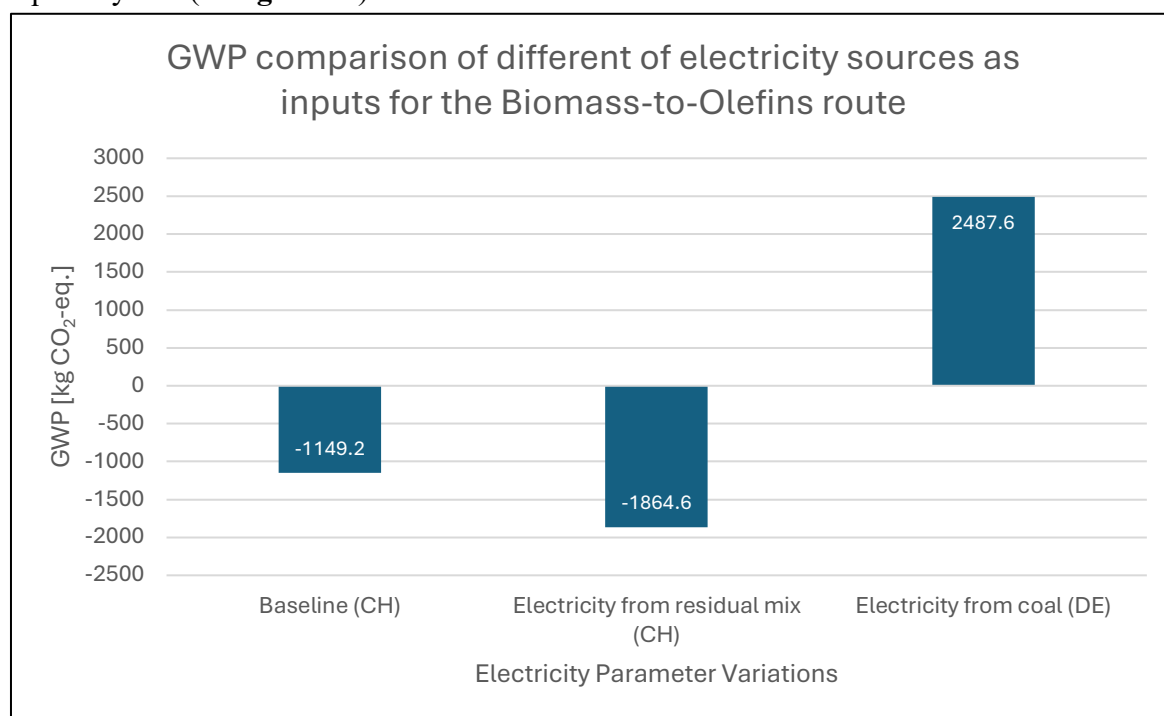
Figure 58: Bar chart of GWP comparison of the Biomass-to-Olefins route with different electricity sources expressed in CO_2-eq./t ethylene for Switzerland in the 2020 (BASE) scenario

These findings reinforce the significant role of electricity sources in determining the overall GWP for electricity-intensive routes like Biomass- and H_2+CCU-to-Olefins. The results highlight the critical need to prioritize low-carbon electricity sources to achieve meaningful reductions in environmental impact, which reaffirms the conclusion made in the paper of Liu et al., 2024.

4. Conclusion and Outlook

4.1 Summary

Recent catastrophic floods in Valencia highlight the IPCC's warnings that failing to urgently mitigate the Anthropogenic Climate Change, driven by GHG emissions from unsustainable practices, will lead to increasingly frequent and severe extreme weather events with significant socioeconomic impacts. The petrochemical industry, heavily reliant on fossil fuels for energy and feedstock supply, is a major contributor to these emissions but remains locked into carbon-intensive practices. Ethylene, a key petrochemical product with high production volumes and diverse applications, serves as a case study for addressing these challenges.

The reviewed literature highlights that low-carbon pathways offer notable environmental improvements from a GHG perspective, especially under future scenarios with increased reliance on renewable energy. However, these technologies face significant challenges which is why this study employs prospective Life Cycle Assessments to compare climate related GWP impacts of the conventional Steam Cracking process with two innovative low-carbon pathways based on the MTO production process. These pathways derive MeOH either from direct CO_2 hydrogenation with electrolytic hydrogen or from pretreated syngas from biomass gasification, both incorporating promising low-carbon technologies. The analysis evaluates these routes under a cradle-to-gate perspective across different scenarios built on Integrated Assessment Models (2020 (BASE), 2030 (BASE), 2050 (BASE), 2050 (PkBudg500)), geographies (China and Switzerland) and process modifications, exploring their potential to break the sector's carbon lock-in while also considering various feedstock and several state-of-the-art technology configurations. Economic Allocation is used to account for co-products, and a Sensitivity Analysis identifies the key factors influencing overall results.

To conduct these different LCAs, it is an imperative to define and explain the LCA system boundaries, providing extensive descriptions, chemical equations and process schematics, which serve as basis for specific in- and outputs summarized in the respective LCI tables giving the reader a more comprehensive understanding of each route.

The conventional Steam Cracking process serves as the baseline case, covering pre-heating, high-temperature cracking, subsequent scrubbing and distillation steps, using naphtha as feedstock. Modifications to this baseline included replacing conventional furnaces with low-emission or e-furnaces reducing the fuel demand, incorporating other pre-dominant cracking feedstocks (LPG and ethane) and integrating CCS to capture and store CO_2 emissions in geological formations.

For the novel pathways, the H2+CCU-to-Olefins route involves MeOH production of electrolytic hydrogen via PEMEC suitable for fluctuating renewable energy and CO_2 captured from cement plants using regeneratable MEA solvents as industrial benchmark technology. Process configurations included replacing low-temperature PEMEC with high-temperature SOEC with higher energy efficiency, deploying carbon capture solvents with smaller energy penalties and substituting point-source capture with DAC following the *Climeworks* technology as alternative carbon capture technology. Nevertheless, the captured CO_2 is always assigned to the ethylene product in both cases. The Biomass-to-Olefins route begins with gasifying bark chips to produce crude syngas, followed by post-treatment to remove acid impurities and adjust gas composition of CO, CO_2 and H_2 for MeOH synthesis. Process

modifications included feedstock alternatives like miscanthus and wood chips and employing CCS at the post-treatment stage. Furthermore, energy integration was applied in both routes to reduce demand, leveraging improvements in the post-treatment stage for the Biomass-to-Olefins route and optimizing CCU in the H_2+CCU-to-Olefins route. After MeOH precursor production, both routes utilize a *Lurgi* reactor for MeOH synthesis employing an $Al_2O_3/MgO/ZnO/CuO$ catalyst and finally, a fluidized bed reactor with a highly selective SAPO-34 catalyst for converting MeOH to ethylene during the MTO process.

The future scenarios were implemented two-fold: On the one hand, Integrated Assessment Models scenarios from REMIND were integrated adjusting respective energy mixes accordingly. On the other hand, efficiency improvements were anticipated for future years based on literature.

The prospective cradle-to-gate Life Cycle Impact Assessment and Interpretation of ethylene production pathways across the four scenarios reveals that the Biomass-to-Olefins route achieves the best GWP performance, with cradle-to-gate GWP values as low as -2910 kg CO_2-eq./t ethylene in the 2050 (PkBudg500) scenario attributed to the CO_2 sequestration properties of biomass. Electricity, initially a noticeable positive GWP contributor of the Biomass-to-Olefins route, diminishes in impact over time due to the integration of renewable sources and energy efficiency measures, which is the main driver of GWP reduction from the 2020 (BASE) to the 2050 (PkBudg500) scenario. While the H_2+CCU-to-Olefins route starts with the highest GWP scores of all three routes, its GWP performance improves significantly over time due to the decarbonization of electricity grids, eventually surpassing the conventional Steam Cracking route. The Steam Cracking route only exhibits minor GWP enhancements due to its reliance on the fossil feedstock upstream chain and mature technology.

In earlier scenarios, all pathways perform better in Switzerland compared to China, largely due to Switzerland's more renewable-dominated energy mix, which is a key determinant for both novel ethylene production routes. However, global electricity decarbonization in the 2050 (PkBudg500) scenario eliminates these disparities, leading to convergent GWP values for both locations. Despite these geographic differences, the Biomass-to-Olefins route consistently delivers superior environmental performance from a GWP viewpoint.

Process modifications yield moderate GWP reductions in most cases. For Steam Cracking, incorporating low-emission furnace and CCS reduces GWP, especially from the Steam Cracking process itself, by up to 40% from +1648.8 to +976.8 kg CO_2-eq./t ethylene although the naphtha-related upstream activities remain dominant GWP contributors, accounting between 40 to almost 70% of the total GWP impact depending on the configuration. These limitations highlight the need for alternative feedstocks or entirely new production pathways although technological improvements contribute to lower GWP by reducing or capturing combustion-related emissions of the Steam Cracking process. These emissions can be reduced to a negligible level in the best-case scenario, while e-furnaces eliminate combustion emissions entirely, yet shifting the environmental burden to electricity consumption.

In the Biomass-to-Olefins route, changing feedstocks to miscanthus or wood chips, implementing CCS at the post-treatment process stage and adopting integrated process designs by recycling heat waste enhance GWP performance, with the best-case configuration achieving a GWP reduction of close to -340%, reaching -4959.8 kg CO_2-eq./t ethylene compared to -

1149.2 kg CO_2-eq./t ethylene in the baseline case. The CCS of biogenic CO_2 during the post-treatment process stage, substantially reduces its GWP impact.

In the H_2+CCU-to-Olefins route, replacing PEMEC with SOEC, using advanced carbon capture solvents, and optimizing process designs can reduce electricity consumption and hence, GWP by up to -30%, lowering impacts from +9324.7 to +6566.2 kg CO_2-eq./t ethylene in the best-case scenario. In contrast, the DAC configuration performs worse than the baseline case due to higher electricity demands than PSC. GWP reductions for this route are largely driven by the decarbonization of electricity grids and a more efficient use of electricity, especially for the hydrogen production. This is evident since the SOEC configurations exhibits the biggest individual reduction potential of all other H_2+CCU-to-Olefins configurations and the biggest GWP contributors are mainly composed of different electricity sources throughout different process modifications.

By the 2050 PkBudg500 scenario, cradle-to-gate GWP values for Biomass-to-Olefins and H_2+CCU-to-Olefins reach exceptionally low levels of -2911.1 and -2804.4 kg CO_2-eq./t ethylene, respectively. When considering cradle-to-grave emissions, assuming no emissions during the use phase and complete combustion at end-of-life, net GWP values remain low, ranging from +231.76 to +388.46 kg CO_2-eq./t ethylene. These results highlight their feasibility as low-carbon alternatives.

Key insights from this analysis underscore the critical importance of feedstock selection, electricity source and technological advancements in achieving substantial GWP reductions. While feedstocks and process-specific efficiencies play crucial roles, the alignment of energy systems with renewable sources is fundamental to minimizing GWP impacts for these two novel routes, which is highlighted once more in the Sensitivity Analyses. Contrarily, the Steam Cracking route shows relative insensitivity to changes of its biggest GWP contributors. Nonetheless, applying CCS to the Steam Cracking and the Biomass-to-Olefins route can substantially decrease their GWP impact.

4.2   Conclusion

In light of the accelerating impacts of Anthropogenic Climate Change, the development of novel production pathways for large-volume chemicals heavily reliant on fossil resources, such as ethylene, is imperative. These alternatives must demonstrate superior environmental performance compared to conventional routes. This Master Thesis contributed to it by assessing two innovative production routes for manufacturing the large-volume chemical ethylene via MTO technology compared to the conventional Steam Cracking route from a cradle-to-gate p-LCA perspective considering only GWP impacts.

Among the scenarios and different process configurations evaluated, these are the most important take-home messages:

- The Biomass-to-Olefins route consistently outperforms the conventional Steam Cracking and the H_2+CCU-to-Olefins route across different scenarios and locations from a GWP perspective mainly due to its CO_2 sequestration properties.
- The H_2+CCU-to-Olefins route's GWP performance extremely relies on the source of electricity.

- Both novel routes, but especially the H_2+CCU-to-Olefins route, are highly sensitive to different electricity sources performing better in GWP impact in regions with cleaner electricity mixes due to their electricity-intensive processes.
- The Steam Cracking route offers less GWP improvement potential than the other two pathways due to the reliance on its fossil feedstock upstream chain and high technological maturity.
- CCS can be a viable option for mitigating GWP impacts of the Biomass-to-Olefins and Steam Cracking route.

4.3 Limitations and Outlook

As the impacts of anthropogenic climate change continue to intensify, the urgency of identifying effective solutions to decarbonize carbon-intensive industries grows. Such efforts are critical to mitigating future climate impacts. This Master Thesis contributes to these efforts by evaluating three production routes for ethylene from a GWP perspective, providing a solid foundation for further research. Nevertheless, these results should always be viewed in relation to each other and not as absolute values, since there are variations in boundary setting and retrieved LCI values. Although the data provided only reflects literature data, which can obviously not be as precise as applying real-life process inputs, these results should reflect the respective trends accurately, which is backed-up from literature sources.

While transitioning to de-fossilized feedstocks and renewable energy is a crucial step, it is not a panacea for addressing the carbon lock-in problem. Trade-offs and competitions with other environmental resources – such as land use, water consumption, use of rare earth metals and biomass availability – must also be carefully considered, which have not been assessed in this Master Thesis (Gabrielli et al., 2023; Palm et al., 2024). Therefore, even though GWP is a crucial metric for assessing climate-related impacts, it is equally important to consider other environmental dimensions. Future analyses could explore additional environmental impacts, as outlined in **Table 1**, to provide a more holistic understanding of the routes' environmental implications.

Furthermore, environmental performance alone is insufficient for driving practical implementation; economic viability must also be evaluated. A production pathway that lacks economic feasibility is unlikely to be adopted, regardless of its environmental advantages. Consequently, future research should also be conducted on the economical side for these routes.

Lastly, this study focuses exclusively on cradle-to-gate impacts, omitting considerations of downstream processes. Future exploration should contain a analysis including these phases, which would offer a more comprehensive assessment of the environmental and economic impacts associated with ethylene production. Such expanded evaluations will be essential for developing actionable strategies to address the climate and environmental challenges posed by carbon-intensive industries.

Above all, a comprehensive solution will likely require a combination of low carbon strategies, including alternative feedstocks, renewable energy, green hydrogen, CCS and many more (Meng et al., 2023). Though, regardless of the route, all pathways are resource-intensive, underscoring the need to prioritize reducing overall consumption over simply substituting existing technologies (Rootzén et al., 2023).

5. Bibliography

Abuagela, M., & Ahmed, M. (**2022**): Techno-economic and environmental assessment of CO_2 Utilization processes for the production of Dimethyl ether and Olefins, https://eprints.nottingham.ac.uk/id/eprint/71550 [last retrieved on the 14.11.2024].

Ahbabi Saray, J., Gharehghani, A., & Hosseinzadeh, D. (**2024**): Towards sustainable energy Carriers: A solar and Wind-Based systems for green liquid hydrogen and ammonia production, in: *Energy Conversion and Management,* 304, https://doi.org/10.1016/j.enconman.2024.118215.

Joao Vilhena Moreira (**2015**): Steam Cracking: Kinetics and Feed Characterization, https://fenix.tecnico.ulisboa.pt/downloadFile/1126295043834327/JVM_ExtendedAbstract.pdf [last retrieved on the 114.11.2024].

Arber, Justin (**2024**): "Es ist beängstigend": So erleben Schweizer das Unwetter, in: *20 Min.*, https://www.20min.ch/story/valencia-ueberschwemmungen-das-erleben-schweizer-103211253 [last retrieved on 11.11.2024].

Arvidsson, M., Haro, P., Morandin, M., & Harvey, S. (**2016**): Comparative thermodynamic analysis of biomass gasification-based light olefin production using methanol or DME as the platform chemical, in: *Chemical Engineering Research and Design*, 115, 182–194. https://doi.org/10.1016/j.cherd.2016.09.03.

Babu, S. P. (2005): Biomass gasification for hydrogen production-process description and research needs, in: *Biomass and Bioenergy*, 35 https://www.researchgate.net/publication/228850748.

Barahmand, Z., & Eikeland, M. S. (**2022**): Life Cycle Assessment under Uncertainty: A Scoping Review, *World*, 3(3), 692–717, https://doi.org/10.3390/world3030039.

Bareiß, K., de la Rua, C., Möckl, M., & Hamacher, T. (**2019**): Life cycle assessment of hydrogen from proton exchange membrane water electrolysis in future energy systems, *Applied Energy*, 237, 862–872, https://doi.org/10.1016/j.apenergy.2019.01.001.

Bauer, F., Kulionis, V., Oberschelp, C., Pfister, S., Tilsted, J. P., Finkill, G. D., & Fjäll, S. (**2022**): Petrochemicals and Climate Change: Tracing Globally Growing Emissions and Key Blind Spots in a Fossil-Based Industry, in: *IMES/EESS report* (Vol. 126), https://lucris.lub.lu.se/ws/portalfiles/portal/117494791/Petrochemicals_climate_change_review_web.pdf [last retrieved on 20.11.2024].

Bauer, F., Nielsen, T. D., Nilsson, L. J., Palm, E., Ericsson, K., Fråne, A., & Cullen, J. (**2022**): Plastics and climate change breaking carbon lock-ins through three mitigation pathways, in: *One Earth* (Vol. 5, Issue 4, pp. 361–376), Cell Press. https://doi.org/10.1016/j.oneear.2022.03.007.

Biernacki, P., Röther, T., Paul, W., Werner, P., & Steinigeweg, S. (**2018**): Environmental impact of the excess electricity conversion into methanol, in: *Journal of Cleaner Production*, 191, 87–98, https://doi.org/10.1016/j.jclepro.2018.04.232.

Bilandžija, D., Stuparić, R., Galić, M., Zgorelec, Ž., Leto, J., & Bilandžija, N. (**2022**): Carbon Balance of Miscanthus Biomass from Rhizomes and Seedlings, in: *Agronomy*, 12(6), https://doi.org/10.3390/agronomy12061426.

Bisinella, V., Hulgaard, T., Riber, C., Damgaard, A., & Christensen, T. H. (**2021**): Environmental assessment of carbon capture and storage (CCS) as a post-treatment technology in waste incineration, in: *Waste Management*, 128, 99–113, https://doi.org/10.1016/j.wasman.2021.04.046.

Bork, Henrik (**2021**): Chinas Ethylen-Produktion erreicht neuen Höhepunkt, in: *Process*, https://www.process.vogel.de/chinas-ethylen-produktion-erreicht-neuen-hoehepunkt-a-1121bce4ab6876660f3cd2f84ce73718/ [last retrieved on 11.10.2024].

Brightway (**2024**): Brightway LCA Software Framework, https://docs.brightway.dev/en/latest/ [last retrieved on 22.11.2024].

Budinis, S., Krevor, S., Dowell, N. mac, Brandon, N., & Hawkes, A. (**2018**): An assessment of CCS costs, barriers and potential, in: *Energy Strategy Reviews*, 22, 61–81, https://doi.org/10.1016/j.esr.2018.08.003.

Caprio, Frank (**2017**): Understanding Naphtha and Ethane Cracking Processes, https://www.hosemaster.com/understanding-naphtha-ethane-cracking-processes/ [last retrieved on 11.10.2024].

Carbon Brief Ltd. (**2018**): Explainer: How 'Shared Socioeconomic Pathways' explore future climate change, https://www.carbonbrief.org/explainer-how-shared-socioeconomic-pathways-explore-future-climate-change/ [last retrieved on 08.10.2024].

Carbon Brief Ltd. (**2024**): Q&A: How 'integrated assessment models' are used to study climate change, https://www.carbonbrief.org/qa-how-integrated-assessment-models-are-used-to-study-climate-change/ [last retrieved on 08.10.2024].

Carbon Chain (**n.d.**): Deep-Dive: Allocation Methods in Product Carbon Footprinting, https://www.carbonchain.com/carbon-accounting/economic-allocation-product-carbon-footprint#methodslast [retrieved on 11.11.2024].

Carmo, M., Fritz, D. L., Mergel, J., & Stolten, D. (**2013**): A comprehensive review on PEM water electrolysis, in: *International Journal of Hydrogen Energy* (Vol. 38, Issue 12, pp. 4901–4934), https://doi.org/10.1016/j.ijhydene.2013.01.151.

Carvalho, L., Furusjö, E., Kirtania, K., Wetterlund, E., Lundgren, J., Anheden, M., & Wolf, J. (**2017**): Techno-economic assessment of catalytic gasification of biomass powders for methanol production, in: *Bioresource Technology*, 237, 167–177, https://doi.org/10.1016/j.biortech.2017.02.019.

Cefic (2023): The Journey Of Petrochemicals Explained: From Raw Materials To 95% Of All Manufactured Goods, https://cefic.org/media-corner/newsroom/the-journey-of-petro-chemicals-explained-from-raw-materials-to-95-of-all-manufactured-goods/ [last retrieved on 22.11.2024]

Chemie (**2024**): Petrochemie, https://www.chemie.de/lexikon/Petrochemie.html# [last re-trieved on 20.11.2024].

CEM-WAVE (**2022**): The Life Cycle Analysis, a great tool for a greener future, https://www.cem-wave.eu/blog/life-cycle-analysis-great-tool-greener-future [last re-trieved on 26.11.2024].

Cherubini, F., Strømman, A. H., & Ulgiati, S. (**2011**): Influence of allocation methods on the environmental performance of biorefinery products - A case study, in: *Resources, Conservation and Recycling*, 55(11), 1070–1077, https://doi.org/10.1016/j.rescon-rec.2011.06.001.

Cnudde, P., Demuynck, R., Vandenbrande, S., Waroquier, M., Sastre, G., & Speybroeck, V. van. (**2020**): Light Olefin Diffusion during the MTO Process on H-SAPO-34: A Complex Interplay of Molecular Factors, in: *Journal of the American Chemical Society*, 142(13), 6007–6017, https://doi.org/10.1021/jacs.9b10249.

Council of the European Union (**2024**). Maßnahmen der EU gegen den Klimawandel, https://www.consilium.europa.eu/de/policies/climate-change/ [last retrieved on 11.11.2024].

Cruz, T. T. da, Perrella Balestieri, J. A., de Toledo Silva, J. M., Vilanova, M. R. N., Oliveira, O. J., & Ávila, I. (**2021**): Life cycle assessment of carbon capture and storage/utilization: From current state to future research directions and opportunities, in: *International Journal of Greenhouse Gas Control* (Vol. 108), https://doi.org/10.1016/j.ijggc.2021.103309.

Deutz, S., & Bardow, A. (**2021**): Life-cycle assessment of an industrial direct air capture process based on temperature–vacuum swing adsorption, in: *Nature Energy*, 6(2), 203–213, https://doi.org/10.1038/s41560-020-00771-9.

Dolezal, S., Franz, Mötzl, Hildegund, Spitzbart, & Christina. (**2014**): Survey of Allocation Methods in Life Cycle Assessments of Wood Based Products, https://www.irbnet.de/daten/iconda/null_DC28103.pdf [last retrieved on 20.22.2024].

ecoinvent (**2023**). Ecoinvent Version 3.9, https://support.ecoinvent.org/ecoinvent-version-3.9# [last retrieved on 25.11.2024].

ecoivent (**2024**): Introduction to the Database, https://support.ecoinvent.org/introduction-to-the-database [last retrieved on 09.11.2024].

Enerkem (**2024**): Edmonton, Alberta, Canada, https://enerkem.com/projects/edmonton [last retrieved on 08.10.2024].

European Commission (**2016**): European Platform on LCA – EPLCA, https://eplca.jrc.ec.europa.eu/LCDN/EN15804.html [last retrieved on 09.11.2024].

Fattouh, B., & Brown, C. (**2014**): US NGLs Production and Steam Cracker Substitution: What will the Spillover Effects be in Global Petrochemical Markets?, https://www.oxfordenergy.org/wpcms/wp-content/uploads/2014/09/US-NGLs-Production-and-Steam-Cracker-Substitution.pdf [last retrieved on 09.10.2024].

Gabrielli, P., Rosa, L., Gazzani, M., Meys, R., Bardow, A., Mazzotti, M., & Sansavini, G. (**2023**): Net-zero emissions chemical industry in a world of limited resources, in: *One Earth* (Vol. 6, Issue 6, pp. 682–704), Cell Press, https://doi.org/10.1016/j.oneear.2023.05.006.

Galán-Martín, Á., Tulus, V., Díaz, I., Pozo, C., Pérez-Ramírez, J., & Guillén-Gosálbez, G. (**2021**): Sustainability footprints of a renewable carbon transition for the petrochemical sector within planetary boundaries, in: *One Earth*, 4(4), 565–583. https://doi.org/10.1016/j.oneear.2021.04.001.

Gholami, Z., Gholami, F., Tišler, Z., & Vakili, M. (**2021**): A review on the production of light olefins using steam cracking of hydrocarbons, in: *Energies*, 14(23). https://doi.org/10.3390/en14238190.

Global Energy Infrastructure (**2021**). Hydrogen - data telling a story, https://globalenergyinfrastructure.com/articles/2021/03-march/hydrogen-data-telling-a-story/ [last retrieved on 20.08.2024].

Gogate, M. R. (**2019**): Methanol-to-olefins process technology: current status and future prospects, in: *Petroleum Science and Technology* (Vol. 37, Issue 5, pp. 559–565), Taylor and Francis Inc, https://doi.org/10.1080/10916466.2018.1555589.

Gu, J., Kim, H., & Lim, H. (**2022**): Electrified steam cracking for a carbon neutral ethylene production process: Techno-economic analysis, life cycle assessment, and analytic hierarchy process, in: *Energy Conversion and Management*, 270, https://doi.org/10.1016/j.enconman.2022.116256.

Guinée, J.B., Heijungs, R., Huppes, G (**2004**): Economic allocation: examples and derived decision tree, in: *The International Journal of Life Cycle Assessment* (Vol. 9, pp. 23-33), https://doi.org/10.1065/lca2003.10.136.

Hall, Anja (**2024**): Flut in Spanien führt zu Milliardenschäden, https://versicherungsmonitor.de/2024/10/31/flut-in-spanien-fuehrt-zu-milliardenschaeden/ [last retrieved on 10.11.2024].

Hank, C., Lazar, L., Mantei, F., Ouda, M., White, R. J., Smolinka, T., Schaadt, A., Hebling, C., & Henning, H. M. (**2019**): Comparative well-to-wheel life cycle assessment of OME3-5 synfuel production via the power-to-liquid pathway, in: *Sustainable Energy and Fuels*, 3(11), 3219–3233, https://doi.org/10.1039/c9se00658c.

Heldebrant, D. J., Koech, P. K., Glezakou, V. A., Rousseau, R., Malhotra, D., & Cantu, D. C. (**2017**) : Water-Lean Solvents for Post-Combustion CO_2 Capture: Fundamentals, Uncertainties, Opportunities, and Outlook, in: *Chemical Reviews* (Vol. 117, Issue 14, pp. 9594–9624), American Chemical Society, https://doi.org/10.1021/acs.chemrev.6b00768.

Hoppe, W., Thonemann, N., & Bringezu, S. (**2018**): Life Cycle Assessment of Carbon Dioxide–Based Production of Methane and Methanol and Derived Polymers, in: *Journal of Industrial Ecology*, 22(2), 327–340. https://doi.org/10.1111/jiec.12583.

Hrbek, J., Oberndorfer, C., Zanzinger, P., & Pfeifer, C. (**2021**): Influence of $Ca(OH)_2$ on ash melting behaviour of woody biomass, in: *Carbon Resources Conversion*, 4, 84–88. https://doi.org/10.1016/j.crcon.2021.01.008.

IEA (**2023**): Chemicals, https://www.iea.org/energy-system/industry/chemicals [last retrieved on 10.08.2024].

Intratec (**2024**): Butene Prices – Current and Forecast, https://www.intratec.us/chemical-markets/butene-price [last retrieved on 20.11.2024].

IPCC (**2023**): Sections. In: Climate Change 2023: Synthesis Report. Contribution of Working Groups I, II and III to the Sixth Assessment Report of the Intergovernmental Panel on Climate Change [Core Writing Team, H. Lee and J. Romero (eds.)], IPCC, Geneva, Switzerland, pp. 35-115, doi: 10.59327/IPCC/AR6-9789291691647.

ISO 14040:2006 (**2006a**): Environmental management - life cycle assessment - requirements and guidelines, https://www.iso.org/standard/37456.html [last retrieved on 03.10.2024].

ISO 14044:2006 (**2006b**): Environmental management - life cycle assessment - requirements and guidelines, https://www.iso.org/standard/38498.html [last retrieved on 04.10.2024].

Jiang, P., Li, L., Zhao, G., Zhang, H., Ji, T., Mu, L., Lu, X., & Zhu, J. (**2024**): Seeking the Low-Carbon Route of Methanol Production with Sustainable Resources by Tracking Energy and Environment Indicators, in: *Industrial and Engineering Chemistry Research*, 63(18), 8261–8272, https://doi.org/10.1021/acs.iecr.3c03667.

Kansy, M., Neuner, P., Bajohr, S., Rauch, R., & Kolb, T. (**2023**): Comparison of Different Approaches for Sustainable Olefin Production Using the MtO and FT Processes, in: *Chemie-Ingenieur-Technik*, 95(9), 1476–1481, https://doi.org/10.1002/cite.202200032.

Katumwesigye, A., Researcher Lauri Leppakoski, J., & Professor Ville Uusitalo, A. (**2023**): Life Cycle Assessment of Green hydrogen: Wind-based hydrogen vs Solar based hydrogen, https://urn.fi/URN:NBN:fi-fe202301041425 [last retrieved on 14.11.2024].

Keller, F., Lee, R. P., & Meyer, B. (**2020**): Life cycle assessment of global warming potential, resource depletion and acidification potential of fossil, renewable and secondary feedstock for olefin production in Germany, in: *Journal of Cleaner Production*, 250. https://doi.org/10.1016/j.jclepro.2019.119484.

Kixmüller, Jan (**2024**): "Die Menschen wussten einfach nicht, was sie tun sollten" Warum die Flut in Spanien zur Katastrophe wurde, in: *Tagesspiegel*, https://www.tagesspiegel.de/wissen/die-menschen-wussten-einfach-nicht-was-sie-tun-sollen-warum-die-flut-in-spanien-zur-katastrophe-wurde-12623780.html [last retrieved on 11.10.2024].

Koornneef, J., van Keulen, T., Faaij, A., & Turkenburg, W. (**2008**): Life cycle assessment of a pulverized coal power plant with post-combustion capture, transport and storage of CO_2, in: *International Journal of Greenhouse Gas Control*, 2(4), 448–467, https://doi.org/10.1016/j.ijggc.2008.06.008.

Krishnan, S., Corona, B., Kramer, G. J., Junginger, M., & Koning, V. (**2024**): Prospective LCA of alkaline and PEM electrolyser systems, in: *International Journal of Hydrogen Energy*, 55, 26–41, https://doi.org/10.1016/j.ijhydene.2023.10.192.

Lalonde, Emily (**2024**): Explained: LCIA methods, https://helpcenter.ecochain.com/en/articles/9055669-explained-lcia-methods [last retrieved on 11.11.2024].

Lerche Raadal, H., & Saur Modahl, I. (**2022**): LCA of CCS and CCU compared with no capture: How should multi-functional systems be analysed?, in: *E3S Web of Conferences*, 349, https://doi.org/10.1051/e3sconf/202234903001.

Liu, J., Zhao, J., Wei, H., Zhu, Q., & Li, Y. (**2024**): Comparative environmental assessment of methanol production technologies: A cradle-to-gate life cycle analysis, in: *Energy Conversion and Management*, 302, https://doi.org/10.1016/j.enconman.2024.118128.

Liu, Y., Li, G., Chen, Z., Shen, Y., Zhang, H., Wang, S., Qi, J., Zhu, Z., Wang, Y., & Gao, J. (**2020**): Comprehensive analysis of environmental impacts and energy consumption of biomass-to-methanol and coal-to-methanol via life cycle assessment, in: *Energy*, 204. https://doi.org/10.1016/j.energy.2020.117961.

Luderer G, Bauer N, Baumstark L, Bertram C, Leimbach M, Pietzcker R, Strefler J, Abo-umahboub T, Auer C, Bi S, Dietrich J, Dirnaichner A, Giannousakis A, Haller M, Hilaire J, Klein D, Koch J, Karner A, Kriegler E, Levesque A, Lorenz A, Ludig S, Laken M, Malik A, Manger S, Merfort L, Mouratiadou I, Pehl M, Piontek F, Popin L, Rauner S, Rodrigues R, Roming N, Rottoli M, Schmidt E, Schreyer F, Schultes A, Sargel B, Ueckerdt F (**2020**): REMIND – Regional Model of INvestments and Development - Version 2.1.3, https://www.pik-potsdam.de/research/transformation-pathways/models/remind [last retrieved on 26.11.2024].

Lv, B., Guo, B., Zhou, Z., & Jing, G. (**2015**): Mechanisms of CO2 Capture into Monoethanolamine Solution with Different CO2 Loading during the Absorption/Desorption Processes, in: *Environmental Science and Technology*, 49(17), 10728–10735, https://doi.org/10.1021/acs.est.5b02356.

Markowitsch, C., Lehner, M., & Maly, M. (**2023**): Comparison and techno-economic evaluation of process routes for lower olefin production via Fischer–Tropsch and methanol synthesis in: *International Journal of Greenhouse Gas Control*, 129, https://doi.org/10.1016/j.ijggc.2023.103985.

Marlin, D. S., Sarron, E., & Sigurbjörnsson, Ó. (**2018**): Process Advantages of Direct CO_2 to Methanol Synthesis, in: *Frontiers in Chemistry*, 6, https://doi.org/10.3389/fchem.2018.00446.

Meng, F., Wagner, A., Kremer, A. B., Kanazawa, D., Leung, J. J., Goult, P., Guan, M., Herrmann, S., Speelman, E., Sauter, P., Lingeswaran, S., Stuchtey, M. M., Hansen, K., Masanet, E., Serrenho, A. C., Ishii, N., Kikuchi, Y., & Cullen, J. M. (**2023**): Planet-compatible pathways for transitioning the chemical industry, in: *Proceedings of the National Academy of Sciences of the United States of America*, 120(8), https://doi.org/10.1073/pnas.2218294120.

Meunier, N., Chauvy, R., Mouhoubi, S., Thomas, D., & de Weireld, G. (**2020**): Alternative production of methanol from industrial CO_2, in: *Renewable Energy*, 146, 1192–1203, https://doi.org/10.1016/j.renene.2019.07.010.

Mynko, Oleksii, Mike Bonheure, Ismaël Amghizar, David J. Brown, Lin Chen, Guy Marin, Rodrigo Freitas de Alvarenga, Didem Civancik Uslu, Jo Dewulf, and Kevin Van Geem (**2023**): Electrification of Steam Cracking as a Pathway to Reduce the Impact of the Petrochemical Industry on Climate Change, in: *Journal of cleaner Production,* 427, doi:10.1016/j.jclepro.2023.139208.

Nonnast, Thomas (**2021**): BASF, SABIC und Linde arbeiten gemeinsam an der Realisierung des weltweit ersten elektrisch beheizten Steamcracker-Ofens. https://www.basf.com/global/de/media/news-releases/2021/03/p-21-165 [last retrieved on 09.10.2024].

Nonnast, Thomas (**2024**): BASF, SABIC und Linde feiern Inbetriebnahme der weltweit ersten großtechnischen elektrisch beheizten Steamcracker-Öfen, https://www.basf.com/global/de/media/news-releases/2024/04/p-24-177 [last retrieved on 09.10.2024].

Øi, L. E., & Kvam, S. H. P. (**2014**): Comparison of energy consumption for different CO2 absorption configurations using different simulation tools, in: *Energy Procedia*, 63, 1186–1195, https://doi.org/10.1016/j.egypro.2014.11.128.

Osman, A. I., Mehta, N., Elgarahy, A. M., Al-Hinai, A., Al-Muhtaseb, A. H., & Rooney, D. W. (**2021**): Conversion of biomass to biofuels and life cycle assessment: a review, in: *Environmental Chemistry Letters* (Vol. 19, Issue 6, pp. 4075–4118), Springer Science and Business Media Deutschland GmbH, https://doi.org/10.1007/s10311-021-01273-0.

Palm, E., Tilsted, J. P., Vogl, V., & Nikoleris, A. (**2024**): Imagining circular carbon: A mitigation (deterrence) strategy for the petrochemical industry, in: *Environmental Science and Policy*, 151, https://doi.org/10.1016/j.envsci.2023.103640.

Petrochemicals Europe (**2023**): European Market Overview, https://www.petrochemistry.eu/about-petrochemistry/petrochemicals-facts-and-figures/european-market-overview/ [last retrieved on 15.10.2024].

Plastics Europe (**2017**): Plastics Europe recommendation on Steam Cracker allocation, https://plasticseurope.org/wp-content/uploads/2021/12/PlasticsEurope_recommendation_on_Steam_Cracker_allocation-_Juillet_2018.pdf [last retrieved on 17.08.2024].

Premise Dash (**n.d.**): Premise Scenario Explorer, https://premisedash-6f5a0259c487.herokuapp.com [last retrieved on 12.11.2024].

Procurement Resource (**2024**): Pyrolysis Oil Price Trend and Forecast, https://www.procurementresource.com/resource-center/pyrolysis-oil-price-trends [last retrieved on 20.11.2024].

PubChem (**2024**): Ethylene, https://pubchem.ncbi.nlm.nih.gov/compound/Ethylene [last retrieved on 14.11.2024].

Oud, P. (**2020**): Low-emission cracking furnace with air preheat, www.technipenergies.com [last retrieved on 09.11.2024].

Quicker, Peter (**2023**): Status, potentials and risks of chemical recycling of plastics, https://www.bafu.admin.ch/dam/bafu/en/dokumente/international/externe-studien-berichte/status-potentials-and-risks-of-chemical-recycling-of-waste-plastics.pdf.download.pdf/risks-chemical-recycling-plastics.pdf [last retrieved on 18.10.2024].

Ren, T., Patel, M., & Blok, K. (**2006**): Olefins from conventional and heavy feedstocks: Energy use in steam cracking and alternative processes, in: *Energy*, 31(4), 425–451, https://doi.org/10.1016/j.energy.2005.04.001.

Ren, Y., Liao, Z., Yang, Y., Sun, J., Jiang, B., Wang, J., & Yang, Y. (**2022**): Direct prediction of steam cracking products from naphtha bulk properties: Application of the two sub-networks ANN, in: *Frontiers in Chemical Engineering*, 4, https://doi.org/10.3389/fceng.2022.983035.

Riahi, K., van Vuuren, D. P., Kriegler, E., Edmonds, J., O'Neill, B. C., Fujimori, S., Bauer, N., Calvin, K., Dellink, R., Fricko, O., Lutz, W., Popp, A., Cuaresma, J. C., KC, S., Leimbach, M., Jiang, L., Kram, T., Rao, S., Emmerling, J., … Tavoni, M. (**2017**): The Shared Socioeconomic Pathways and their energy, land use, and greenhouse gas emissions implications: An overview, in: *Global Environmental Change*, *42*, 153–168, https://doi.org/10.1016/j.gloenvcha.2016.05.009.

Rodríguez-Vallejo, D. F., Guillén-Gosálbez, G., & Chachuat, B. (**2020**): What Is the True Cost of Producing Propylene from Methanol? The Role of Externalities, in: *ACS Sustainable Chemistry and Engineering*, 8(8), 3072–3081, https://doi.org/10.1021/acssuschemeng.9b05516.

Rootzén, J., Nyberg, T., Karltorp, K., & Åhman, M. (**2023**): Turning the tanker? Exploring the preconditions for change in the global petrochemical industry, in: *Energy Research and Social Science*, 104, https://doi.org/10.1016/j.erss.2023.103256.

Rosental, M., Fröhlich, T., & Liebich, A. (**2020**): Life Cycle Assessment of Carbon Capture and Utilization for the Production of Large Volume Organic Chemicals, in: *Frontiers in Climate*, 2, https://doi.org/10.3389/fclim.2020.586199.

Sacchi, R., Terlouw, T., Siala, K., Dirnaichner, A., Bauer, C., Cox, B., Mutel, C., Daioglou, V., & Luderer, G. (**2022**): PRospective EnvironMental Impact asSEment (premise): A streamlined approach to producing databases for prospective life cycle assessment using integrated assessment models, in: *Renewable and Sustainable Energy Reviews*, *160*, https://doi.org/10.1016/j.rser.2022.112311.

Sammarchi, S., Li, J., Izikowitz, D., Yang, Q., & Xu, D. (**2022**): China's coal power decarbonization via CO2 capture and storage and biomass co-firing: A LCA case study in Inner Mongolia, in: *Energy*, 261, https://doi.org/10.1016/j.energy.2022.125158.

Santos, R. O. dos, Santos, L. de S., & Prata, D. M. (**2018**): Simulation and optimization of a methanol synthesis process from different biogas sources, in: *Journal of Cleaner Production*, 186, 821–830, https://doi.org/10.1016/j.jclepro.2018.03.108.

Schropp, E., Naumann, G. & Gaderer, M. (**2020**): Life Cycle Assessment of a Polymer Electrolyte Membrane Water Electrolysis, in: Albrecht, S., Fischer, M., Leistner, P., Schebek, L. (eds) *Progress in Life Cycle Assessment 2019. Sustainable Production, Life Cycle Engineering and Management*, Springer, Cham, https://doi.org/10.1007/978-3-030-50519-6_5.

SG H$_2$ Energy (**2020**): Economics – Cost Comparison, https://www.sgh2energy.com/economics [last retrieved on 20.11.2024].

Shell (**2021**): Quest Facility Spotlight: showing how large-scale CO$_2$ capture can be safe and effective, https://www.shell.ca/en_ca/about-us/projects-and-sites/quest-carbon-capture-and-storage-project.html [last retrieved on 08.10.2024].

Shi, X., Xiao, H., Azarabadi, H., Song, J., Wu, X., Chen, X., & Lackner, K. S. (**2020**): Sorbents for the Direct Capture of CO2 from Ambient Air, in: *Angewandte Chemie - International Edition* (Vol. 59, Issue 18, pp. 6984–7006), Wiley-VCH Verlag, https://doi.org/10.1002/anie.201906756.

Shiva Kumar, S., & Himabindu, V. (**2019**): Hydrogen production by PEM water electrolysis – A review, in: *Materials Science for Energy Technologies* (Vol. 2, Issue 3, pp. 442–454), KeAi Communications Co, https://doi.org/10.1016/j.mset.2019.03.002.

Sinan, M., Neumann, M., & Hasenauer, H. (**2024**): How much carbon is stored in the stem bark of Austrian trees?, in: *Carbon Management*, 15(1), https://doi.org/10.1080/17583004.2024.2363747.

Singh, N., & Walker, T. R. (**2024**): Plastic recycling: A panacea or environmental pollution problem, in: *Npj Materials Sustainability*, 2(1), https://doi.org/10.1038/s44296-024-00024-w.

Sodiq, A., Abdullatif, Y., Aissa, B., Ostovar, A., Nassar, N., El-Naas, M., & Amhamed, A. (**2023**): A review on progress made in direct air capture of CO2, in: *Environmental Technology and Innovation* (Vol. 29), Elsevier B.V. https://doi.org/10.1016/j.eti.2022.102991.

SRF (**2024**): Spanien: Bald weitere 10000 Soldaten und Polizisten im Einsatz, in *SRF*, https://www.srf.ch/news/international/heftige-regenfaelle-spanien-bald-weitere-10-000-soldaten-und-polizisten-im-einsatz [last retrieved on 11.11.2024].

Statista (**2024a, May 16th**): Natural gas commodity prices in Europe and the United States from 1980 to 2023, with a forecast for 2024 and 2025, https://www.statista.com/statistics/252791/natural-gas-prices/ [last retrieved on 20.11.2024].

Statista (**2024b, August 23rd**): Price of ethylene worldwide from 2017-2023, https://www.statista.com/statistics/1170573/price-ethylene-forecast-globally/ [last retrieved on 20.11.2024].

Statista (**2024c, August 23rd**): Price of propylene worldwide from 2017-2023, https://www.statista.com/statistics/1170576/price-propylene-forecast-globally/ [last retrieved on 20.11.2024].

Statista (**2024d, August 26th**): Price of benzene worldwide from 2017-2023, https://www.statista.com/statistics/1171072/price-benzene-forecast-globally/ [last retrieved on 20.11.2024].

Stagge, M, Kolbe, N., Haakmann, F. (**2024**): Unser Projekt Carbon2Chem®, https://www.thyssenkrupp-steel.com/de/unternehmen/nachhaltigkeit/carbon2chem/carbon2chem.html [last retrieved on 08.10.2024].

Steubing, B., de Koning, D., Haas, A., & Mutel, C. L. (**2020**): The Activity Browser – An open source LCA software building on top of the brightway framework, in: *Software Impacts*, *3*, https://doi.org/10.1016/j.simpa.2019.100012.

Sun, Q., Xie, Z., & Yu, J. (**2018**): The state-of-the-art synthetic strategies for SAPO-34 zeolite catalysts in methanol-to-olefin conversion, in: *National Science Review* (Vol. 5, Issue 4, pp. 542–558), Oxford University Press, https://doi.org/10.1093/nsr/nwx103.

Umwelt Bundesamt (**2022**): Die Treibhausgase, https://www.umweltbundesamt.de/themen/klima-energie/klimaschutz-energiepolitik-in-deutschland/treibhausgas-emissionen/die-treibhausgase [last retrieved on 11.11.2024].

UN Climate Change (**n.d.**): The Paris Agreement, https://unfccc.int/process-and-meetings/the-paris-agreement [last retrieved on 20.09.2024].

Unfccc. (**2015**): Adoption of the Paris Agreement – Paris Agreement text English, https://unfccc.int/resource/docs/2015/cop21/eng/l09r01.pdf [last retrieved on 03.09.2024].

US Department of Energy (**n.d.**): Rectisol, https://netl.doe.gov/research/coal/energy-systems/gasification/gasifipedia/rectisol [last retrieved on 25.09.2024].

Vaithyanathan, V. K., Goyette, B., & Rajagopal, R. (**2023**): A critical review of the transformation of biomass into commodity chemicals: Prominence of pretreatments, in: *Environmental Challenges* (Vol. 11), Elsevier B.V., https://doi.org/10.1016/j.envc.2023.100700.

Vega, F., Baena-Moreno, F. M., Gallego Fernández, L. M., Portillo, E., Navarrete, B., & Zhang, Z. (**2020**): Current status of CO_2 chemical absorption research applied to CCS: Towards full deployment at industrial scale, in: *Applied Energy*, 260. https://doi.org/10.1016/j.apenergy.2019.114313.

Vilbergsson, K. v., Dillman, K., Emami, N., Ásbjörnsson, E. J., Heinonen, J., & Finger, D. C. (**2023**): Can remote green hydrogen production play a key role in decarbonizing Europe in the future? A cradle-to-gate LCA of hydrogen production in Austria, Belgium, and Iceland, in: *International Journal of Hydrogen Energy*, 48(46), 17711–17728, https://doi.org/10.1016/j.ijhydene.2023.01.081.

Von Eichhorn, Christian (**2024**): *So kam es zur Katastrophe*, in: Tagesspiegel, https://www.tagesanzeiger.ch/unwetter-spanien-klimawandel-ist-schluesselfaktor-fuer-regenfaelle-142531153892 [last retrieved on 11.11.2024].

Wang, Y., Zhu, L., He, Y., Zeng, X., Hao, Q., Huang, Y., & Han, X. (**2024**): Life cycle assessment of an efficient biomass power plant supported by semi-closed supercritical CO_2 cycle and chemical looping air separation, in: *Science of the Total Environment*, 919, https://doi.org/10.1016/j.scitotenv.2024.170832.

Wei, S., Sacchi, R., Tukker, A., Suh, S., & Steubing, B. (**2024**): Future environmental impacts of global hydrogen production, in: *Energy and Environmental Science*, 17(6), 2157–2172, https://doi.org/10.1039/d3ee03875k.

Wei, W., Larrey-Lassalle, P., Faure, T., Dumoulin, N., Roux, P., & Mathias, J. D. (**2015**) : How to conduct a proper sensitivity analysis in life cycle assessment: Taking into account correlations within LCI data and interactions within the LCA calculation model, in: *Environmental Science and Technology*, 49(1), 377–385, https://doi.org/10.1021/es502128k.

Weidner, T., Merlich, J., & Gosálbez, G. (**2022**): Environmental sustainability assessment of large-scale hydrogen production using prospective life cycle analysis Rights / license: Creative Commons Attribution 4.0 International, in: *International Journal of Hydrogen Energy*, 48(22), https://doi.org/10.3929/ethz-b-000599075.

Wiesinger, Helen (**2024**): Recycling plastic is not a quick fix, https://baug.ethz.ch/en/news-and-events/news/2024/03/blog-recycling-plastic-is-not-a-quick-fix.html [last retrieved on 01.11.2024].

World Nuclear Association (**2020**): Heat Values of Various Fuels, https://world-nuclear.org/information-library/facts-and-figures/heat-values-of-various-fuels [last retrieved on 13.11.2024].

Yang, M., & You, F. (**2017**): Comparative Techno-Economic and Environmental Analysis of Ethylene and Propylene Manufacturing from Wet Shale Gas and Naphtha, in: *Industrial and Engineering Chemistry Research*, 56(14), 4038–4051, https://doi.org/10.1021/acs.iecr.7b00354.

Ye, Z., Han, X., Hu, G., & Zhao, L. (**2023**): Comparative life cycle environmental, exergteic, and economic assessment of three hydrocarbon-based ethylene production routes, in: *Fuel*, 333, https://doi.org/10.1016/j.fuel.2022.126359.

Young, B., Hawkins, T. R., Chiquelin, C., Sun, P., Gracida-Alvarez, U. R., & Elgowainy, A. (**2022**): Environmental life cycle assessment of olefins and by-product hydrogen from steam cracking of natural gas liquids, naphtha, and gas oil, in: *Journal of Cleaner Production*, 359, https://doi.org/10.1016/j.jclepro.2022.131884.

Zhao, Z., Chong, K., Jiang, J., Wilson, K., Zhang, X., & Wang, F. (**2018**): Low-carbon roadmap of chemical production: A case study of ethylene in China, in: *Renewable and Sustainable Energy Reviews*, 97, 580–591, https://doi.org/10.1016/j.rser.2018.08.008.

Zhou, S., Wang, S., & Chen, C. (**2012**): Thermal degradation of monoethanolamine in CO_2 capture with acidic impurities in flue gas, in: *Industrial and Engineering Chemistry Research*, 51(6), 2539–2547, https://doi.org/10.1021/ie202214y.

Ziegler, J., Reck, R., & Haas, S. (**2024**): Global Warming Potential, https://www.ffe.de/veroeffentlichungen/global-warming-potential-gwp/ [last retrieved on 11.11.2024].

Zuiderveen, E. A. R., Caldeira, C., Vries, T., Schenk, N. J., Huijbregts, M. A. J., Sala, S., Hanssen, Steef. v., & van Zelm, R. (**2024**): Evaluating the Environmental Sustainability of Alternative Ways to Produce Benzene, Toluene, and Xylene, in: *ACS Sustainable Chemistry & Engineering*, 12(13), 5092–5104, https://doi.org/10.1021/acssuschemeng.3c06996.

6. Appendix

6.1 Economic Allocation

6.1.1 Steam Cracking

Appx. Table 1: Economic Allocation calculation for the Steam Cracking process in 2020 with respective prices between 2020-2022, the yields/amount of feedstock and quantities as well as their proceeds based on Chapter 3.1.1.1

Naphtha 2020	Price 2020 [US-$ t]	Price 2021 [US-$/t]	Price 2022 [US-$/t]	3-years Average [US-$/kg]	Amount of Feedstock [kg]	Yield [% of feedstock]	Quantity [kg]	Proceeds [US-$]	Sum [US-$]	Allocation Factor []	Sources
Ethylene Price	780	1000	1060	0.95	3.33	0.3	1.00	0.95		0.35128	Amount of Feedstock & Yield: Young et al., 2022; Prices: Statista, 2024b
Propylene Price	778	983	997	0.92	3.33	0.17	0.57	0.52		0.19331	Amount of Feedstock & Yield: Young et al., 2022; prices: Statista, 2024c
Butene Price	981	1258	1333	1.19	3.33	0.058	0.19	0.23		0.08542	Amount of Feedstock & Yield: Young et al., 2022; Prices: Intratec, 2024
Methane Price	136	525	1226	0.63	3.33	0.14	0.00	0.00	2.69	0.00000	Amount of Feedstock & Yield: Young et al., 2022; Prices: Statista, 2024a
Benzene	498	935	1107	0.85	3.33	0.064	0.21	0.18		0.06702	Amount of Feedstock & Yield: Young et al., 2022; Prices: Statista, 2024d
Pyrolysis Gasoline	759	973	1032	0.92	3.33	0.11	0.37	0.34		0.12534	Amount of Feedstock & Yield: Young et al., 2022; Prices: Procurement Resource, 2024
Other products Average Price	655	946	1126	0.91	3.33	0.158	0.53	0.48		0.17763	Amount of Feedstock & Yield: Young et al., 2022; Prices: Average of the prices above

Appx. Table 2: *Economic Allocation calculation for the Steam Cracking process in the LPG as feedstock configuration with respective prices between 2020-2022, the yields/amount of feedstock and quantities as well as their proceeds based on Chapter 3.1.1.2*

LPG	Price 2020 [US-$ t]	Price 2021 [US-$/ t]	Price 2022 [US-$/ t]	3-years Average [US-$/kg]	Amount of Feedstock [kg]	Yield [% of feedstock]	Quantity [kg]	Proceeds [US-$]	Sum [US-$]	Allocation Factor []	Sources
Ethylene Price	780	1000	1060	0.95	2.35	0.425	1.00	0.95		0.6552	Amount of Feedstock & Yield: Young et al., 2022; Prices: Statista, 2024b
Propylene Price	778	983	997	0.92	2.35	0.18	0.42	0.39		0.2695	Amount of Feedstock & Yield: Young et al., 2022; prices: Statista, 2024c
Methane Price	136	525	1226	0.63	2.35	0.24	0.10	0.06	1.44	0.0426	Amount of Feedstock & Yield: Young et al., 2022; Prices: Statista, 2024a
Other Products Average Price	565	836	1094	0.13	2.35	0.155	0.36	0.05		0.0327	Amount of Feedstock & Yield: Young et al., 2022; Prices: Average of the prices above

Appx. Table 3: *Economic Allocation calculation for the Steam Cracking process in the ethane as feedstock configuration with respective prices between 2020-2022, the yields/amount of feedstock and quantities as well as their proceeds based on Chapter 3.1.1.2*

Ethane	Price 2020 [US-$ t]	Price 2021 [US-$/ t]	Price 2022 [US-$/ t]	3-years Average [US-$/kg]	Amount of Feedstock [kg]	Yield [% of feedstock]	Quantity [Kg]	Proceeds [US-$]	Sum [US-$]	Allocation Factor []	Sources
Ethylene Price	780	1000	1060	0.95	1.25	0.8	1.00	0.95		0.5827	Amount of Feedstock & Yield: Young et al., 2022; Prices: Statista, 2024b
Hydrogen Price	3000	3846	4077	3.64	1.25	0.062	0.08	0.28	1.62	0.1737	Amount of Feedstock &Yield: Young et al., 2022; Prices: SG H2 Energy, 2020
Other Products Average Price	1890	2423	2569	2.29	1.25	0.138	0.17	0.40		0.2436	Amount of Feedstock & Yield: Young et al., 2022; Prices: Average of the prices above

Appx. **Table 4**: *Economic Allocation calculation for the Steam Cracking process in the low-emission-furnace configuration with respective prices between 2020-2022, the yields/amount of feedstock and quantities as well as their proceeds based on Chapter 3.1.2*

Low emission furnace	Price 2020 [US-$ t]	Price 2021 [US-$/t]	Price 2022 [US-$/t]	3-years Average [US-$/kg]	Amount of Feedstock [kg]	Yield [% of feedstock]	Quantity [kg]	Proceeds [US-$]	Sum [US-$]	Allocation Factor []	Sources
Ethylene Price	780	1000	1060	0.95	3.33	0.3	1.00	0.95		0.3402	Amount of Feedstock & Yield: Young et al., 2022; Prices: Statista, 2024b
Propylene Price	778	983	997	0.92	3.33	0.17	0.57	0.52		0.1872	Amount of Feedstock & Yield: Young et al., 2022; prices: Statista, 2024c
Butene Price	981	1258	1333	1.19	3.33	0.058	0.19	0.23		0.0827	Amount of Feedstock & Yield: Young et al., 2022; Prices: Intratec, 2024
Benzene	498	935	1107	0.85	3.33	0.064	0.21	0.18	2.78	0.0649	Amount of Feedstock & Yield: Young et al., 2022; Prices: Statista, 2024d
Methane Price	136	525	1226	0.63	3.33	0.14	0.14	0.09		0.0316	Amount of Feedstock & Yield: Young et al., 2022; Prices: Statista, 2024a
Pyrolysis Gasoline	759	973	1032	0.92	3.33	0.11	0.37	0.34		0.1214	Amount of Feedstock & Yield: Young et al., 2022; Prices: Procurement Resource, 2024
Other products Average Price	655	946	1126	0.91	3.33	0.158	0.53	0.48		0.1720	Amount of Feedstock & Yield: Young et al., 2022; Prices: Average of the prices above

Appx. **Table 5:** *Economic Allocation calculation for the Steam Cracking process in the e-furnace configuration with respective prices between 2020-2022, the yields/amount of feedstock and quantities as well as their proceeds based on Chapter 3.1.1.2*

E-fur-nace	Price 2020 [US-$ t]	Price 2021 [US-$/t]	Price 2022 [US-$/t]	3-years Average [US-$/kg]	Amount of Feedstock [kg]	Yield [% of feedstock]	Quantity [kg]	Proceeds [US-$]	Sum [US-$]	Allocation Factor []	Sources
Ethylene Price	780	1000	1060	0.95	3.33	0.3	1.00	0.95		0.3168	Amount of Feedstock & Yield: Young et al., 2022; Prices: Statista, 2024b
Propylene Price	778	983	997	0.92	3.33	0.17	0.57	0.52		0.1743	Amount of Feedstock & Yield: Young et al., 2022; prices: Statista, 2024c
Butene Price	981	1258	1333	1.19	3.33	0.058	0.19	0.23		0.0770	Amount of Feedstock & Yield: Young et al., 2022; Prices: Intratec, 2024
Benzene	498	935	1107	0.85	3.33	0.064	0.21	0.18	2.99	0.0604	Amount of Feedstock & Yield: Young et al., 2022; Prices: Statista, 2024d
Methane Price	136	525	1226	0.63	3.33	0.14	0.47	0.29		0.0982	Amount of Feedstock & Yield: Young et al., 2022; Prices: Statista, 2024a
Pyrolysis Gasoline	759	973	1032	0.92	3.33	0.11	0.37	0.34		0.1130	Amount of Feedstock & Yield: Young et al., 2022; Prices: Procurement Resource, 2024
Other products Average Price	655	946	1126	0.91	3.33	0.158	0.53	0.48		0.1602	Amount of Feedstock & Yield: Young et al., 2022; Prices: Average of the prices above

Appx. Table 6: Economic Allocation calculation for the Steam Cracking process in 2030 with respective prices between 2020-2022, the yields/amount of feedstock and quantities as well as their proceeds based on Chapter 3.1.1.1 and Chapter 3.2

Naphtha 2030	Price 2020 [US-$ t]	Price 2021 [US-$/ t]	Price 2022 [US-$/ t]	3-years Average [US-$/kg]	Amount of Feedstock [kg]	Yield [% of feedstock]	Quantity [kg]	Proceeds [US-$]	Sum [US-$]	Allocation Factor []	Sources
Ethylene Price	780	1000	1060	0.95	3.33	0.3	1.00	0.95		0.3503	Amount of Feedstock & Yield: Young et al., 2022; Prices: Statista, 2024b
Propylene Price	778	983	997	0.92	3.33	0.17	0.57	0.52		0.1928	Amount of Feedstock & Yield: Young et al., 2022; prices: Statista, 2024c
Butene Price	981	1258	1333	1.19	3.33	0.058	0.19	0.23		0.0852	Amount of Feedstock & Yield: Young et al., 2022; Prices: Intratec, 2024
Methane Price	136	525	1226	0.63	3.33	0.14	0.01	0.01	2.70	0.0027	Amount of Feedstock & Yield: Young et al., 2022; Prices: Statista, 2024a
Benzene	498	935	1107	0.85	3.33	0.064	0.21	0.18		0.0668	Amount of Feedstock & Yield: Young et al., 2022; Prices: Statista, 2024d
Pyrolysis Gasoline	759	973	1032	0.92	3.33	0.11	0.37	0.34		0.1250	Amount of Feedstock & Yield: Young et al., 2022; Prices: Procurement Resource, 2024
Other products Average Price	655	946	1126	0.91	3.33	0.16	0.53	0.48		0.1771	Amount of Feedstock & Yield: Young et al., 2022; Prices: Average of the prices above

Appx. Table 7: Economic Allocation calculation for the Steam Cracking process in 2050 with respective prices between 2020-2022, the yields/amount of feedstock and quantities as well as their proceeds based on Chapter 3.1.1 and Chapter 3.2

Naphtha 2050	Price 2020 [US-$ t]	Price 2021 [US-$ / t]	Price 2022 [US-$ / t]	3-years Average [US-$/kg]	Amount of Feedstock [kg]	Yield [% of feedstock]	Quantity [kg]	Proceeds [US-$]	Sum [US-$]	Allocation Factor []	Sources
Ethylene Price	780	1000	1060	0.95	3.33	0.3	1.00	0.95		0.3494	Amount of Feedstock & Yield: Young et al., 2022; Prices: Statista, 2024b
Propylene Price	778	983	997	0.92	3.33	0.17	0.57	0.52		0.1923	Amount of Feedstock & Yield: Young et al., 2022; prices: Statista, 2024c
Butene Price	981	1258	1333	1.19	3.33	0.058	0.19	0.23		0.0850	Amount of Feedstock & Yield: Young et al., 2022; Prices: Intratec, 2024
Methane Price	136	525	1226	0.63	3.33	0.14	0.02	0.01	2.71	0.0053	Amount of Feedstock & Yield: Young et al., 2022; Prices: Statista, 2024a
Benzene	498	935	1107	0.85	3.33	0.064	0.21	0.18		0.0667	Amount of Feedstock & Yield: Young et al., 2022; Prices: Statista, 2024d
Pyrolysis Gasoline	759	973	1032	0.92	3.33	0.11	0.37	0.34		0.1247	Amount of Feedstock & Yield: Young et al., 2022; Prices: Procurement Resource, 2024
Other products Average Price	655	946	1126	0.91	3.33	0.16	0.53	0.48		0.1767	Amount of Feedstock & Yield: Young et al., 2022; Prices: Average of the prices above

6.1.2 MTO-Process

Appx. Table 8: Economic Allocation calculation for the MTO process with respective prices between 2020-2022, the quantities and proceeds

Parameter	Price 2020 [US-$ t]	Price 2021 [US-$/ t]	Price 2022 [US-$/ t]	3-years Average [US-$/kg]	Quantity [kg]	Proceeds [US-$]	Sum [US-$]	Allocation Factor []	Sources
Ethylene Price	780	1000	1060	1.03	1000.0	1030.00		0.43203	Quantity from Rosental et al., 2020; Prices from Statista, 2024b
Propylene Price	778	983	997	0.99	800.0	792.00		0.33220	Quantity from Rosental et al., 2020; prices from Statista, 2024c
Butene Price	981	1258	1333	1.30	230.0	297.96	2384.09	0.12498	Quantity from Rosental et al., 2020; Prices from Intratec, 2024
Aliphatics	846	1080	1130	1.11	239.0	264.13		0.11079	Quantity from Rosental et al., 2020; Price: average of prices above

6.2 Sankey Diagrams of selected ethylene production routes

6.2.1 H₂+CCU-to-Olefins route located in China for the 2020 (BASE) scenario
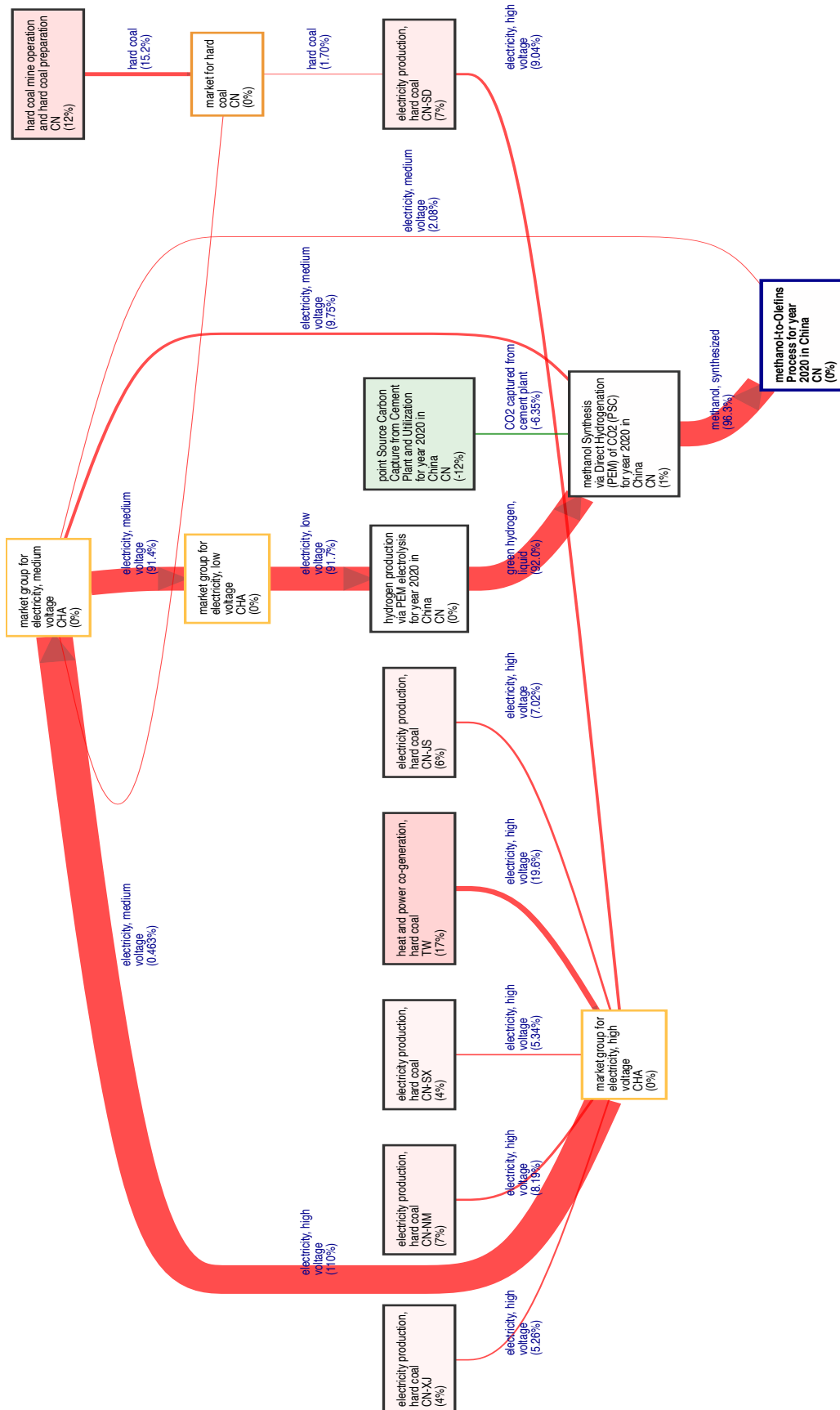
Appx. Figure 1: *Sankey Diagram of the H₂+CCU-to-Olefins route with a cut-off value of 0.05 located in China for the 2020 (BASE) scenario*

6.2.2 Steam Cracking route located in Switzerland for the 2020 (BASE) scenario
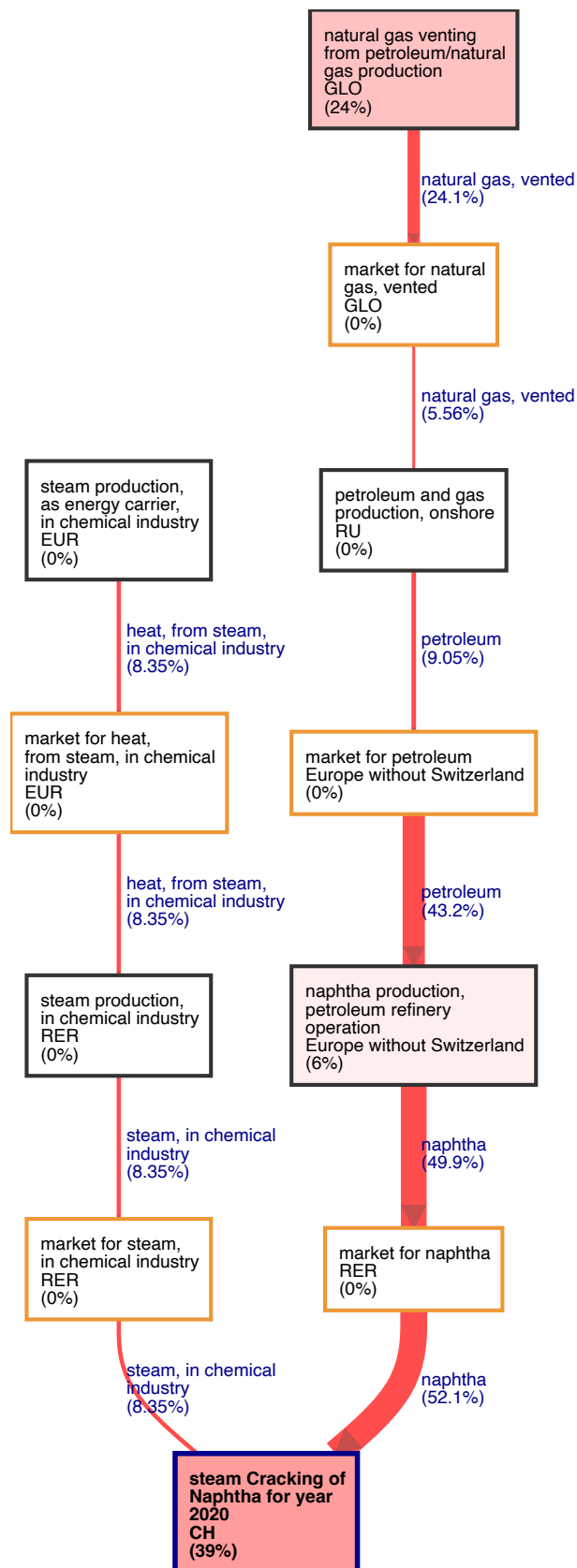
Appx. ***Figure 2:*** *Sankey-Diagram of the Steam Cracking route with a cut-off value of 0.08 located in Switzerland for the 2020 (BASE) scenario*

6.2.3 Swiss high voltage electricity mix in the 2020 (BASE) scenario
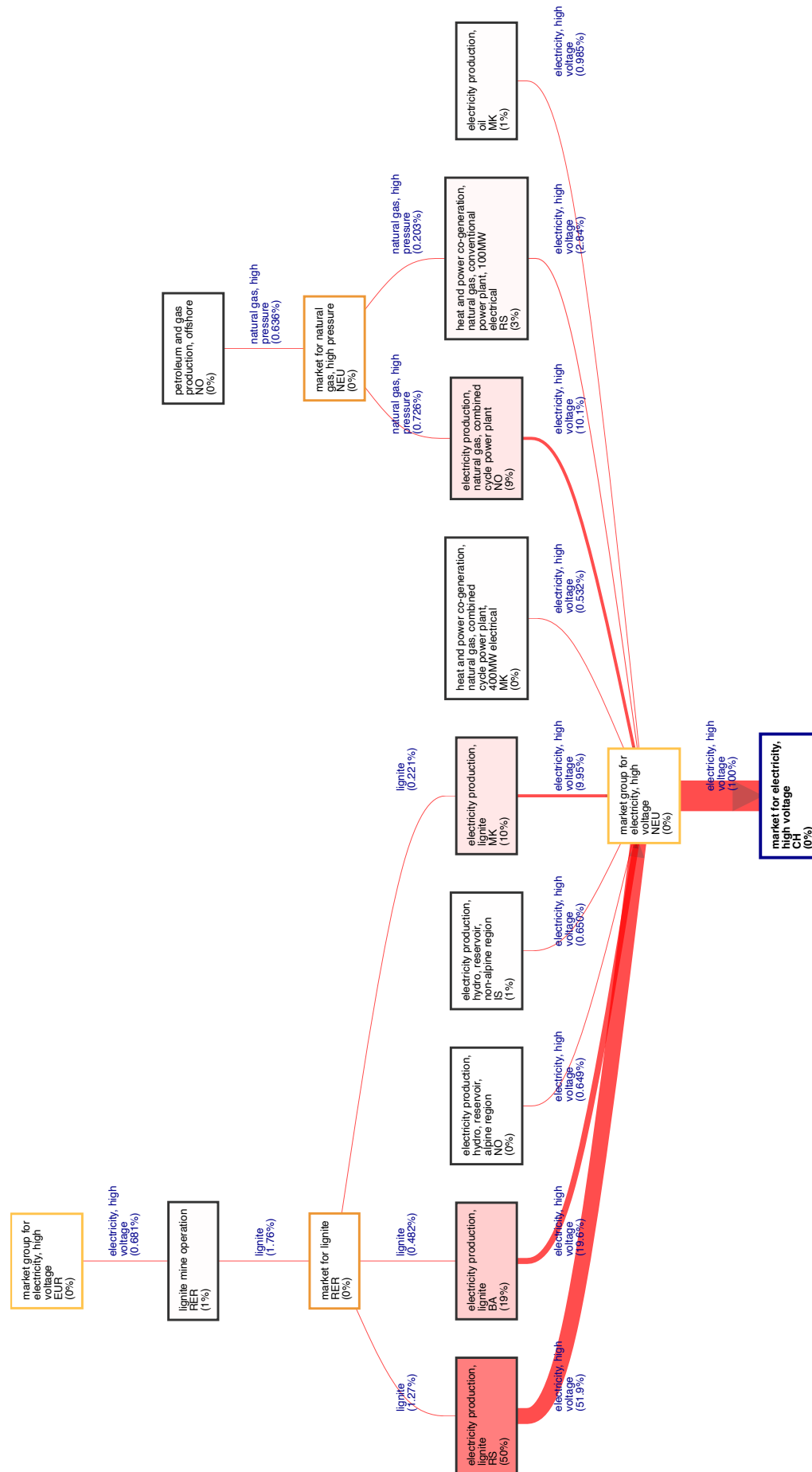
Appx. Figure 3: Sankey Diagram of the Swiss high voltage electricity mix with a cut-off value of 0.005 for the 2020 (BASE) scenario

6.3   Complete LCIs of H₂+CCU- & Biomass-to-Olefins

All values presented in this chapter have already been reported in this Master Thesis with their respective sources in Chapter 3.1individually yet have not been integrated and adjusted throughout the whole production route to 1 t of ethylene.

6.3.1 Integrated LCIs of different Biomass-to-Olefins Routes

6.3.1.1   Integrated LCI of baseline case and future scenarios (2030 & 2050)

Appx. Table 9: *Integrated LCIs of the Biomass-to-Olefins route with adjusted values for the years 2020, 2030 and 2050 according to Chapter 3.2 in Switzerland*

Process	Parameter	Unit/kg FU	Amount		
			Baseline Case	**2030**	**2050**
	Product:				
	Crude Syngas	**kilogram**	**4.8960**	**4.8960**	**4.8960**
	Inputs:				
Biomass Gasification	Bark Chips	kilogram	3.2020	3.2020	3.2020
	O_2	kilogram	1.7530	1.7530	1.7530
	Electricity	kilowatt hour	0.0780	0.0740	0.0710
	Emissions:				
	Ash	kilogram	0.0440	0.0440	0.0440
	Heat (in form of steam), waste	megajoule	4.0150	4.0150	4.0150
	Coke	kilogram	0.0150	0.0150	0.0150
	Product:				
	Sweet Syngas	**kilogram**	**2.5369**	**2.5369**	**2.5369**
	Inputs:				
Post Treatment (AGR&WGS)	Crude Syngas	kilogram	4.8960	4.8961	4.8961
	Electricity	kilowatt hour	0.0100	0.0092	0.0087
	Heat	megajoule	3.3490	3.1812	3.0222
	Emissions:				
	CO_2, non-fossil	kilogram	2.3810	2.3811	2.3811
	H_2S	kilogram	0.0013	0.0013	0.0013
	Product:				
	MeOH	**kilogram**	**2.3490**	**2.3490**	**2.3490**
	Inputs:				
	Sweet Syngas	kilogram	2.5370	2.5369	2.5369
	Electricity	kilowatt hour	3.6170	3.5269	3.4388
	MgO	kilogram	0.0000	0.0004	0.0003
	ZnO	kilogram	0.0060	0.0051	0.0043
MeOH Production	CuO	kilogram	0.0150	0.0135	0.0115
	Al_2O_3	kilogram	0.0020	0.0021	0.0018
	Emissions:				
	H_2O	cubic meter	0.0002	0.0002	0.0002
	CO	kilogram	0.0014	0.0014	0.0014
	CO_2, non-fossil	kilogram	0.0070	0.0070	0.0070
	VOC	kilogram	0.0235	0.0235	0.0235
	Heat, waste	megajoule	6.2440	6.2444	6.2444
	Waste:				
	Zeolite waste	kilogram	-0.0230	-0.0211	-0.0179
	Allocation Factor:		0.43203	0.4320	0.4320	0.4320
	Product:				
	Ethylene	**kilogram**	**1.0000**	**1.0000**	**1.0000**
	Inputs:				
	MeOH	kilogram	2.3490	2.3490	2.3490
	Electricity	kilowatt hour	0.6520	0.6200	0.5270
MTO-Process	Metallurgical Al_2O_3	kilogram	0.2010	0.1910	0.1623
	PO_4^{3-}-rock beneficiation	kilogram	0.2010	0.1910	0.1623
	sodium silicate production	kilogram	0.2010	0.1910	0.1623
	Emissions:				
	Heat	megajoule	1.9270	1.9270	1.9270
	H_2O	cubic meter	0.0010	0.0010	0.0010
	CO_2, non-fossil	kilogram	0.0630	0.0630	0.0630
	Waste:				
	Zeolite waste	kilogram	-0.6030	-0.5430	-0.4610

6.3.1.2   Integrated LCI of different process modifications

Appx. Table 10: *Integrated LCIs of different process modifications of the Biomass-to-Olefins route with adjusted values from Chapter 3.1.2.2 for production location in Switzerland and the year 2020*

Process	Parameter	Unit/kg FU	Amount				
			Wood Chips	Miscan-thus	Advanced Process	CCS	Best Case
Biomass Gasification	**Product:**						
	Crude Syngas	**kilogram**	**4.8960**	**4.8960**	**4.8960**	**4.8960**	**4.8960**
	Inputs:						
	Bark Chips/Wood Chips or Miscanthus	kilogram	3.5570	3.5570	3.2020	3.2020	3.5570
	O_2	kilogram	1.3980	1.3980	1.7530	1.7530	1.3980
	Electricity	kilowatt hour	0.0780	0.0780	0.0780	0.0740	0.0780
	Emissions:						
	Ash	kilogram	0.0440	0.0440	0.0440	0.0440	0.0440
	Heat (in form of steam), waste	megajoule	4.0150	4.0150	0.0000	4.0150	0.0000
	Coke	kilogram	0.0150	0.0150	0.0150	0.0150	0.0150
Post Treatment (AGR&WGS)	**Product:**						
	Sweet Syngas	**kilogram**	**2.5370**	**2.5370**	**2.5370**	**2.5370**	**2.5370**
	Inputs:						
	Crude Syngas	kilogram	4.8960	4.8960	4.8960	4.8960	4.8960
	Electricity	kilowatt hour	0.0100	0.0100	0.0100	0.0100	0.0100
	Heat	megajoule	3.3490	3.3490	0.0000	3.3490	0.0000
	CO_2 compression, transport & storage	kilogram	0.0000	0.0000	0.0000	2.3810	2.3810
	Emissions:						
	CO_2, non-fossil	kilogram	2.3810	2.3810	2.3810	0.0000	0.0000
	H_2S	kilogram	0.0013	0.0013	0.0013	0.0013	0.0013
MeOH Production	**Product:**						
	MeOH	**kilogram**	**2.3490**	**2.3490**	**2.3490**	**2.3489**	**2.3489**
	Inputs:						
	Sweet Syngas	kilogram	2.5370	2.5370	2.5370	2.5369	2.5369
	Electricity	kilowatt hour	3.6170	3.6170	1.1640	3.5269	1.1640
	MgO	kilogram	0.0005	0.0005	0.0005	0.0005	0.0005
	ZnO	kilogram	0.0060	0.0060	0.0060	0.0051	0.0060
	CuO	kilogram	0.0150	0.0150	0.0150	0.0135	0.0150
	Al_2O_3	kilogram	0.0020	0.0020	0.0020	0.0021	0.0020
	Emissions:						
	H_2O	cubic meter	0.0002	0.0002	0.0002	0.0002	0.0002
	CO	kilogram	0.0014	0.0014	0.0010	0.0014	0.0010
	CO_2, non-fossil	kilogram	0.0070	0.0070	0.0070	0.0070	0.0070
	VOC	kilogram	0.0235	0.0235	0.0235	0.0235	0.0235
	Heat, waste	megajoule	6.2440	6.2440	0.0000	6.2444	0.0000
	Waste:						
	Zeolite waste	kilogram	-0.0230	-0.0230	-0.0230	-0.0230	-0.0230
MTO-Process	**Allocation Factor:**	0.43203	0.4320	0.4320	0.4320	0.4320	0.4320
	Product:						
	Ethylene	**kilogram**	**1.0000**	**1.0000**	**1.0000**	**1.0000**	**1.0000**
	Inputs:						
	MeOH	kilogram	2.3490	2.3490	2.3490	2.3490	2.3490
	Electricity	kilowatt hour	0.6520	0.6520	0.6520	0.6520	0.6520
	Metallurgical Al_2O_3	kilogram	0.2010	0.2010	0.2010	0.2010	0.2010
	PO_4^{3-}-rock beneficiation	kilogram	0.2010	0.2010	0.2010	0.2010	0.2010
	sodium silicate production	kilogram	0.2010	0.2010	0.2010	0.2010	0.2010
	Emissions:						
	Heat	megajoule	1.9270	1.9270	0.0000	0.0000	0.0000
	H_2O	cubic meter	0.0010	0.0010	0.0010	0.0010	0.0010
	CO_2, non-fossil	kilogram	0.0630	0.0630	0.0630	0.0630	0.0630
	Waste:						
	Zeolite waste	kilogram	-0.6030	-0.6030	-0.6030	-0.6030	-0.6030

6.3.2 Complete LCIs of different H₂+CCU-to-Olefins Routes

6.3.2.1 Integrated LCI of baseline and future scenarios (2030 & 2050)

Appx. Table 11: *Integrated LCIs of the H₂+CCU-to-Olefins route with adjusted values for the years 2020, 2030 and 2050 according to Chapter 3.2 in Switzerland*

Process	Parameter	Unit/kg FU	Amount		
			Baseline Case	2030	2050
PEM-Electrolysis	**Product:**				
	H_2	**kilogram**	**0.4768**	**0.4768**	**0.4768**
	Inputs:				
	PEM Stack (1 MW)	unit	4.96E-07	6.44E-07	6.44E-07
	PEM BoP Production	unit	1.65E-07	1.51E-07	1.34E-07
	De-ionized H_2O	kilogram	5.7220	6.3505	5.5785
	Electricity	kilowatt hour	27.4038	22.6774	19.1259
	Emissions:				
	O_2	kilogram	3.8147	3.3596	2.8335
	Wastes:				
	Waste Treatment of PEM BoP	unit	-4.96E-07	-6.44E-07	-6.44E-07
	Waste Treatment of PEM Stack	unit	-1.65E-07	-1.51E-07	-1.34E-07
CCU-PSC	**Product:**				
	Captured CO_2	**kilogram**	**3.3848**	**3.3848**	**3.3848**
	Inputs:				
	Electricity	kilowatt hour	1.8102	1.7650	1.6767
	MEA	kilogram	0.0068	0.0066	0.0063
	CO_2, from air	kilogram	3.7609	3.7609	3.7609
	Emissions:				
	CO_2, fossil	kilogram	0.3761	0.3761	0.3761
	Ethylene diamine	kilogram	0.0068	0.0066	0.0063
MeOH Production	**Product:**				
	MeOH	**kilogram**	**2.3489**	**2.3489**	**2.3489**
	Inputs:				
	CO_2	kilogram	3.3848	3.3848	3.3848
	H_2	kilogram	0.4768	0.4768	0.4768
	Electricity	kilowatt hour	3.0583	2.9819	2.8328
	MgO	kilogram	0.0005	0.0004	0.0004
	ZnO	kilogram	0.0056	0.0051	0.0043
	CuO	kilogram	0.0150	0.0135	0.0115
	Al_2O_3	kilogram	0.0023	0.0021	0.0018
	Emissions:				
	H_2O	cubic meter	0.0014	0.0014	0.0014
	CO_2, fossil	kilogram	0.1550	0.1503	0.1503
	Heat, waste	megajoule	3.2885	3.2885	3.2885
	Waste:				
	Zeolite waste	kilogram	-0.0235	-0.0211	-0.0180
MTO-Process	**Allocation Factor:**		0.43203	0.43203	0.43203
	Product:				
	Ethylene	**kilogram**	**1.0000**	**1.0000**	**1.0000**
	Inputs:				
	MeOH	kilogram	2.3489	2.3489	2.3489
	Electricity	kilowatt hour	0.6524	0.6197	0.5268
	Metallurgical Al_2O_3	kilogram	0.2010	0.1910	0.1623
	PO_4^{3-}-rock beneficiation	kilogram	0.2010	0.1910	0.1623
	sodium silicate production	kilogram	0.2010	0.1910	0.1623
	Emissions:				
	Heat	megajoule	1.9273	1.9273	1.9273
	H_2O	cubic meter	0.0013	0.0013	0.0013
	CO_2, fossil	kilogram	0.0626	0.0626	0.0626
	Waste:				
	Zeolite waste	kilogram	-0.6031	-0.5729	-0.4870

6.3.2.2 Integrated LCIs of different process modifications

Appx. Table 12: *Integrated LCIs of different process modifications of the H_2+CCU-to-Olefins route with adjusted values from Chapter 3.1.2.2 for production location in Switzerland and the year 2020*

Process	Parameter	Unit/kg FU	Amount				
			SOEC	Advanced Process	Novel Solvents	DAC	Best Case
PEM-Electrolysis	**Product:**						
	H₂	**kilogram**	**0.4768**	**0.4768**	**0.4768**	**0.4768**	**0.4768**
	Inputs:						
	PEM/SOEC Stack (1 MW)	unit	1.10E-06	4.96E-07	4.96E-07	4.96E-07	1.10E-06
	PEM/SOEC BoP Production	unit	1.22E-07	1.65E-07	1.65E-07	1.65E-07	1.22E-07
	De-ionized H₂O	kilogram	5.6951	3.0553	5.7220	5.7220	3.0553
	Electricity	kilowatt hour	20.28	27.4038	27.4038	27.4038	20.28
	Heat	mega joule	8.95	0.0000	0.0000	0.0000	8.95
	Emissions:						
	O₂	kilogram	3.80	3.8147	3.8147	3.8147	3.80
	Wastes:						
	Waste Treatment of PEM/SOEC BoP	unit	-1.22E-07	-4.96E-07	-4.96E-07	-4.96E-07	-1.22E-07
	Waste Treatment of PEM/SOEC Stack	unit	-1.10E-06	-1.65E-07	-1.65E-07	-1.65E-07	-1.10E-06
CCU-PSC/DAC	**Product:**						
	Captured CO₂	**kilogram**	**3.3848**	**3.3848**	**3.3848**	**3.3848**	**3.3848**
	Inputs:						
	Electricity	kilowatt hour	1.8102	1.0735	1.2824	3.4431	0.7667
	MEA/Amine-based silica	kilogram	0.0068	0.0068	0.0068	0.0101	0.0068
	CO₂, from air	kilogram	3.7609	3.7609	3.7609	3.7609	3.7609
	Sorbent based DAC System	unit	0.0000	0.0000	0.0000	1.684E-09	0.0000
	Emissions:						
	CO₂, fossil	kilogram	0.3761	0.3761	0.3761	0.3761	0.3761
	Ethylene diamine	kilogram	0.0068	0.0068	0.0068	0.0101	0.0068
	Waste:						
	Waste Treatment of DAC system	unit	0.0000	0.0000	0.0000	-1.684E-09	0.0000
MeOH Production	**Product:**						
	MeOH	**kilogram**	**2.3489**	**2.3489**	**2.3489**	**2.3489**	**2.3489**
	Inputs:						
	CO₂	kilogram	3.3848	3.3848	3.3848	3.3848	3.3848
	H₂	kilogram	0.4768	0.4768	0.4768	0.4768	0.4768
	Electricity	kilowatt hour	3.0583	3.0583	3.0583	3.0583	3.0583
	MgO	kilogram	0.0005	0.0005	0.0005	0.0005	0.0005
	ZnO	kilogram	0.0056	0.0056	0.0056	0.0056	0.0056
	CuO	kilogram	0.0150	0.0150	0.0150	0.0150	0.0150
	Al₂O₃	kilogram	0.0023	0.0023	0.0023	0.0023	0.0023
	Emissions:						
	H₂O	cubic meter	0.0014	0.0000	0.0014	0.0014	0.0000
	CO₂, fossil	kilogram	0.1550	0.1550	0.1550	0.1550	0.1550
	Heat, waste	megajoule	3.2885	0.0000	3.2885	3.2885	0.0000
	Waste:						
	Zeolite waste	kilogram	-0.0235	-0.0235	-0.0235	-0.0235	-0.0235
MTO-Process	**Allocation Factor:**		0.43203	0.43203	0.43203	0.43203	0.43203
	Product:						
	Ethylene	**kilogram**	**1.0000**	**1.0000**	**1.0000**	**1.0000**	**1.0000**
	Inputs:						
	MeOH	kilogram	2.3489	2.3489	2.3489	2.3489	2.3489
	Electricity	kilowatt hour	0.6524	0.6524	0.6524	0.6524	0.6524
	Metallurgical Al₂O₃	kilogram	0.2010	0.2010	0.2010	0.2010	0.2010
	PO₄³⁻-rock beneficiation	kilogram	0.2010	0.2010	0.2010	0.2010	0.2010
	sodium silicate production	kilogram	0.2010	0.2010	0.2010	0.2010	0.2010
	Emissions:						
	Heat	megajoule	1.9273	0.0000	1.9273	1.9273	0.0000
	H₂O	cubic meter	0.0013	0.0000	0.0013	0.0013	0.0000
	CO₂, fossil	kilogram	0.0626	0.0626	0.0626	0.0626	0.0626
	Waste:						
	Zeolite waste	kilogram	-0.6031	-0.6031	-0.6031	-0.6031	-0.6031

7. Statement of Authorship

I expressly declare that the written work I have submitted with the following title:

"Shaping Tomorrow`s Ethylene: A Prospective Life Cycle Assessment of Emerging Production Alternatives"

is an original work composed by me independently, without unauthorized assistance and in my own words. In addition, I did not use any tools other than those specified in this work. I also confirm that the work has not yet been submitted to any other examination authority in the same or similar form and has not yet been published as a whole or in parts. I expressly declare that I have identified all references to sources and secondary literature contained in the above-mentioned work as such. I particularly verify that I have, without exception and to the best of my knowledge, indicated the authorship both for directly quoted statements (quotations) and for statements of other authors paraphrased in my own words (indirect quotations). I acknowledge that works that violate the principles of the declaration of independence - especially those that contain direct or indirect quotations without indication of origin - are considered plagiarism and may result in corresponding legal and disciplinary consequences. With my signature I confirm that I have read and understood the declaration of independence and confirm its contents.

Zurich, 28.11.2024

_____
(Signature of Student)